NSIRC RESEARCH AND INNOVATION CONFERENCE 2021

INDUSTRY-LED POSTGRADUATE RESEARCH

8-9 SEPTEMBER 2021

nsirc

ENQUIRIES@NSIRC.CO.UK
+44 (0) 1223 899 000
NSIRC.COM/CONFERENCE

00.10.09.21.00

TWI HELLAS

Technology | Innovation | Consulting

Client New Product Development

TWI Hellas develops & integrates new technologies to make products & services more competitive.

Our work on **Solbotix** automated & autonomous PV cleaning systems for arid regions aims at resolving the existing soiling problem & recovering the lost revenue.

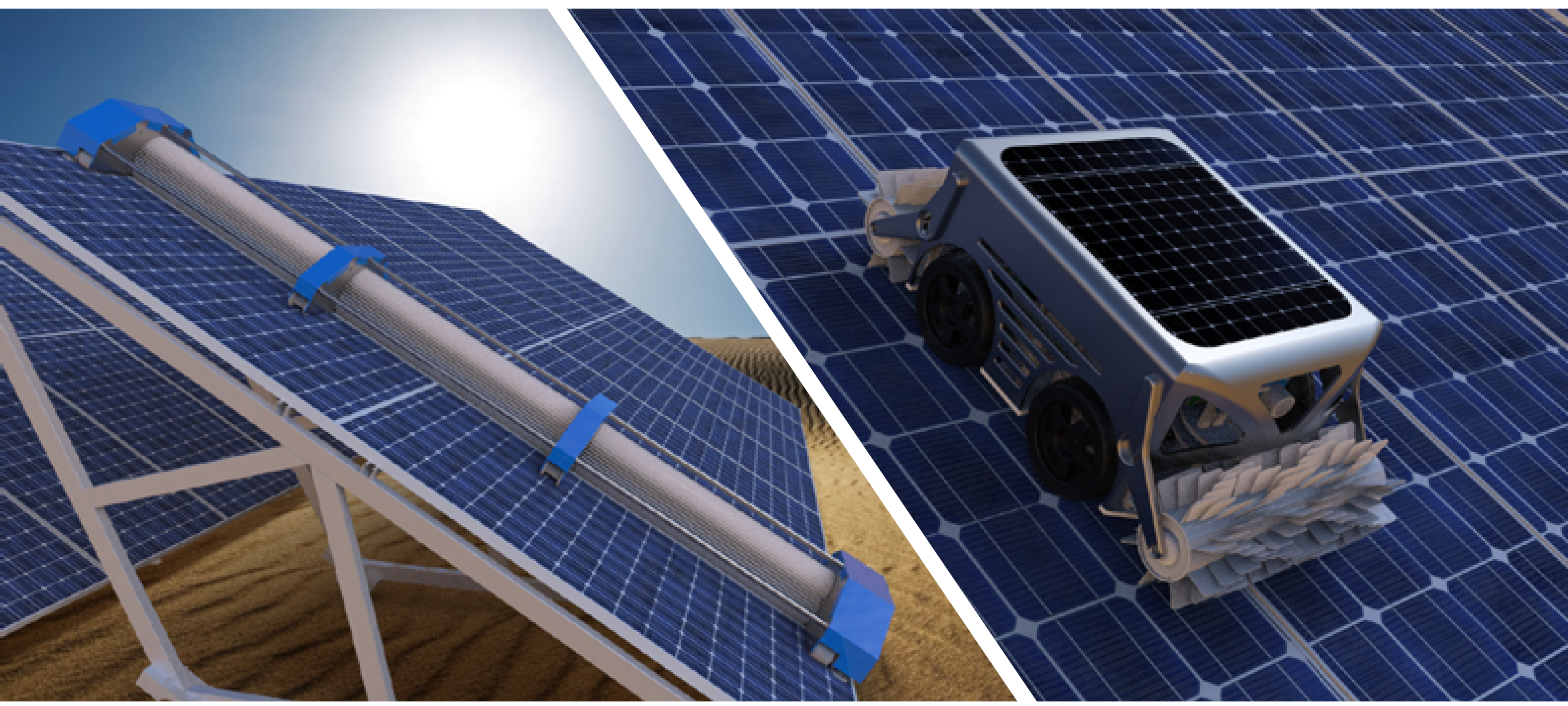

Contact us!

info@twi-hellas.com

www.linkedin.com/company/twi

CATAPULT Digital

Intelligent Infrastructure

In the UK, we are rapidly approaching an inflection point for how we future proof our critical infrastructure and lower its environmental impact. Digital technologies have the potential to improve the interoperability, resilience and intelligence of our supply chains. These opportunities will mean as an industry we can adapt to shifts in energy mixes, the electrification of transportation and the gas network transition to hydrogen.

As the UK authority on advanced digital technology Digital Catapult welcomes you to join two online events covering digitalising infrastructure:

Digital Supply Chain - Why and how the UK food and drink industry should lead the way

16 September 10:00 - 11:30

Explore how digitalising the UK food and drink supply chain can improve efficiency, resilience and sustainability.

Sign-up here:

bit.ly/DigiSupplyChainFood

Intelligent Energy Infrastructure Forum - The benefits of greater intelligence

05 October 14:00 - 15:30

Discuss with leaders in the energy sector how advanced digital innovation can address the challenges of energy transformation.

Sign-up here:

bit.ly/IntelligentEnergyInfrastructure

Digital Catapult is proud to be partners with TWI to establish a new industrial net-zero hub

Established as a joint initiative between two of the UK's leading innovation organisations in the engineering and digital sectors, INZIC targets asset and energy intensive industries such as aerospace, utilities and energy.

Find out more bit.ly/INZIC

WELCOME - NSIRC RESEARCH AND INNOVATION CONFERENCE 2021

I am delighted to inform you that this year, for the first time, we will also be including TWI's Core Research Programme (CRP) in our two-day conference, and shining the spotlight on some of its activities, alongside our usual coverage of NSIRC and its students' achievements in the past year.

Building on the success of NSIRC 2020 LIVE, we are also bringing you this year's event in an online format, so that our students, partners and associates can join us for the conference, no matter where they are in the world currently.

NSIRC was established in 2012, by founding partners Lloyd's Register Foundation and TWI, as a postgraduate education and research centre to train over 500 postgraduate qualified engineers and employ 61 professionals in its first ten years, and advance fundamental research with real world applications in industry.

The CRP invests half of TWI's Industrial Membership subscriptions to develop new technology capabilities for industrial application in 3-5 years' time. It comprises a rolling programme of 30-40 projects, with 10-15 new projects starting every year, some of which provide opportunities for NSIRC students to work on them.

Now in its penultimate year, I am pleased to report that NSIRC continues to flourish and is on track to achieve its ten year objectives. Some of the ways in which NSIRC is impacting industry and society are:

- Enabling 280 postgraduate research students to work at a state-of-the-art facility to enhance their knowledge and make scientific breakthroughs
- 100% employment rate for PhD students within one year of graduating
- 184 PhDs and 148 MScs successfully completed by students in an industrial setting
- Promoting the inclusion of underrepresented communities in engineering. 31% of NSIRC PhD students are female, compared to a UK engineering workforce representation of 11%.
- A network of more than 40 academic partners via signed agreements with leading universities in the UK and overseas
- Two new Masters' courses launched in January 2021: MSc in Lightweight Structures Impact Engineering and Masters of Business Administration
- 350 days of community outreach activities delivered by students to young engineers, schools and universities
- £150m invested in facilities, equipment and studentships

TWI's CRP is steered and monitored by TWI's Research Board which is composed of representatives from around 40 Industrial Member companies. Technology themes for CRP projects are identified through facilitated technology mapping workshops with Industrial Members and TWI's technical experts, conferences, and day-to-day interactions with industry, other research organisations and academia.

This year's CRP showcase will demonstrate the breadth of research that TWI conducts at low TRLs, and the link between NSIRC's PhD Programme and the CRP. It will include a number of project presentations looking at industry pull, benefits to TWI Industrial Members and how the CRP builds upon or underpins other TWI technical work.

Lastly I would like to thank everyone involved in NSIRC and the CRP – TWI and university staff, partners and TWI Industrial Members, and our sponsors for their support – and wish you a very warm welcome to the NSIRC 2021 Research and Innovation Conference.

Tat-Hean

Professor Tat-Hean Gan
NSIRC Director
TWI Director, Innovation & Skills

DPS_9535 0720

OFFICIAL 2021 CONFERENCE SPONSORS

We would like to sincerely thank all our sponsors of NSIRC 2021. Without their support, our annual conference would not have been possible.

33

Number of countries NSIRC students come from.

£150m

Invested in PhD research facilities, equipment and studentships

ABOUT NSIRC

The National Structural Integrity Research Centre (NSIRC) was established in October 2012 with the aim of becoming the world centre for structural integrity research.

NSIRC is a state-of-the-art postgraduate engineering facility established and managed by structural integrity specialist TWI. It works closely with industrial partners Lloyd's Register Foundation and BP plc, and lead academic partner Brunel University London.

NSIRC collaborates with almost 40 world-leading universities, including University of Cambridge, University of Oxford and National University of Singapore, to meet industrial challenges. The collaborating partners provide academic excellence to address the need for fundamental research, as well as high-quality, industry-relevant training for the next generation of structural integrity engineers.

NSIRC advances fundamental research to:

- Support the safe operation of products and structures
- Develop innovative, fit-for-purpose technologies and design rules
- Demonstrate solutions for long-term asset management

This includes risk-based management, engineering critical assessment, non-destructive testing, structural health and condition monitoring, and health management for use in real world settings.

180

PhDs successfully completed

Research Institute
Future Transport and Cities

Coventry University

Materials and Structural Integrity

Coventry University is an award winning, modern university with a track record in running effective collaborations and partnerships with academic peers and industrial partners from around the world.

Under the global challenge of Clean Growth and Future Mobility, our research is concerned with advancing powertrain electrification, future and disruptive mobility solutions, advanced manufacturing technology and next-generation materials to ensure a more sustainable future.

Our support for manufacturing industries is underpinned by our research in Materials Engineering and Structural Integrity which focuses on safety-critical applications, and the fundamental scientific knowledge required to assure and improve safety. By understanding in-service material behaviour, we support our industrial partners in producing superior and more cost-effective products with longer lifespans.

Since 2014, we are delighted to have been awarded 22 PhD studentships from NSIRC, sponsored by the Lloyd's Register Foundation, TWI and BP. The success of our research in this area drives our ambition to grow our collaboration with the sponsors, NSIRC and wider industry and develop innovative solutions to new challenges.

Research Coventry | discover more online www.coventry.ac.uk/research

coventry.ac.uk/iftc

UNIVERSITY OF LEICESTER

TWI

MatIC at the University of Leicester

The Materials and Innovation Centre (MatIC), an international collaboration between The Welding Institute and the University of Leicester, creates a shared research and technology capability. Bringing together the expertise of the two organisations, it will specialise in small and full-scale materials testing in harsh environments, it will undertake joint research programmes and it will develop the next generation of technologies and engineers in this discipline.

Core areas:

- Materials performance in simulated service conditions
- Physical metallurgy of welding and other fusion-based processes
- Materials characterisation and analysis
- Failure mechanism of weldments and other components made by fusion-based processes
- Computational mechanics
- Digital manufacturing and materials modelling
- Thermal and cold spray coatings
- Thin films and metal matrix systems
- Electrochemistry and corrosion

www.le.ac.uk/matic

AFFILIATED UNIVERSITIES

At NSIRC we combine academia with industry, working closely alongside lead academic partner Brunel University London, as well as more than 35 other affiliated universities...

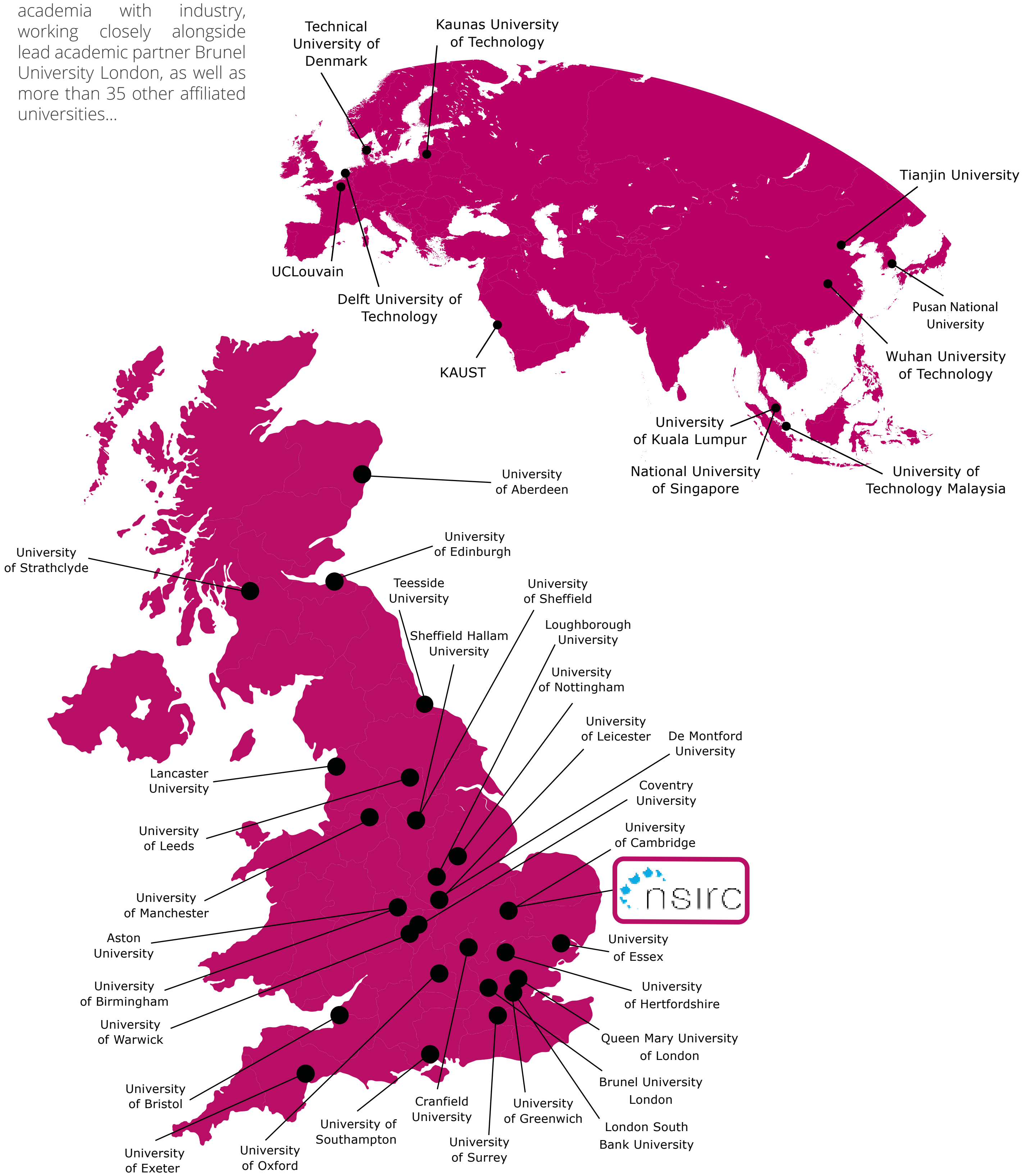

KEYNOTE SPEAKERS

Luca Corradi
Innovation Network Director, Net Zero Technology Centre

Luca is the Innovation Network Director at the Net Zero Technology Centre, working to bring "the outside in", connecting innovators and organisations across sectors and disciplines, to explore the latest technologies that could be adopted to address industry transition challenges. Leading The Net Zero Technology Centre's horizon scanning activity, he identifies emerging technology trends, cutting through the hype to identify potential areas of impact and application. He came to this role after more than twenty years of experience in management consulting. After a Master Degree in Economics and Business with a specialisation in Organisation and Change Management, he worked internationally for Accenture, mostly with energy related projects and clients. Luca led and grew the global network of Accenture Energy Hubs, and led transformational projects across multiple countries and cultures. Outside work Luca loves reading, music and travel. He lives in Aberdeen, is married and has two young daughters and a dog. He enjoys the rare motorbike ride in Scotland and even rarer ski trip to the Alps.

Prof Mark Thomson
Executive Chair, Science and Technology Facilities Council

Professor Thomson is Executive Chair of the Science and Technology Facilities Council (STFC). STFC, which is one of the nine councils of UK Research and Innovation, is responsible for particle physics, astrophysics, space science and nuclear physics. As well as STFC, Prof Thomson is also responsible for the large-scale multidisciplinary research facilities at the UK National Laboratories. Within UKRI, Prof Thomson leads on infrastructure, including e-Infrastructure, and directed the work to produce the UK's first Research and Innovation Infrastructure Roadmap, which was released in 2019. Having held national and international research leadership roles in both neutrino physics and collider physics, before joining STFC, Prof Thomson was the co-leader of the Deep Underground Neutrino Experiment (DUNE), an international collaboration of over 1000 scientists and engineers. Beyond his own research, Prof Thomson has held numerous research oversight roles in the UK and abroad and has published a textbook "Modern Particle Physics", which has been widely adopted for undergraduate courses at universities around the globe.

DAY 1 (8TH) AGENDA

Time	Session
09:30	**Welcome and Introduction to NSIRC (National Structural Integrity Research Centre) and CRP (Core Research Programme)** Prof Tat-Hean Gan, NSIRC Director
09:45	**Scanning the Horizon for a Net Zero Future** Keynote Speaker: Luca Corradi, Innovation Network Director, *Net Zero Technology Centre*

Time	SESSION A	SESSION B
	Composites and Polymers Sponsored by **Brunel Composites Centre** and **Teesside University**	**Additive Manufacturing** Sponsored by **Anglia Ruskin University** and **Malvern Panalytical**
10:15	Alessandro Sergi Influence of Powder Characteristics on Hot Isostatically Pressed pure Niobium for Space Application	Helen Elkington Laser Beam Direct Energy Deposition – Effect of Process Parameters on Material Properties of Inconel 718
10:30	Mohammad Alghfeli An Approach to Enhanced HDPE nanocomposites	Sameera Weeratunga Determine influence of local microstructure features on crack initiation in additively manufactured Inconel-718
10:45	BREAK	
11:00	**Core Research Programme Showcase Presentation:** Chris Worrall Preliminary Mechanical Properties of Thermoplastic Composites Containing Multiple Pierced Perforations	Marie-Salome Duval-Chaneac Effect of heat treatment on fatigue crack growth in Multiple Material Additive Manufacturing (MMAM)
11:15		Saad Ahmed Correlating Defects to Fatigue Performance in Selective Laser Melted Al-Si10-Mg Alloys
11:30	Minghui Wu Assessing life cycle costs and environmental performance of composite material in aircraft application	**Core Research Programme Showcase Presentation:** Adrian Addison Welding of Additively Manufactured Materials: Preliminary Assessment
11:45	Thamasha Dona Design and Development of Composite Panels with Variable Thermal Conductivity for Li-ion Battery Module	
12:00	LUNCH	

Time	Session A	Session B
13:00	Hamad Raheem Evaluation of Polymer Ageing Due to Gas Permeation using Piezoelectric Micromachined Ultrasonic Transducers	Corentin Penot Investigation of the corrosion performance of a WAAM deposited 316L alloy in NaCl environment
		Industry 4.0 Sponsored by the **University of Leicester**
13:15	Malallah Al Lawati Powder Hot Isostatic Pressing of Ti-based Metal Matrix Composites (TMCs)	Yi Yin Electron Beam Weld Penetration Depth Prediction Based on Artificial Neural Network and Numerical Modelling
13:30	Burak Sakarya Design of Composite Pressure Vessels with built-in "Leak-Before-Break" Capability	Marco Berchiolli Deep Learning Based Chest Cavity Segmentation in T1-Weighted Contrast-Enhanced Breast MRI
13:45	Maciej Gierulski Electrofusion couplers for Thermoplastic Composite Pipe	Norbert Sieczkiewicz Electron beam characterisation using time series imaging and deep learning
14:00	BREAK	
	Joining Technologies Sponsored by **TWI Certification Limited** and **Coventry University**	**Structural Integrity** Sponsored by **Brunel University London** and **Coventry University**
14:15	Mohammad Khairy Effect of partial pressure of hydrogen on vacuum brazing of 316L stainless steel	Chiamaka Mbanusi Dynamic Fracture Toughness of Metallic Materials at Very High Loading Rates
14:30	Tianmiao Li Cold Atmospheric Plasma (CAP) Treatment to Enhance Adhesive Bonding	Zeng Chen Evaluation of applicability of different constraint parameters in brittle SEN(B) specimens
14:45	**Core Research Programme Showcase Presentation:** Mike Dodge Hydrogen Embrittlement of High Strength Precipitation Hardenable Nickel Alloys	Hanwei Zhou Numerical Simulation of Fatigue Crack Propagation
15:00		Vishal Vats Characterization of arc welding fume samples by FT-IR spectroscopy
15:15	**Closing Words**	
15:30	**End of Day 1**	

DAY 2 (9TH) AGENDA

Time	Session A	Session B
09:30	**Welcome and Introduction** Ameni Lounissi, Research and Innovation Operations Section Manager, TWI Ltd Daisy Martlew, Commercial Operations Team Manager, TWI Ltd	
09:45	**Technology Matters** Keynote Speaker: Mark Thomson, Executive Chair, *Science and Technology Facilities Council (STFC)*	
	SESSION A	**SESSION B**
	Inspection and Monitoring Sponsored by **TWI Hellas,** the **Industrial Net Zero Innovation Centre** and **Castalia**	**Structural Integrity and Standards** Sponsored by **Brunel Innovation Centre**
10:15	Rukhshinda Wasif Development of permanently installed magnetic eddy current sensor for corrosion monitoring	Faris Nafiah Quantitative Data Analysis of Pulsed Eddy Current Responses For Pipeline Profiling
10:30	Dandan Liu Hydrogen Induced Cracking in Oil and Gas Pipelines and Its Monitoring	Paul Sukpe Crack Tip Constraint In Typical High Strength Steel Components In Arctic Conditions
10:45	BREAK	
11:00	**Core Research Programme Showcase Presentation:** Channa Nageswaran Influencing Parameters For The Ultrasonic Inspection Of Austenitic Welds	Matthew Weltevreden Parametric Statistics using Austenitic Girth Weld Residual Stress Data
11:15		Oliver Logan Constraint Analysis – Application to Notched Cases
11:30	Xuening Zou Simulation-based training of CNN for detection of cracking	**Core Research Programme Showcase Presentation:** Muhammad Ali Refill Friction Stir Spot Welding Parameter Development for Transport Industry Aluminium Alloys
11:45	Nagu Sathappan Development of an underwater and high temperature sensor for a permanently installed corrosion monitoring system	
12:00	LUNCH	

Time	Coatings Technologies Sponsored by **the Materials Innovation Centre**	Joining Technologies Sponsored by **TWI Certification Limited** and **Coventry University**
13:00	Ana Carolina Araujo-Lascano Performance of Painted TSA in Simulated Marine Environment	Dimitrios Gaitanelis Thermal degradation of thermoplastic composites in laser processing: An investigation for composite-metal joining
13:15	Adamantini Loukodimou Development of Novel Coating Systems for Mitigating Corrosion of Offshore Wind Turbines	Bowei Li Laser riveting: an innovative technique for dissimilar materials joining
13:30	**Core Research Programme Showcase Presentation:** Ewen Kellar Gas Plasma as a Universal Dry Pre-treatment for Structural Bonding Applications	Amarachi Frances Obilor Laser Surface texturing of Polymer materials for surface energy control
13:45		George Brooks Investigation Into The Influence Of Friction Stir Welding In Thick Section Aluminium Alloys
14:00	Aamna Asad Understanding the structure function relationships of super-omniphobic nano-particles	
14:15	**Closing Words**	
14:30	**End of Day 2**	

Alessandro Sergi

Alessandro obtained his MSc degree in Mechanical Engineering at University of Calabria (Italy) in May 2017. He started his PhD with University of Birmingham in January 2018. His research is focused on Powder Hot Isostatic Pressing (P-HIP) of high-temperature materials, including Ni-base superalloys, refractory metals and Ni-base metal matrix composites (MMCs).

Influence of Powder Characteristics on Hot Isostatically Pressed pure Niobium for Space Application

R.H.U. Khan [1], Martina Meisner[2], M.M. Attallah [3]
[1]TWI, [2]ESA, [3]Univeristy of Birmingham
3rd Year of PhD

Keywords: powder characteristics, oxygen levels, microstructure, mechanical properties.

I. INTRODUCTION

Niobium (Nb) and Nb alloys are widely used in spacecraft components due to their excellent high-temperature capabilities and relatively low density if compared to other refractory metals. However, producing Nb with the conventional manufacturing processes is challenging due to the high melting temperature of Nb and high reactivity. For these reasons, powder hot isostatic pressing (P-HIP) consolidation process was assessed to see the HIP response of pure Nb powder material. In fact, P-HIP process is performed in a controlled atmosphere and with the use of a sacrificial canister, thus there are no issues related to the powder reactivity. Moreover, since P-HIP involves the simultaneous application of both high temperature and isostatic pressure, the final microstructure is isotropic with high densification levels. The main scope of this work was to gain a comprehensive understanding of the P-HIP response of pure Nb and evaluate the influence of powder characteristics on the microstructure and mechanical properties. To this end, four different Nb powders (fine, mid-range, mid-range sieved and coarse) were consolidated through P-HIP. It was found that the powder oxygen content plays a crucial role in the mechanical properties of the consolidated material. Furthermore, it was explored that the powder oxygen levels can be altered to obtain an increase in strength while maintaining good levels of ductility.

II. DESIGN/METHODOLOGY/APPROACH

In this study, four different pure Nb powders classified as fine (<44µm), mid-range (15–100µm), sieved mid-range (15-63µm) and coarse (<500µm) were analysed. In particular, a detailed powder characterisation including powder morphology, chemical analysis and particle size distribution (PSD) was performed on these pure Nb powders. After assessing the characteristics, all the four Nb powders were encapsulated separately in low carbon steel (ISO 3574 Grade CR4) cylindrical canisters (Ø50mm x 90mm) with 2 mm wall thickness. Due to the reactive nature of the powders, the powder filling procedure was performed inside a glove box in argon atmosphere. After the filling procedure, the four canisters were degassed, crimped and hot isostatically pressed (HIPed) using EPSI HIP system. After the HIP process, samples for microstructural characterisation and testing work were extracted using electrical discharge machine (EDM) cutting method. The four samples were polished using standard metallographic techniques and characterised using scanning electron microscope (SEM), energy dispersive X-ray (EDX), electron backscatter diffraction (EBSD) and microhardness. Whereas, three tensile samples were extracted from as-HIPed Nb mid-range and sieved mid-range to evaluate the room temperature tensile properties and to understand the influence of oxygen on the tensile properties of the material.

III. FINDINGS/RESULTS

1. Powder Characterisation

Figure 1 shows the powder morphology of the three initial Nb powders. Nb powders are characterised by a rock shape, typical of the hydrogenation–dehydrogenation (HDH) process. Another important result concerns the oxygen levels present in Nb powders. In fact, it was observed that Nb fine showed the highest level of oxygen contamination (1189ppm) followed by Nb coarse (1172ppm), sieved Nb mid-range (756ppm) and Nb mid-range (302ppm).

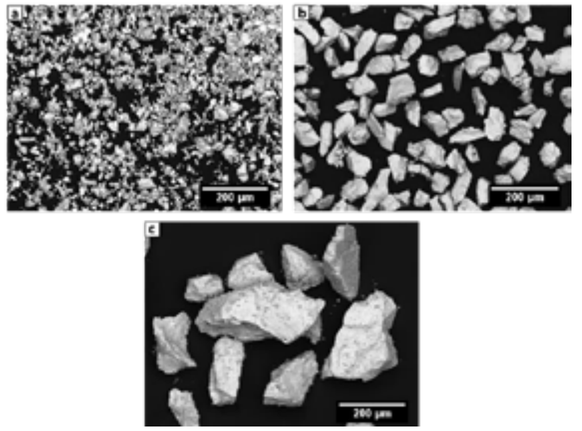

Figure 1 SEM powder morphology of Nb fine (a), mid-range (b) and coarse (c).

2. Microstructure and Mechanical Properties

The microstructure of the as-HIPed Nb powders is shown in Figure 2. The Nb microstructure showed fully dense isotropic material. A clear difference in grain size can be observed between the three HIPed microstructures with an average grain size of 33µm for Nb-fine, 53µm for Nb mid-range and 67µm for Nb coarse, suggesting that the grain size is a function of the powder particle size. Moreover, Nb mid-range powders were subjected to a sieve operation to increase the surface to volume ratio and consequently the oxygen concentration. The microstructure also, in this case, shows a direct correlation between powder particle size with an average grain size of 45µm Figure 2d.

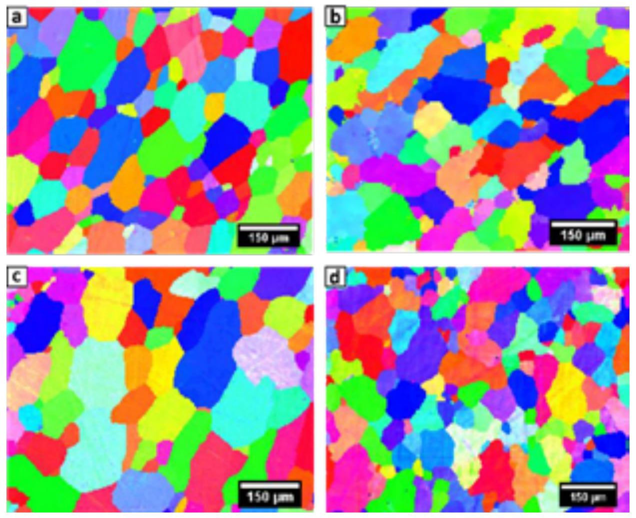

Figure 2 EBSD maps of as-HIPed Nb fine (a), Nb mid-range (b), Nb coarse (c), sieved Nb mid-range (d).

Microhardness tests performed on the four powders highlight the influence of oxygen on the strength of pure Nb. Nb fine having the highest O concentration, showed the highest hardness (250HV), followed by Nb coarse (194HV), while Nb mid-range exhibits the lowest levels of microhardness just above 100HV. However, it is worth noting that the sieving operation resulted in a considerable increase in strength for Nb mid-range up to (135HV).

Tensile tests were performed on Nb mid-range and Nb mid-range sieved to understand the increase in tensile strength, but also the influence of oxygen levels on the ductility for pure Nb. The results reported in Figure 3 show a considerable increase in both YS and UTS, while retaining excellent levels of %EL.

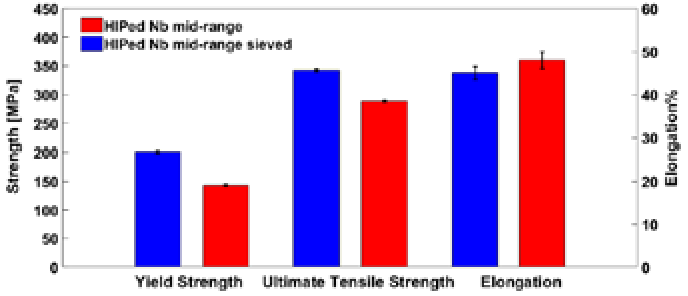

Figure 3 Tensile properties of as-HIPed Nb mid-range and sieved Nb mid-range.

IV. DISCUSSION/CONCLUSIONS

In this work, the P-HIP response of pure Nb was investigated. The as-HIPed Nb resulted in a fully dense isotropic microstructure. Moreover, it was demonstrated that powder oxygen levels have a considerable influence on the mechanical properties of pure Nb. In addition, sieving Nb mid-range resulted in a finer microstructure, with higher oxygen levels which consequently increases the tensile strength, while retaining good ductility levels. This suggests the possibility of tailoring the as-HIPed mechanical properties by altering the initial powder characteristics.

V. FUTURE PLAN/DIRECTION

Despite the excellent mechanical properties exhibited by as-HIPed Nb, high temperature tensile and creep tests are required to assess the high-temperature properties and understand the role of oxygen solid solution in hindering the high-temperature grain boundary sliding.

VI. ACKNOWLEDGEMENTS

The authors acknowledge the financial support provided by Centre of Doctoral Training in Innovative Metal Processing (IMPaCT) funded by the Engineering and Physical Sciences Research Council (EPSRC). The authors warmly acknowledge ESA for funding this work in the frame of the General Studies Technology Programme (ESA GSTP ITT 8899) under contract 4000122901/18/NL/BJ. The work was enabled through the National Structural Integrity Research Centre (NSIRC).

Mohammad AlGhfeli

Graduated with a BEng in Chemical and Process Engineering from Arizona State University (ASU), USA in 2018. He later pursued an MSc in Chemical Engineering at ASU with a research focused on the gas separation analysis of thermoplastics using He, CO2 and N2 and graduated with distinction. He then went for a 3-month internship at Abu Dhabi National Oil Company (ADNOC) in the research & development department and focused on repellent polymer coatings and the ongoing industrial problem of pipeline corrosion. The primary objective of his PhD project is to establish the feasibility of building on the know-how on surface modification within TWI with the analytical expertise of Cambridge University in developing new surface functionalized nanostructured fillers into HDPE.

An Approach to Enhanced HDPE Nanocomposites

Dr. Alan Taylor, Dr. Mick Mantle
TWI - NIC, Univeristy of Cambridge
2nd Year of PhD

Key Words: compatibility, interfacial chemistry

I. INTRODUCTION

Pipeline corrosion is an industrial problem that leads to high maintenance costs. Around 2% of the oil & gas revenue is spent on pipeline corrosion [1]. There are a number of approaches to mitigate corrosion in production to reduce maintenance and replacement costs and lengthen operational lifetimes. Such approaches include the use of polymer liners. Augmentation of the properties of polymers by the addition of additives and fillers has long been carried out [2]. Such additives/fillers fundamentally change the composition of the polymer and can have both impacts on structure at the molecular and microscale. Structural changes can be hierarchical and introduce additional regions of anisotropy.

Thermoplastic polymers that are widely accepted for use as liners include high-density polyethylene (HDPE) and polyamide [3]. Compositional, microstructural and chemical differences in these polymers dictate their inherent properties, processing characteristics and ultimately their functional performance in operational environments. There is considerable interest in the use of fillers to enhance the properties of HDPE [4]. The importance of the interface between organic polymers and inorganic fillers has long been recognised in fibre-reinforced composites. However, in the field of particulate enhancement of thermopolymers it is only recently that this topic has received attention. The emerging consensus is that increasing the compatibility between the filler and the matrix leads to improved and enhanced material properties. However, there is a notable absence of detailed and specific data regarding the key factors that dictate such compatibility, how they are identified and measured.

This PhD studentship will therefore focus on developing a deeper understanding of the importance of the interfacial chemistry between inorganic (specifically silica) fillers and HDPE. Silane functionalisation agents will form the basis of the surface modification. Reactive and non-reactive silanes will be examined to allow the influence of chemical bonding to be determined. The primary output of the programme will be the establishment of design rules and guidelines enabling optimisation of the interfacial chemistry. A secondary output will be provisional data relating to the mechanical, thermal and chemical properties of selected candidate HDPE-silica nanocomposites.

II. DESIGN/METHODOLOGY/APPROACH

The technical approach for the development of the HDPE nanocomposite will follow the following methodology which is broadly the first part of a technology readiness level (TRL) scale. Commercially available silica of different sizes will be surface functionalized using different silanes with a main focus on hexamethyldisilazane (HMDZ) at different reaction conditions & ratios to facilitate the functionalization process (TRL 1). The silica filler will undergo several characterization techniques such as thermogravimetric analysis (TGA), Scanning Electron Microscopy (SEM), Fourier Transform Infrared and (FTIR) spectroscopy. In addition, solid-state ^{1}H, ^{29}Si and ^{13}C nuclear magnetic resonance (NMR) techniques will be used to determine the structure of the functionalized silica particles and to quantify the extent of functionalization/TMS coverage. To indicate the most effective functionalized silica fillers there will be an iterative loop between the different functionalisation and the characterisation process. Once the optimal functionalised fillers are chosen, there will be a laboratory scale synthesis of the fillers (TRL 2). The prepared fillers will be incorporated into HDPE using solvent based methodologies, then the silica-HDPE compatibility will be assessed (TRL 3). Subsequently, the nanocomposite samples with the most compatible functional fillers will be prepared by melt processing methods followed by a material characterisation process (TRL 4). The final stage will be the assessment of manufacturability.

III. DISCUSSION

The key challenge to the material property enhancement is the improved chemical compatibility between the inorganic filler and the polymer matrix to allow higher filler loading [5] and thus improved properties such as barrier properties [6], mechanical properties, thermomechanical, chemical and rheological properties [7]. But there is still a gap in the specific data needed to achieve such improved compatibility. Selection of a functionalized filler that most effectively provides commonality with the polymer will minimize incompatibilities and so reduces the drive and mechanism for aggregation, thus allowing higher filler loadings before viscosity increases are seen [8]. Figure 1 demonstrates the viscosity increases based on the filler loading volumes of hydrophilic and hydrophobic fillers in xylene (analog to HDPE).

Figure 1 Thickeing effect of hydrophilic & hydrophobic pyrogenic silicon dioxide in xylene [8]

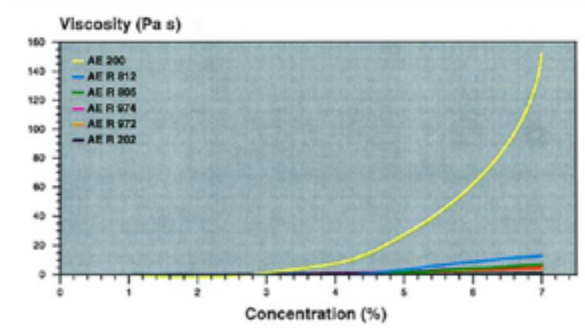

Untreated inorganic nanoparticles such as silica are hydrophilic due to the presence of hydroxyls that dominate their surfaces [8]. Incorporation of these particles into polymer materials often leads to phase segregation, agglomeration of the inorganics ultimately giving inhomogeneous dispersions. The chemistry of silica is studied through history using TGA & ^{1}H and ^{29}Si NMR methods. The different species found on the surface of silica are demonstrated in Figure 2. These species can be determined by the TGA analysis & certain chemical shifts on the NMR spectrum.

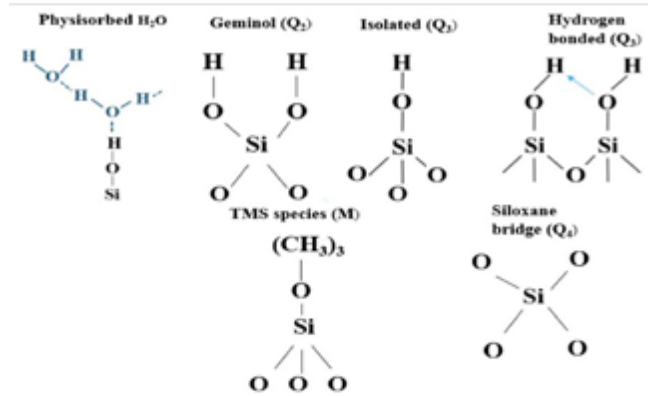

Figure 2 The different types of species present on the silica surface

IV. FUTURE DIRECTION

The commercially available silica will be functionalised using different reactive and non-reactive silanes to allow the influence of chemical bonding to be determined followed by a characterisation process. The designed fillers will be compared and evaluated and the most promising candidates will be chosen and incorporated in HDPE. The fillers will be mixed with HDPE using melt processing techniques at different loading weights. The mechanical, thermomechanical, rheological and chemical properties of the prepared HDPE-silica nanocomposites will be characterized at a laboratory scale. Finally, the HDPE-silica nanocomposites will be assessed for manufacturability.

REFERENCES

[1] A. Al-Khowaiter, Sep. (2019). "Future of Plastic and Composite Pipeline Technologies", NIC, TWI UK.
[2] Harito C, Bavykin D V, Yuliarto B. Dipojono H K and Walsh F C, 2019: 'Polymernanocomposites having a high filler content: synthesis, structures, properties and applications.' Nanoscale, 11 4653.
[3] Non-metallic Innovation Centre (NIC), 2019. 'Foresight Review: Application of Non-metallics in the Oil and Gas industry.
[4] Savino V, Fallatah G M and Medhi M S, 2009: 'Applications of nanocomposite materials in the oil and gas industry'. Advanced Materials Research.' Vol 83-86, 771-776, doi:10.4028/www.scientific.net/AMR.83-86.771
[5] Šupová, M.; Martynková, G. S.; Barabaszová, K. Effect of Nanofillers Dispersion in Polymer Matrices: A Review. *Science of Advanced Materials* 2011, *3* (1), 1–25.
[6] Alexandre M, Dubois P. Polymer-layered silicate nanocomposites: preparation, properties and uses of a new class of materials: *Materials Science and Engineering 28 (2000) 1-63.*
[7] Adewole et al. Bulk and Surface Mechanical Properties of Clay Modified HDPE used in Liner Applications. *Canadian Journal of Chemical Engineering, 2012, 90(4), pp 1066-1078*
[8] Ettlinger, M.; Ladwig, T.; Weise, A. Surface Modified Fumed Silicas for Modern Coatings. *Progress in Organic Coatings* 2000, *40* (1-4), 31–34.

Helen Elkington

I am a third year PhD student based at TWI Yorkshire and Sheffield Hallam University where I originally came to to study a Masters in Mechanical Engineering.

Laser Beam Direct Energy Deposition – Effect of Process Parameters on Material Properties of Inconel 718

Dr. Carl Hauser[1], Dr. Stephen Magowan[2], Dr. Quanshun Luo[2]
[1]TWI, [2]Sheffield Hallam University
3rd Year of PhD

Keywords: Laser Beam Direct Energy Deposition, microstructure, Inconel 718

I. INTRODUCTION

Laser Beam Direct Energy Deposition (DED-LB) is an Additive Manufacturing (AM) process that utilises a laser to create a molten pool in a metallic substrate. An inert gas is used to blow metal powder into the melt pool via a nozzle [1]. Upon interaction with the molten pool, the powder melts and binds to the substrate or previously deposited material. As the laser continues to move along its projected toolpath the deposited material cools and solidifies. Figure 1 shows a schematic of the DED-LB process.

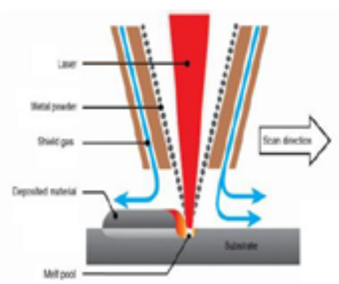

Figure 1 Schematic of the DED-LB process.

Process parameters are variables which can be changed, altering the process. In DED-LB these include those related to the laser such as power, scan speed and laser profile, and others such as powder feed rate and gas flow rate. Due to the relationships between DED-LB process parameters and the properties of the deposited material, small variations to parameters can cause large changes to the microstructure and material properties [2].

Three key process parameters have been identified to be key due to their significant effect on the heat input – a factor which is crucial to microstructure formation and thus final mechanical properties. These are laser power (LP), scan speed (SS) and powder feed rate (PFR).

II. DESIGN/METHODOLOGY/APPROACH

A Trumpf DMD 505 system with a 1.8kW CO2 laser was used to manufacture samples using Inconel 718 powder. Process parameters from previous work on this system were used to determine process parameter values, and the range examined for LP, SS and PFR.

A Taguchi Design of Experiments (DOE) using 3 levels of the 3 process parameters (LP, SS, PFR) was utilised.

This generated 9 combinations of the process parameters. The highest level of each process parameter was also used for a 10th combination. These were used to manufacture sample blocks of two sizes (large - 140mm x 65mm x 25mm and small - 50mm x 20mm x 15mm). Samples were analysed in their as-deposited state, using Optical Light Microscopy (OLM), Scanning Electron Microscopy (SEM), Vickers hardness, and tensile testing (larger block only).

III. FINDINGS/RESULTS

Of the 9 Taguchi DOE generated process parameter combinations only 3 could be completed. Other combinations produced insufficiently wide and/or high tracks, did not fuse to the substrate, or failed during building the blocks. Thus, despite choosing a range of process parameter values that have been used successfully previously, building all Taguchi DOE combinations was not feasible in practice. Therefore, the inputs are not appropriate for this Taguchi DOE approach. This suggests that this DOE approach may not be entirely suitable for the DED-LB process unless very narrow ranges of process parameter values are being investigated.

OLM found samples to be metallurgically similar. Regions which had undergone re-melting as subsequent tracks and layers were deposited were clearly distinct. Heat-affected regions containing refined phases were noted. SEM observed 4 phases present. This included a white globular phase, identified as Laves phase (Figure 2). This phase was greater in volume within large blocks.

Other phases included the γ-matrix, Al-oxides and an unknown phase (pending further investigation) surrounding Laves phase.

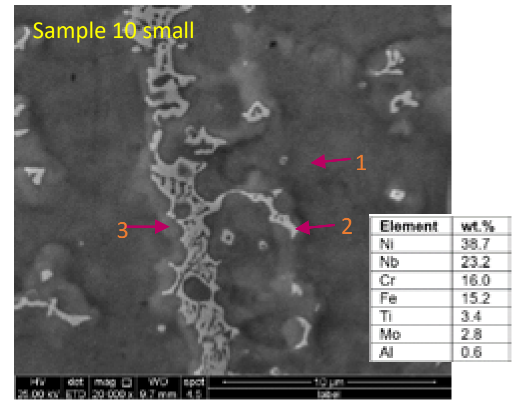

Element	wt.%
Ni	38.7
Nb	23.2
Cr	16.0
Fe	15.2
Ti	3.4
Mo	2.8
Al	0.6

Figure 2 SEM image showing γ-matrix (1), Laves (2) and unknown phase (3).

Tensile specimens were taken in two orientations from the large blocks (horizontal and vertical). Tensile values differed significantly (Figure 3). This occured due to grain orientation with regards to the tensile specimens – grains lie perpendicular to horizontal tensile specimens and parallel to vertical. No significant difference was observed between process parameter combinations.

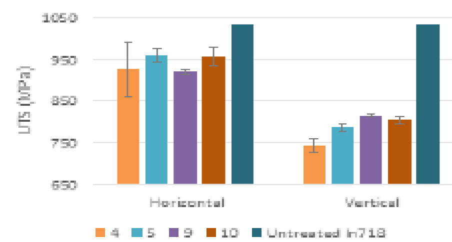

Figure 3 UTS values for tensile specimens machined from 4 large blocks in two orientations. UTS untreated Inconel 718 is shown [3].

Macrohardness did not vary significantly between the sets of small blocks, or between the sets of large blocks. Variation between small block microhardness was observed. No significant difference was present between large block microhardness. Macro/microhardness was greater in small blocks when compared to large blocks, except for one set of process parameters (no. 5) whose small block value was akin to microhardness of large blocks (Figure 4).

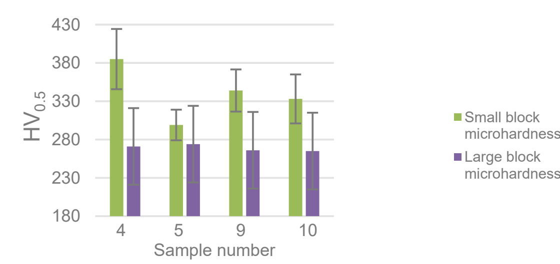

Figure 4 Microhardness values for small and large blocks. Standard deviation error bars are shown.

The decreased volume of the white globular phase seen in small samples may be linked to their greater microhardness. Surrounding this phase is another unknown phase, this may also link to the greater microhardness observed. These phases are distributed heterogeneously throughout samples, caused by the variation in thermal cycling during the build. This heterogenous distribution may cause the difference between micro and macrohardness as the area tested in macrohardness is greater in size, hence the Inconel 718 matrix surrounding the white and unknown phase plays a greater role in affecting macro measurements.

These results show that the different combinations of process parameters result in property variation at a micro-scale in the small blocks. However, when looking at larger areas of a deposited part the significance of the differences decrease, and in the large blocks, variation is negligible. This indicates that the lower heat build-up during building the larger blocks may prevent greater hardness properties initially being reached. Alternatively the increased time that the larger blocks are at higher temperatures may deteriorate properties, causing them to decline until reaching a certain range of values (in this case for microhardness between 257 HV0.5 to 287 HV0.5).

IV. DISCUSSION/CONCLUSIONS

Differences between process parameter combinations were noted at a micro-scale in small blocks. No significant difference could be seen at a macro scale, or in large blocks. The interactions between LP, SS and PFR should be considered when determining what values to use for process parameters. Identical process parameters for different geometries can result in significantly different properties, meaning process parameters are not interchangeable between geometries.

V. FUTURE PLAN/DIRECTION

Future work should include linking LP, SS, and PFR mathmatically. Building different sized blocks in increments to determine when, and why, properties change and investigation into heat-treatments.

REFERENCES

[1] Gu, D. (2015). Laser additive manufacturing of high-performance materials. Springer.
[2] Segerstark, A., Andersson, J., & Svensson, L. (2014). Review of laser deposited superalloys using powder as an additive. 8th International symposium on superalloy 718 and derivatives, 393-408.
SAE International. (2016). Nickel Alloy, Corrosion and Heat Resistant, Sheet, Strip, and Plate, 52.5Ni - 19Cr - 3.0Mo - 5.1Cb (Nb) - 0.90Ti - 0.50Al - 18Fe, Consumable Electrode or Vacuum Induction Melted, 1950 °F (1066 °C) Solution Heat Treated AMS5597. Aerospace Material Specification.

Sameera Weeratunga
Sameera Weeratunga graduated from Sri Jayewardenepura University, Sri Lanka with a Bachelor's Degree, and a Master's in Advance Engineering Materials from University of Manchester, UK where he achieved distinction and course prize. He started his career working at Sheffield Hallam University as a KTP associate, primarily focusing on developing process capabilities of a Sheffield based company. Soon after, he return to Sri Lanka where he worked as a process development engineer, lead process engineer and finally as the head of process for a multinational yacht component manufacturer. Sameera is pursuing a PhD with Coventry University on the topic of Mechanistic Basis for defect acceptance criteria in additively manufactured Inconel 718 sponsored by Lloyd's Register foundation and he is currently in his 3rd year of studies.

Local Microstructure Features Influence on Crack Initiation in Additively Manufactured Inconel-718

Yanhui Zhang[1], David Parfitt [2]
[1]TWI Ltd, Cambridge, UK , [2]Coventry University, Coventry, UK
3rd Year of PhD

Keywords: Additive manufacturing, defect influence on HCF, Microstructure influence on HCF, Crystal plasticity modelling,

I. INTRODUCTION

The industrial application of Additive Manufacturing (AM) is severely hampered by the inconsistent mechanical properties exhibit due to the existence of defects in the structure. These defects are produced due to the processing condition variations, scanning strategy variations, and quality of the materials. In addition to this inherent nature of the AM process induced directional cooling leads to forms highly textured materials and secondary particles that further complicate the consistency of the mechanical properties.

The objective of this project is to establish the influence of defects and texture of the material on high-cycle fatigue. This is by initially identifying the critical defect characteristics and microstructure features that influence the fatigue properties by conducting endurance fatigue tests and later simulating these conditions using crystal plasticity modelling to establish the level of influence from each of these critical characteristics. Hence, increasing the predictability of fatigue performance in additively manufactured Inconel-718 materials, and establishing defect acceptance criteria for industry use.

II. METHODOLOGY

Initially, the defects were identified and characterized by optical microscopy (OM), Scanning electron microscopy (SEM), and X-ray computer tomography imaging techniques. As shown in Figure 1, the type of defects, their size, and distribution were closely analysed to later use to determine the criticality of these features on fatigue performance.

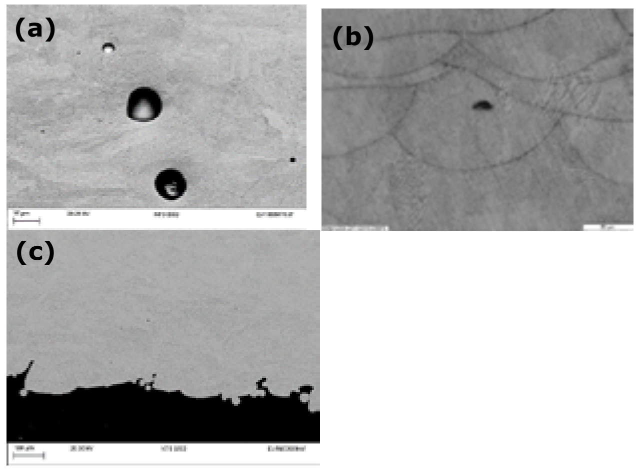

Figure 1: type of defects found in additively manufactured Inconel-718, (a) gas porosity; (b) Lack of fusion porosity; (c) rough surface

Fatigue tests were carried out on two separate sets of samples produced with variable-level recycled powder. Further, the samples were produced in line with the fatigue loading direction and 900 to the loading direction to assess the influence of the process-oriented defects on the fatigue properties. As the samples were received in as-built condition, they were heat-treated prior to fatigue testing. The fatigue tests were carried out in a force-controlled manner with a constant stress amplitude of 630MPa initially and in a sinusoidal waveform with an R ratio of 0.1 at room temperature. Later, the stress amplitude was increased to 720MPa with the same R ratio to eliminate any runouts.

Crystal Plasticity modelling was done based on the work carried out by Pritivirajan [1]. A randomly textured microstructure was generated where the properties of Inconel-718 were assigned from the published literature. Open source software Damask[2] was used for crystal plasticity simulation and the simulated test results were compared with the published data for confirmation.

III. RESULTS AND DISCUSSION

Presented in Figure 2 are the fatigue test results comparing with the published data in the literature [3].

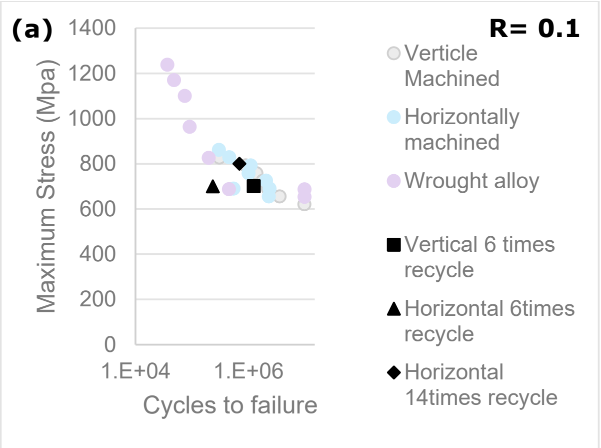

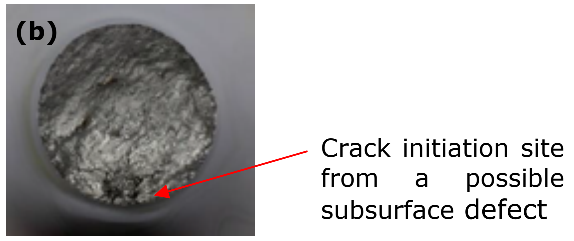

Figure 2: (a) Endurance high cycle fatigue test results compared with the published literature [3]; (b) fracture surface of a failed sample – Horizontal 14 times recycle

Additively manufactured, recycled powder samples behave similarly to the virgin material samples from an overall perspective as illustrated in Figure 2. However the scatter and unpredictability of fatigue performance in recycling material samples seems to exceed and this has been evident from the sample –"horizontal 6 times recycled" which prematurely failed after 240k cycles.

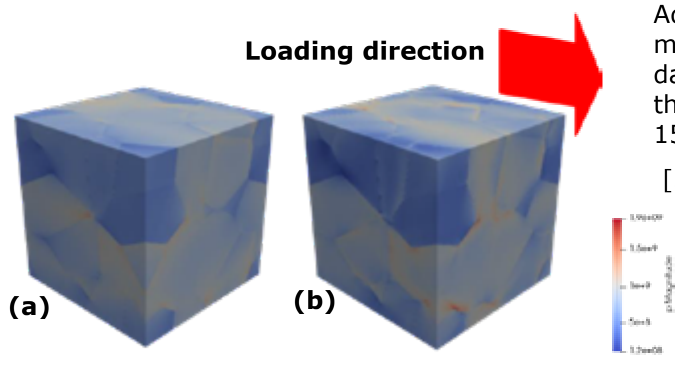

Figure 3: stress distribution of crystal plasticity modelled microstructure; continuous displace and retraction is given in the indicated direction (a) after 1st cycle; (b) after 10th cycle

Crystal plasticity simulation results agree with the literature, wherefrom the simulation it was evident that certain grain orientations and textures lead to stress concentration as illustrated in Figure 3. Further simulating this texture effect with combining the stress concentration from defect can lead to a better predictable model of fatigue performance.

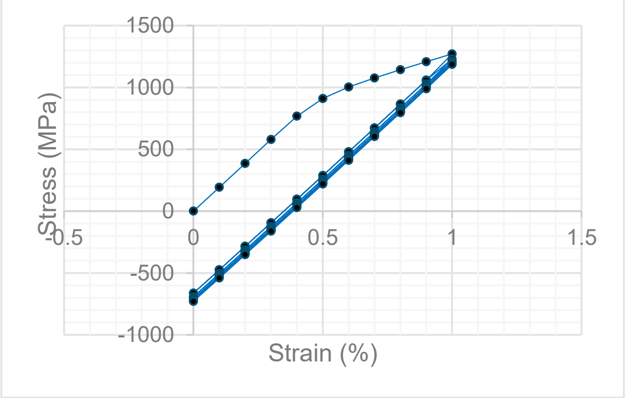

Figure 4: Comparison of CP model data of stress-strain behaviour until 10th cycle.

IV. FUTURE PLAN/DIRECTION

Further work will be comprised of carrying out fatigue tests on samples produce with virgin powder to establish the effect on fatigue from the degradation of material by comparing the results with early experiments.

Crystal plasticity modelling work will primarily focus on using EBSD mapping coordination from microstructures to incorporate the additive manufacture texture and defects to the simulations to fully understand the effect of microstructure features on fatigue performance.

REFERENCES

[1] V. Prithivirajan and M. D. Sangid, "The role of defects and critical pore size analysis in the fatigue response of additively manufactured IN718 via crystal plasticity," Mater. Des. , vol. 150, pp. 139–153, 2018.

[2] F. Roters et al., "DAMASK – The Düsseldorf Advanced Material Simulation Kit for modeling multi-physics crystal plasticity, thermal, and damage phenomena from the single crystal up to the component scale," Comput. Mater. Sci., vol. 158, no. December 2018, pp. 420–478, 2019.

[3] D. B. Witkin, D. Patel, T. V Albright, and G. E. Bean, "Influence of Surface Conditions and Specimen Orientation on High Cycle Fatigue Properties of Inconel 718 Prepared by Laser Powder Bed Fusion," Int. J. Fatigue, vol. 132, no. November 2019, p. 105392, 2019.

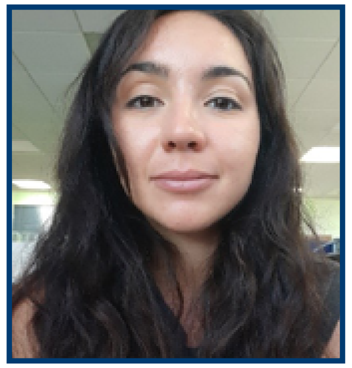

Marie-Salomé Duval-Chanéac

Marie-Salomé is an NSIRC PhD student of Southampton University, partially based in TWI, and sponsored by Lloyd's Register Foundation. She graduated from l'Ecole National d'Ingenieur de Saint-Etienne (ENISE) in France with a Degree in Mechanical Engineering in 2017, with a speciality in Industrial Production. Her education lead her to undertaking various internships related to additive manufacturing processes, working on DMD (Direct Metal deposition) process of Nickel alloy with the CETIM research center (France), and EBM (Electron Beam Melting) of Titanium alloy with the MIRDC research center (Taiwan). She is now working on improving the structural intergity of multi-material structure fabricated by Laser powder bed fusion (L-PBF), including Nickel based alloy and Stainless steel.

Effect of Heat Treatment on Fatigue Crack Growth in Multiple-Material Fabricated by Laser Powder Bed Fusion

Dr Raja Khan[1], Dr Nong Gao[2] , Prof Phillippa Reed[2]
[1]TWI, [2]Southampton University
4th Year of PhD

Keywords: Multi-materials, additive manufacturing (AM), Interface, Heat treatment, Crack growth rate

I. INTRODUCTION

Multiple Material Additive Manufacturing (MMAM) technique allows the production of a new generation of components and the reduction of production cost, lead time, inventory and assembly [1,2]. Inconel 718 (IN718) and 316L stainless steel alloys produced by single-material AM have been extensively investigated due to their specific properties that can be used in systems under extreme conditions [3,4], such alloy combination has been used in pressure tubes for nuclear fission reactor [5,6]. Multi-material specimens have been produced in layered architectures by laser powder bed fusion (L-PBF) process, combining 316L to IN718 in a single operation. Specimen were then heat treated to achieve the better mechanical performance especially for IN718 via precipitation strengthening. A specific heat treatment has been tailored for the combination of 316L and IN718 multi-layered specimen and has been investigated regarding its effect on the mechanisms of fatigue crack propagation. This work aims to control the near tip crack driving force by the combined effect of microstructure strengthening and the shielding effect multiple-layer architecture to mitigate crack propagation.

Objectives of this work:.

- Understanding the effect of heat treatment on the microstructure of L-PBF 316L/IN718 multiple-materials
- Measuring the effect of heat treated layered architecture on fatigue crack propagation

II. DESIGN/METHODOLOGY/APPROACH

Bend bar specimens for fatigue testing were manufactured with dimensions of 10x10x60 mm (see Fig.1). Tensile rods of Ø10x60 mm dimensions were manufactured respectively for IN718 and 316L to test the tensile properties of each alloy separately (see Fig.2). The energy density ratio employed for both materials was $E_{dv} = 140\ \mathrm{J/mm^3}$, and produced using the following set of parameters: P=300W, v=900mm/s, t=0.03mm, h=0.08mm, Rotation between layers = 90°.

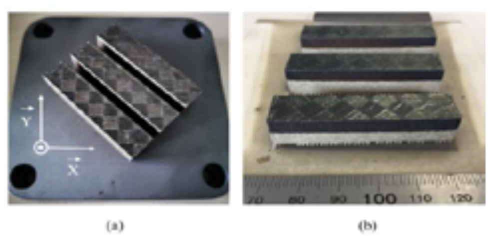

Figure 1. Bi-layer bending specimen a) on building plate after heat treatment, b) cut off building plate

Tensile tests were carried out at room temperature in accordance with the ASTM E8 standard. Long crack tests were performed under three-point bending, on an Instron 8502 servohydraulic machine, with sinusoidal loading at R = 0.1, and frequency f=10Hz. The bend bars were notched in the centre. Subsequent crack growth tests were conducted following the BS EN ISO 12108:2012 standard under constant load, increasing ΔK-conditions. Crack length was monitored by a direct current potential drop (DCPD) method.

The following heat treatment was performed on bilayer specimen: solution annealing at 1050°C/45min, followed by argon gas quench, then ageing at 620°C/8h followed by air cooling.

Heat treatment was performed in a vacuum furnace with argon gas quenching facility.

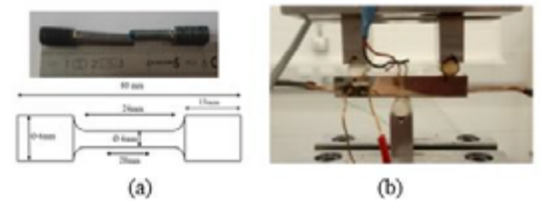

Figure 2. a) Tensile specimen rods, b) bending specimen set up for long crack growth recording by Direct Current Potential Drop (DCPD)

III. FINDINGS/RESULTS

The microstructural study reveals that the heat treatment has suported the diffusion of Iron at the interface over ~140μm depth. Fig.3 shows BSE imaging where a large number of secondary phases in the interface region, expected to be Laves phases, in finer precipitates within the sub-cellular grains structure and in coarser form at grain boundaries and around the ductility dip cracking (DDC) sites.

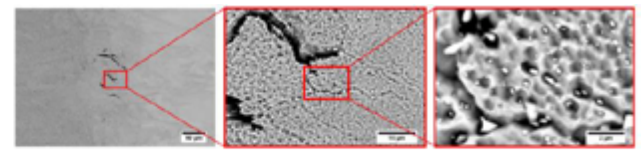

Figure 3. Electron Backscatter magnified image of the heatreted specimen, at the interface within the interdiffusion zone

Heat treatment showed a positive effect on IN718 mechanical response, an increase of 11% in 0.2% yield strength (YS) from its as build (AB) condition, a noticeable 22% increase in UTS and 50% increase in Elongation (El%). However the results for the 316L have demonstrated a loss in YS of about 31% from its AB state, also a decrease in UTS of 5.2%, and a slight increase of 5.8% Elongation (see Fig.4).

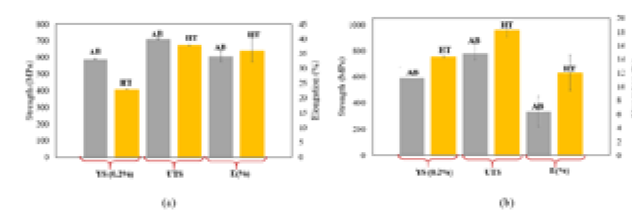

Figure 4. Tensile test results comparing a) 316L properties b) IN718 properties from as-built (AB) to heat treated (HTed)

Fig. 5 shows the crack growth rate versus stress intensity factor, specimen N°1 showing the propagation from IN718 top layer to 316L bottom layer (anti-shielding transition), and specimen N°2 showing the crack propagation from 316L to IN718 (shielding transition). The effect shielding and anti-shielding during the interface transition were limited, because the interface was located at the mid-section of the specimen where the stress intensity factor had already reached a critical level, hence its effect has shown to be less significant than the intrinsic mechanical strength within each alloys.

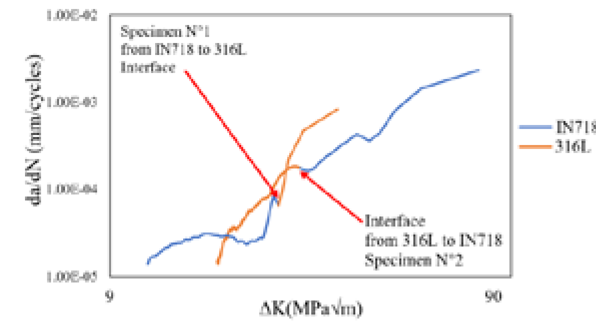

Figure 5. Long-crack propagation test in bi-layer specimen HTed condition

Additionally the final fracture surface exposed in Fig.6 shows the diffrence in the microstructural roughness between each layer. While IN718 shows a flat surface with transgranular cleavage, 316L displays a rough ductile fracture surface with a mix transgranular and intergranular crack propagation, and secondary cracks around the interface in specimen N°2 (due to the shielding effect).

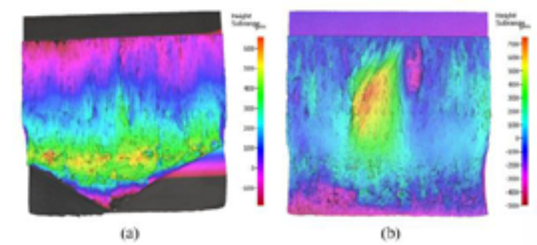

Figure 6. Alicona roughness map of final fracture surface, a) specimen N°1 , b) specimen N°2

IV. DISCUSSION/CONCLUSIONS

The tailoring of the heat treatment was design to support precipitation strengthening within the IN718, while limiting the negative impact on 316L microstructure. However, the mechanical response of each alloy plays a key role on the overall ability of the layered structure to sustain crack propagation. The shielding and anti-shielding mechanisms effect on crack propagation at the dissimilar materials interface, were effective but to a lesser extent.

V. FUTURE PLAN/DIRECTION

The modeling of a geometrical approach can be investigated in order to place a ductile interlayer at a strategic depth in regards to the loading direction and supposed crack initiation location to effectively mitigate crack propagation in MMAM design.

REFERENCES

[1] Busachi A. CIRP J Manuf Sci Technol 2017;
[2] Vaezi M Virtual Phys Prototyp 2013;
[3] Mohd Yusuf S J Alloys Compd 2018;
[4] Trosch T, Mater Lett 2016;
[5] Chlebus E, Materials Science & Engineering A 2015;
[6] Tolosa I, Int J Adv Manuf Technol 2010;

Saad Syed Iqbal Ahmed

Saad graduated with a first class BEng (Hons) in Mechanical Engineering from Heriot-Watt University in 2017. He later pursued an MSc in Advanced Materials Engineering from The University of Manchester where his research focused on developing a comparative study of different data analysis methods to study the residual stresses profiles of aero-engine components by X-ray diffraction. In July 2019, Saad started an Lloyds Register Foundation sponsored PhD with The University of Manchester and TWI Ltd. His work focuses on developing appropriate procedures towards standardizing fatigue design guidance for Selective Laser Melted (SLM) components. This work would try to correlate defects to fatigue performance in SLMed Al-Si10-Mg alloys using X-ray Computed Tomography and microstructure characterisation techniques.

Correlating Defects to Fatigue Performance in Selective Laser Melted Al-Si10-Mg Alloys

Dr. Yanhui Zhang[1], Professor Philip Withers[2], Dr. Matthew Roy[2]
[1]TWI, [2]University of Manchester
2nd Year of PhD

Keywords: Additive Manufacturing, Selective Laser Melting, Fatigue Performance, AlSi10Mg Alloys,

I. INTRODUCTION

Selective Laser Melting (SLM) is a revolutionary technology pertinent to many high-value applications in the biomedical, automotive, and aerospace industries. It has the potential to produce topographically optimized parts comprising of complex geometries previously not possible by traditional subtractive manufacturing methods [1]. SLM technologies have majorly appealed to low volume production of custom parts for specialist applications like medical implants and fine meshed internal structures. It has also enabled on-demand remote manufacturing and repair of functionally-graded parts like turbine blades [2].

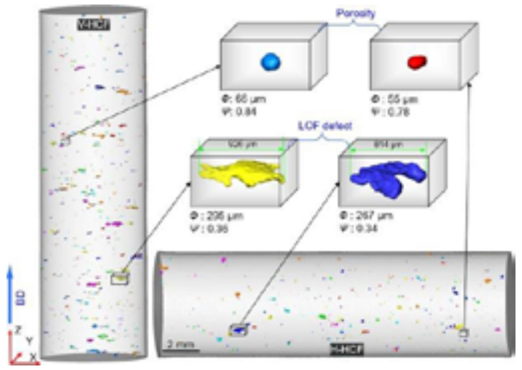

Figure 1 Defect distribution in horizontally and vertically oriented AlSi10Mg alloy samples using X-Ray Computed Tomography (CT) [6]

SLM alloys also have potentially extensive application in mechanical structures [3]. This is a result of SLM components experiencing unique thermal histories specific to their build, significantly affecting the resulting microstructure and the associated mechanical properties [4], resulting in demonstrable tensile behaviour compared to wrought materials. However their implementation is still restricted to non-critical applications due to lower fatigue strength and a larger scatter in fatigue life. To enable their implementation in safety critical applications, it is critical to develop an adept understanding of their fatigue behaviour [5].

To date, defects have been an unavoidable part of the manufacturing process of SLM components. This is due to the lack of fusion (LOF) and gas porosity defects that originate during fabrication of these components. These defects act as crack initiation sites and have largely been associated with short crack initiation and propagation [6]. Certain thermo-mechanical treatments like HIPing and T6 Heat Treatment are known to improve ductility and reduce porosity within these components but have led to an overall reduction in the fatigue strength of the material [3]. These treatments provide a potential solution to obtaining consistent fatigue properties with less scatter in the data. However, even in components that have undergone a post-processing treatment like HIPing, these pores have not been completely eliminated. Thus, it is essential to develop an understanding of the process-microstructure-fatigue relationship of this technique [1].

II. METHODOLOGY

Defects such as gas pores or lack of fusion pores as shown in Fig 1 are formed between two continuous layers and are aligned parallel to them, reducing the effective load-bearing area. When these defects exceed a certain size threshold, they detrimentally impact fatigue properties [2]. These defects also create a large scatter in fatigue lifetimes due to their randomness. This is more critical for situations where there is a higher probability of encountering large irregular pores closer to the surface as this can have more detrimental impact on the fatigue life [5]. Evidence has pointed out that failure cracks usually tend to originate at highly irregular imperfections especially when they are located at the surface or sub-surface developing a local plastic deformation zone around them [1].

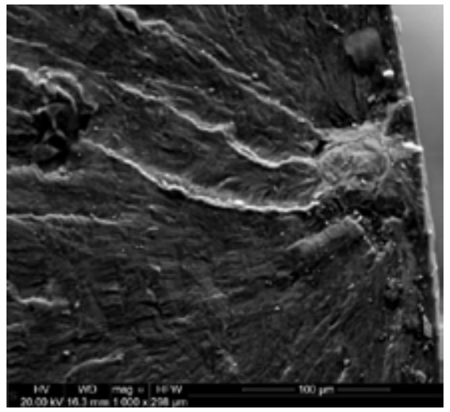

Figure 2 Fatigue Crack Initiation Defect

Thus, the aim of this project is to develop a quantitate method to confidently predict the fatigue life of SLM AlSi10Mg alloys by correlating a critical defect from the fracture surface that has caused fatigue crack initiation, to its pre fatigue examined state. Additionally, it is also needed to correlate the fatigue crack initiation site post-failure to the pre-testing porosity distribution in the high cycle fatigue (HCF) regime of Al-Si10-Mg alloys in order to develop a predictive model for crack initiation. Finally, to predict a probabilistic distribution of pores from a set of distributions available for both horizontally and vertically oriented samples, extending it to predict the fatigue life, this enables us to quantify the fatigue performance of SLM AlSi10Mg alloys in multiple orientations. This can also be used to develop a model to predict the fatigue crack initiation site within AlSi10Mg alloys based on a certain porosity distribution using existing fatigue crack initiation and fatigue crack growth models.

III. RESULTS & DISCUSSION

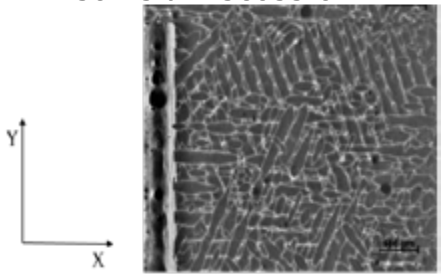

Figure 3 Cross-section view of the Melt pool using Optical Microscopy

Initial results indicate that the most detrimental pores lie on the surface or sub-surface as indicated in Fig 2. The fatigue lives of samples in both orientations is fairly consistent with previous studies. EBSD mapping as shown in Fig 4, of the microstructure was carried out to identify any texture within the material as well as to eliminate the role of microstructure in the fatigue crack initiation within the material. The melt pool cross-section microstructure of the material shown in Fig 3 depicts the laser scan tracks over multiple layers of deposition. The dark phase represents Aluminium while the bright phase represents silicon particles which are scattered indifferently across the surface. The melt pool grain structure can also be identified from the EBSD map wherein there are longitudinal grains across the centre of the melt-pool and small equiaxed grains towards the edges.

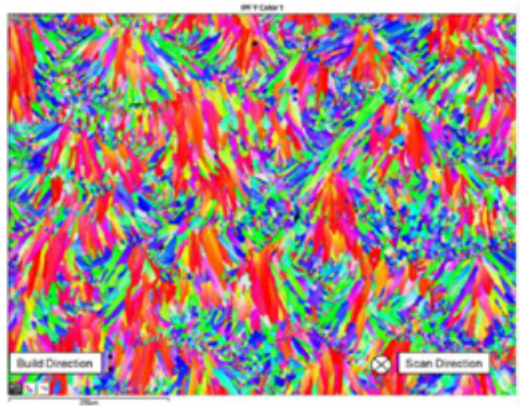

Figure 4 EBSD Map along the Build Direction

IV. FUTURE PLAN

The future plan has been shown in Fig. 5 below.

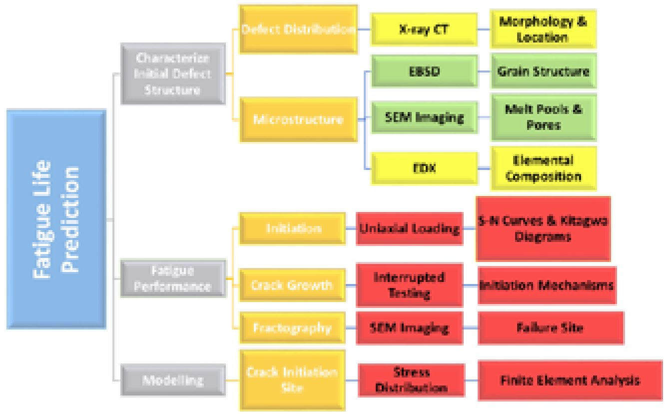

Figure 5 Colour coded Future Testing Plan

REFERENCES

[1] B. Maschinen, A. Investition, G. Beschaffungen, B. Ersatzbeschaffungen, and S. Mittelherkunft.
[2] A. Yadollahi and N. Shamsaei, Int. J. Fatigue, 2017, doi: 10.1016/j.ijfatigue.2017.01.001.
[3] A. Jaafar, A. Rahmat, I. Zainol, and Z. Hussain, J. Appl. Sci., vol. 12, no. 8, pp. 775–780, Aug. 2012, doi: 10.3923/jas.2012.775.780
[4] D. L. McDowell, S. Yip, Ed. Dordrecht: Springer Netherlands, 2005, pp. 1193–1214
[5] Y. N. Hu et al., Int. J. Fatigue, vol. 136, p. 105584, Jul. 2020, doi: 10.1016/j.ijfatigue.2020.105584
[6] Y. N. Hu et al., Mater. Des., vol. 192, 2020, doi: 10.1016/j.matdes.2020.108708.

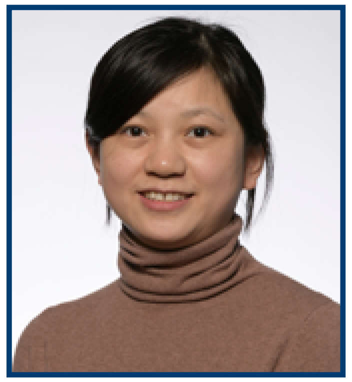

Minghui Wu
Minghui Wu is a third year PhD with the University of Surrey and is currently based in the Asset Integrity Management (AIM) section of TWI. She completed her MSc in the department of mathematics at Southwest Jiaotong University before starting at the National Stuctural Integrity Research Centre (NSIRC). Her research focuses on the development and application of economic and environmental models to assess the use of composites in aircraft structures.

Assessing Life Cycle Costs and Environmental Performance of Composite Material in Aircraft Application

Ujjwal Bharadwaj [1], Jhuma Sadhukhan [2] ,Rachard Murphy[2], Xiaofei Cui[1]
[1]TWI, [2]University of Surrey
3rd Year of PhD

Keywords: : life cycle costing; life cycle assessment; composite door; aluminium door

I. INTRODUCTION

Composite materials have been widely used in the aeronautical industry over the last decade due to their favourable combination of mechanical properties and low weight. There is increasing interest among manufacturers to replace conventional materials, such as aluminium, with composite materials[1]. Under the European Union's Horizon 2020 research, a project titled Thermoplastic on Door (TOD)[2] aims to manufacture a composite door to replace the conventional aluminium door for aircraft, using thermoplastics and thermosets. However, there is a significant gap in terms of assessing the environmental and economic impacts of using these materials for aircraft door. This research conducts life cycle costing (LCC) and life cycle assessment (LCA) of both the composite and aluminium door during the production stage. The research provides new databases and guidance for the manufacturers to choose a more sustainable material and manufacturing processes.

This study presents the LCC and LCA of the composite door in its production stage. A cost model was developed using a 'bottom-up' approach[3]. Key parameters that make the most contribution to the total cost were identified, and sensitivity analysis performed accordingly. Moreover, LCA was carried out to quantify impacts associated with all purchases (materials, energy, etc.), as well as treatment of corporate waste manufacturing process. The dominant parameter for environmental impact was identified. Finally, a comparison between composite doors and aluminium doors was also performed.

II. METHODOLOGY/APPROACH

Estimation of manufacturing costs for each process was carried out using the LCC method, which is based on the bottom-up technique. The overall cost estimating framework is as shown in Figure 1.

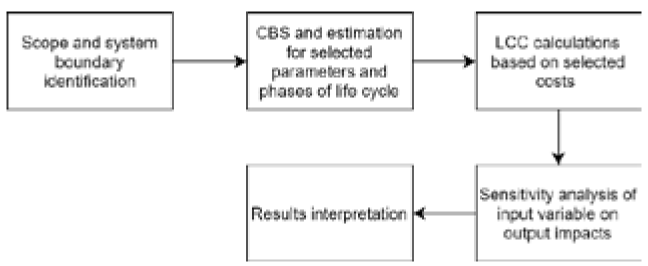

Figure 1. Life cycle costing estimating process

This method develops a cost breakdown structure (CBS) first. In order to estimate the cost breakdown structure, the cost elements associated with production of the aircraft door were identified. The identification process carried out complies with the mutually exclusive and collectively exhaustive (MECE) principle to ensure there is no overlap or gap among these identified elements. The cost elements considered in this study were material cost, labour cost, energy cost and consumable cost. The cost of each element was calculated and then summed up to produce the total product costs.

LCA is an internationally methodological framework used for estimating and assessing environmental impacts attributed to the life cycle of a product or service. The LCA model was developed in accordance with standards ISO 14040-14044 using the software package SimaPro 8.4. The life cycle impact assessment in this model was performed using Impact 2002+ methodology[4], which is widely used in European projects. It enables the impacts to be observed at the midpoint level with 14 impact categories, i.e. human toxicity, respiratory effects, ionizing radiation, ozone layer depletion, photochemical oxidation, aquatic ecotoxicity, terrestrial ecotoxicity, terrestrial acidification/nitrification, aquatic acidification, aquatic eutrophication, land occupation, global warming, non-renewable energy, mineral extraction, and also at endpoint level with four damage categories, i.e. climate change, human health, ecosystem quality and resources

III. FINDINGS/RESULTS

The results indicate that, firstly, for the composite door application, the most significant cost contribution was labour cost, accounting for 63.4% of the total cost. Secondly, energy consumption was the single largest hotspot according to the LCA study contributing to 60.3% changes in the environmental impacts. Thirdly, the composite door was found to be more costly than the counterpart aluminium door that was shown to give limited or negative environmental benefits according to the comparison assessment. The results are shown in Figure 2 and Figure 3.

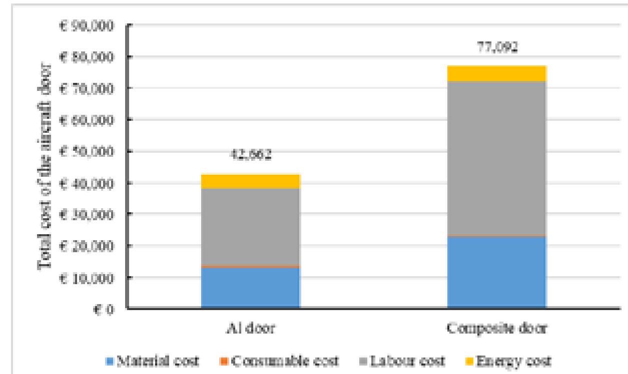

Figure 2. Comparative production cost for Al door vs. composite door

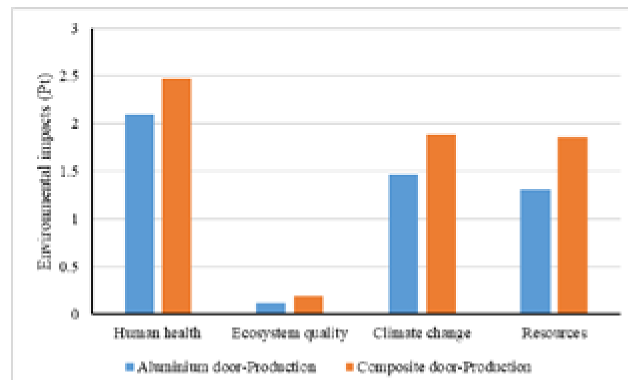

Figure 3. Comparative impact assessment for Al door vs. composite door

Further investigation was also performed on LCA of two doors with the same weight, is shown in Figure 4.

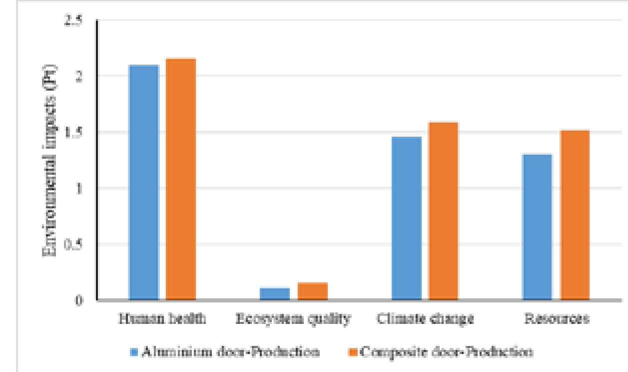

Figure 4. Comparative impact assessment for Al door vs. composite door with the same weight

The result shows that the composite door is not able to achieve the environmental performance of an aluminium door.

IV. DISCUSSION/CONCLUSION

The composite door was heavier than the counterpart aluminium door due to the design engineers adopting more conservative safety factors than those used for the metallic door. However, even if the weight of the novel door is reduced after optimising the structure to reach the same weight as the aluminium door, the composite door is not able to achieve the similar environmental performance as the aluminium door did. This is despite not covering end-of-life costs of the composite door and aluminium door within the remit of the study that is focused only on the manufacturing stage.

IV. FUTURE PLAN

Further research will focus on the operating & maintenance and end of life phase.The composite door is a development product and is not currently available in the market. Therefore, aspects such as maintenance and repair methods and the process used in other related sectors where such materials are in current use will be considered together with further literature review.Additionally, consultations will be carried out with composite experts to gain relevant information about the potential maintenance, repair and inspection methods for a composite door during the operational phase. The same approach will be applied to the end of life phase of the composite door.

REFERENCES

[1] M. Maria, "Advanced composite materials of the future in aerospace industry," Incas Bull., vol. 5, no. 3, pp. 139–150, 2013, doi: 10.13111/2066-8201.2013.5.3.14.
[2] "Thermoplastic on Doors," European Commission. https://trimis.ec.europa.eu/project/thermoplastic-doors.
[3] L. Zijp, "Development of a Life Cycle Cost Model for Conventional and Unconventional Aircraft," Delft University ofTechnology, 2014.
[4] J. Olivier, "IMPACT 2002+: A New Life Cycle Impact Assessment Methodology," Proc. United States Natl. Museum, vol. 32, no. 1531, pp. 411–424, 1907, doi: 10.5479/si.00963801.32-1531.411.

Thamasha Samarasinghe

Thamasha is an NSIRC PhD student of Brunel University, based at TWI. She graduated from University of Moratuwa, Sri Lanka with a BSc.(Hons) degree in Mechanical Engineering in 2016 and completed her MPhil degree in Engineering from University of Liverpool, UK in 2019. Thamasha is currently pursuing a PhD on the "Design and development of composite panels with variable thermal conductivity for Li-ion battery module, funded by Lloyd's Register Foundation.

Design and Development of Composite Panels with Variable Thermal Conductivity for Li-ion Battery Module

Stuart Lewis[1], Mihalis Kazilas[2]
[1]TWI, [2]Brunel University
2nd Year of PhD

Keywords: Heat transfer ,Temperature distribution ,Li-ion battery module

I. INTRODUCTION

The global concerns over reducing the dependence on fossil fuels and ultimately producing less harmful emissions are driving the focus on Electric Vehicles (EVs) and Hybrid Electric Vehicles (HEVs). The performance of EVs and HEVs depends on their energy storage system (battery). Battery performance influences various parameters such as travelling distance and acceleration. Since the cost and life–cycle of batteries affect the reliability of EVs, it is necessary to optimize the parameters which affect the battery efficiency.

Lithium-ion (Li-ion) batteries are considered as the first–choice candidate for EVs and HEVs due to its advantages such as low self-discharge rate and high efficiency [1]. However, thermal performance of Li-ion batteries limits long-term stability and safety characteristics since the optimum operating temperature is typically between 30-40°C [1]. In addition, thermal runaway may occur in a cell when heat is not properly controlled. Fire and explosion are significant risks that can happen due to uncontrolled heat distribution. Therefore, it is necessary to operate battery modules at uniform temperature. Uneven temperature distribution can also cause an electrically unbalanced module and shorten battery life.

Thermal management can be achieved by active or passive built-in sources that provide cooling.

Existing thermal management systems use air, liquid (mainly water) and phase changing materials or a combination of these three methods.

Current solutions with active cooling are adding weight and complexity in EV and HEV batteries. The involvement of Phase Changing Materials (PCMs) as a passive cooling technique is also adding to the complexity, weight and the additional thermal resistance in the heat dissipation process of batteries.

A new idea for a composite casing for car batteries is considered in this project. The composite casing will have variable thermal conductivity, defined by the local volume fraction of carbon fibres and other conductive elements (including graphene) within the composite. The selective high thermal conductivity in areas of the casing will create "thermal avenues" close to the hot areas of the battery in order to provide passive heat dissipation in the areas needed the most. The composite casing will provide a low weight, simple thermal management solution that requires minimum maintenance.

II. DESIGN/METHODOLOGY/APPROACH

We developed a 3D model of a Li-ion battery single cell and designed several geometries of a battery module currently being used by battery manufacturers. Heat transfer simulations are currently being validated by experimental results from a custom jig that emulates the battery geometry. Heating elements of similar size and power/heat output to individual cells have been used for the experiments.

Batteries mainly generate heat during charge and discharge due to enthalpy changes, resistive heating inside the cell and electrochemical polarization. The energy balance equation for a cylindrical Li-ion battery cell is developed by considering the energy conservation laws and the volumetric heat generation of the battery cell. Lumped capacitance model was applied to simplify the Li-ion battery cell heat transfer. The simplified equation can be presented as follows.

$$\rho C_p \frac{\partial T}{\partial t} = hA(T - T_{amb}) + \dot{Q} \quad (1)$$

where, ρ is the density of active battery material (kg/ m^3) and C_p is for specific heat capacity (J/kgK). T and T_{amb} denote the absolute temperature (K) and the absolute temperature in ambient conditions (K) respectively. h denotes the heat transfer coefficient (W/ m^{2}K) and A represents the cross sectional area of the cell (m^2). Furthermore, $\dot{Q}$ denotes the volumetric heat generation rate for the battery (W).

The 3D simulation model for the single cell was developed as a CFD model by using COMSOL Multiphysics 5.5 commercial software. The single cell modelling was then extended for a battery module heat transfer modelling.

A bespoke test rig was designed and built in order to validate the simulation results. In order to replicate the cylindrical battery cells, cylindrical heating elements with similar dimensions were used. In order to emulate the operarion of a battery module, nineteen (19) heating elements were used. In addition to the heating elements, the rig consisted of a bench power supply, a ceramic material base for insulation and K-type thermocouples. The experiments were run for three geometry scenarios by changing the gap between the heating elements.

III. FINDINGS/RESULTS

3D simulations for both single cell and module were run. The square wave function was used in order to model the alternating charge and dischrage of the cells and the 10% of initial state of charge. In order to identify the cell temperature distribution, the simulations run with an airflow which has the velocity of 0.1 m/s at the inlet for X direction and the initial temperature of 298.15 K. The airflow velocity is representative of real EV battery modules. Initial results (Figure 1) indicate that the maximum temperature occurs at the centre core (the active battery material) of the single cell.

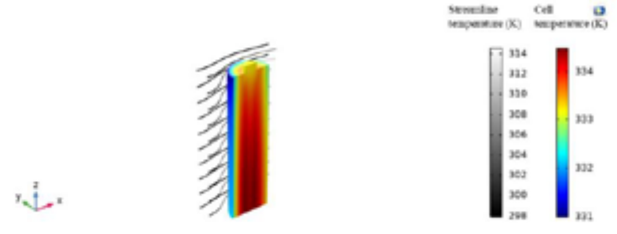

Figure 1. Temperature distribution results of a single cell with the airflow

Simulations were also run on single cell without any airflow. The results indicate that the maximum temperature without any airflow is 365 K. This is about 30°C higher compared to the results obtained with airflow of 0.1 m/s.

Experimental results and their comparison with the simulation are presented in Figure 2 for a single cell and Figure 3 for a battery module, comprising of 19 cells in a hexagonal arrangement.

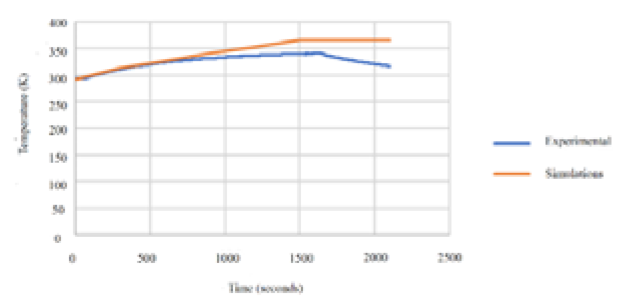

Figure 2. Experimental and simulation results for a single cell

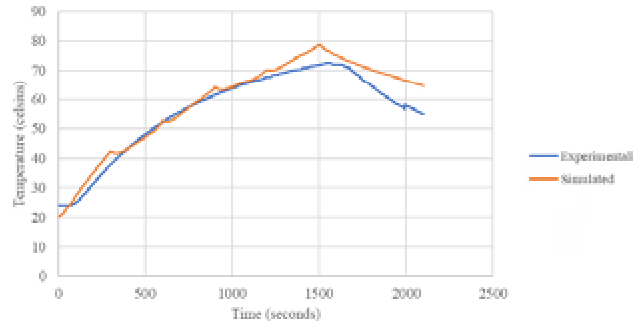

Figure 3. Experimental and simulation results for a centred cell of a battery module

IV. DISCUSSION/CONCLUSIONS

There is good agreement between simulations and experiment results. Minor deviations are attributed to fixing issues of heating elements during the experiments (some elements tilt slightly, creating deviations from the ideal geometry of the battery module).

The temperature distribution in battery modules depends on cells spatial arrangement and the inter -cell distance. Four cell arrangements were considered: 1×24, 3×8, 4×6 rectangular arrays and 19 cells in a hexagonal arrangement. Results confirm that the 4×6 cubic structure is better in terms of cooling capacity. However, since the 19 cells hexagonal arrangement shows good cooling capacity and has optimal space utilisation, this arrangement will be used for further investigation. Finally, simulation and experimental results indicate that the inter cell distance is proportional to the cooling capacity of a module. Hence, a trade-off exists between the size of the battery module and its thermal management.

V. FUTURE PLAN/DIRECTION

A prototype composite case with variable thermal conductivity will be manufactured. The required thermal conductivity of the composite case will be confirmed through the heat dissipation requirements. The thermal behaviour of the composite case will be measured and validated.

REFERENCES

[1] Ahmad A Pesaran, "Battery thermal management in EVs and HEVs : Issues and solutions ," in Advanced automotive battery conference , Las Vegas, 2001

Hamad Raheem

Hamad is an NSIRC PhD student at the University of Cambridge. He graduated with honours from Colorado School of Mines, USA with a BSc in Petroleum Engineering. He then obtained an MSc in Petroleum Engineering with distinction from Imperial College, London. After which, he worked as an intern in Abu Dhabi National Oil Company (ADNOC) who also fund his PhD. His PhD focuses on the effect of prolonged fluid permeation at elevated temperature and pressure on polymer ageing and the feasibility of detecting it through MEMS-based methodologies.

Evaluation of Acoustic Non-Destructive Testing Methods for Polymer Ageing Analysis Due to Gas Permeation

Dr Bernadette Craster[1], Prof. Ashwin Seshia[2]
[1]TWI, [2]University of Cambridge
2nd Year of PhD

Keywords: Resonant, Coupling, PMUT, Polymer, NDT

I. INTRODUCTION

Ageing of polymer samples is characterised as an alteration of polymer crystallinity, which occurs as a result of the consumption of additives and antioxidants in the polymer's crystalline matrix that support its backbone polymeric chain [1]. The induced ageing process is conducted through a gas permeation cell that exposes the samples to high temperatures (up to 90℃), pressures (up to 400 bars) and a mixture of hydrogen sulphide, carbon dioxide, and hydrocarbons. The specimen put to test included 80mm diameter by 2mm thick discs of high-density polyethylene (HDPE) and raised-temperature polyethylene (PE-RT) of known density. Fluxes will be analysed and transport coefficients of diffusion, solubility and permeation calculated. The flux traces will be also studied for an indicator of ageing of the specimen.

Ultrasonic based non-destructive testing (NDT) methods prove to be the best candidates for characterizing solid material and the investigation of change that occurs in them [2]. Proposed NDT methods start with ultrasound broadband spectroscopy (UBS), where a frequency sweep is conducted through the aged specimen by a pair of piezoelectric transducers at either ends. The frequency sweep characterises the natural harmonics of the specimen and the elastic constants of the material are referable from the resonant peaks [3-4]. The analysis of the natural harmonics allows one to detect changes in the material structure as a result of an alteration in the elastic constants and the attenuation coefficient.

II. DESIGN/METHODOLOGY/APPROACH

X-ray diffraction (XRD) and differential scanning calorimetry (DSC) are two destructive methods that are used to keep track of any alterations in the specimen's crystallinity before and after the induced ageing. A visual method is studied along, which is to analyse polymer ageing through acid-etched specimen swollen in toluene and capture microscopic images of spherulites - the building blocks of crystalline structures in polymers - using scanning electron microscopy (SEM).

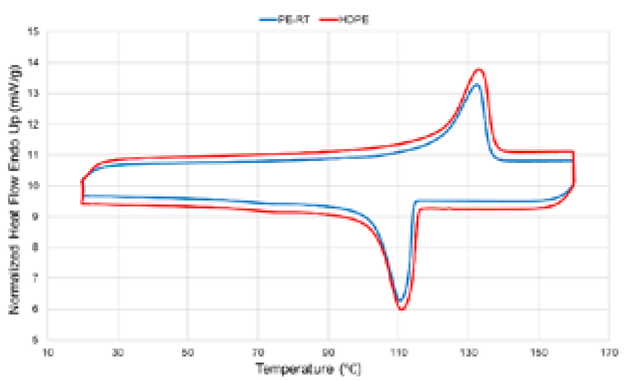

Figure 1: Average weight normalized differential scanning calorimetry (DSC) runs of raise-temperature polyethylene and high-density polyethylene samples

Resonant ultrasound spectroscopy (RUS) is a destructive method that characterises the natural harmonics, and hence all elastic constants, of a material to a very high accuracy [5-7], which is used to compare it with the results of the proposed non-destructive methods.

Previous work by [4] suggest that resolution of the resonant peaks increases with frequency, while the sweep frequency decreases linearly with the increase of the thickness of the piezoelectric layer in the transducer. Microelectromechanical sensors (MEMS) allows one to decrease the size of the transducer while being able to increase the central operating frequency [8]. Hence, two designs of piezoelectric micromachined ultrasonic transducers (PMUT) will be proposed and tested with the aged specimen.

III. FINDINGS/RESULTS

Differential scanning calorimetry tests on virgin samples allowed calculating the percent crystallinity and melt temperatures of the specimen before conducting the ageing experiments (65% and 132℃, and 68% and 133℃ for PE-RT and HDPE, respectively). The wider DSC envelope of HDPE is indicative of carbon-black filling that contributed to an increase in density. See Figure 1. It is predicted that a change in the crystallisation peak will be observed after the exposure of specimen to CO_2 critical fluid. Exposure of HDPE to thermal ageing of 90℃ alone was reported by [1] and [9] to increase crystallinity, melting temperature and elastic moduli through an investigation using XRD, DSC and Fourier-Transform Infrared Spectroscopy (FTIR).

UBS was conducted on virgin PE-RT and HDPE samples and it was found that the two materials, although differ very subtly in the chemical makeup and density (944 kg/m^3 and 960 kg/m^3, respectively), yielded distinguishable harmonic signatures between 1.1GHz and 1.3GHz. See Figure 2. This is an encourageing indication that ultrasonic resonance technique could be able to differentiate an alteration of specimen properties when exposed to damageing conditions. However, the possibility of accurately measuring the extent of the inflicted damage caused by the ageing experiment using the current 15 MHz centre frequency piezoelectric transducers is to be tested. Thus, the magnitude of alteration that could be picked up using the UBS technique is unknown until the on-going ageing experiments are completed.

IV. CONCLUSIONS

Initial experimental runs of ultrasound broadband spectroscopy showed promising results in distinguishing closely chemically related virgin polymer specimen of the same dimensions using harmonic signatures. However, the extent of alteration detection capability of the method is yet to be tested using aged samples (ageing experiments on-going).

V. FUTURE PLAN/DIRECTION

Ageing of the specimen through permeation testing is planned using CO2, H2S and hydrocarbon mixtures at different temperature and pressure ratings. The natural frequency of the aged specimen would then be tested using the bespoke acoustically matched piezoelectric micromachined ultrasonic transducers (PMUT).

Tensile tests are planned for the future to investigate the elastic behaviour of polymer specimens through the proposed ultrasound tests to aid the analysis of correlating elastic moduli and microfracture networks with crystallinity.

The contribution of this research is vital to the understanding of the nature of polymer ageing, and not only adds value to the cost-effective alternative to steel pipes but also provides a non-destructive testing mechanism that avoids shut-in production.

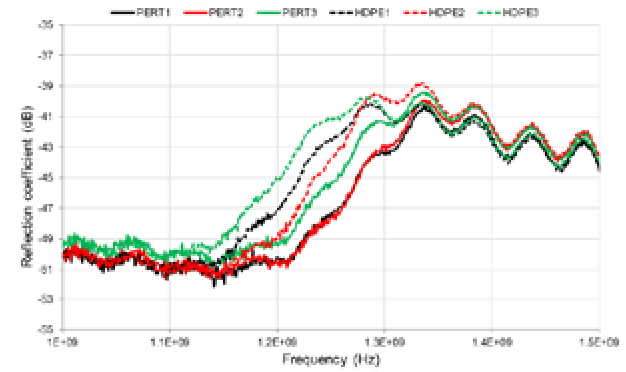

Figure 2: Ultrasound broadband spectroscopy (UBS) of raised-temperature polyethylene (PERT) and high-density polyethylene (HDPE) samples in 3 independent runs.

VI. ACKNOWLEDGEMENT

This publication was made possible by the sponsorship and support of Non-metallic Innovation Centre (NIC). The work was enabled through, and undertaken at, the National Structural Integrity Research Centre (NSIRC), a postgraduate engineering facility for industry-led research into structural integrity established and managed by TWI through a network of both national and international Universities.

VII. REFERENCES

[1] J. Wang et al. "The effect of thermo-oxidative ageing on crystallization, dynamic and static mechanical properties of long glass fibre-reinforced polyamide 10T composites," R. Soc. Open Sci., vol. 5, 6, 2018.
[2] M. Agrawal, "Ultrasonic Resonant Cavity Technique for Materials Characterization," 2015.
[3] M. Agrawal and A. A. Seshia, "Characterization of metallic glasses using ultrasound broadband spectroscopy," IEEE Int. Ultrason. Symp. IUS, 2017.
[4] M. Agrawal et al. , "Characterization of mechanical properties of materials using ultrasound broadband spectroscopy," Ultrasonics, vol. 64, 186–195, 2016.
[5] A. Migliori, "PHYSICA rn," vol. 183, pp. 1–24, 1993.
[6] A. Migliori and T. W. Darling, "Resonant ultrasound spectroscopy for materials studies and non-destructive testing," Ultrasonics, vol. 34, no. 2–5, pp. 473–476, 1996.
[7] H. Ogi et al. "Determination of elastic, anelastic, and piezoelectric coefficients of piezoelectric materials from a single specimen by acoustic resonance spectroscopy," Ultrasonics, 42, 1–9, 183–187, 2004.
[8] M. Agrawal et al. "Design and modeling of an integrated device for acoustic resonance spectroscopy," IEEE IUS, 2183–2186, 2013.
[9] R. Ferhoum, "Analysis of Thermal Ageing Effect (Hold Time - Crystallinity Rate - Mechanical Property) on High Density Polyethylene (HDPE)," Int. J. Mater. Sci. Appl., vol. 2, no. 3, p. 109, 2013.

Malallah Al Lawati

Malallah obtained his BEng degree in Mechanical Engineering at University of Leicester in September 2017. He started his PhD with University of Birmingham in February 2019. His research is focused on the development of novel titanium alloys via powder metallurgy hot isostatic pressing technique. These novel titanium alloys can replace the conventional titanium alloys for the engineering parts needed for harsh industrial applications.

Development of Powder Metallurgy Hot Isostatic Pressing of Titanium Matrix Composites

Raja Khan[1], Moataz Attallah[2]
[1]TWI, [2]University of Birmingham
3rd Year of PhD

Keywords: Titanium matrix composites, powder metallurgy hot isostatic pressing, microstructure, mechanical & tribological properties

I. INTRODUCTION

Titanium (Ti) and its alloys are known to provide excellent corrosion resistance and mechanical properties, ranging from offering high strength to providing weight reductions [1]. On the other hand, they have not been extensively used in a variety of industrial applications due to their poor tribological perfomance [2]. Titanium matrix composites (TMCs) are composites with at least two constituent parts, one being the titanium matrix and the other usually a ceramic which can offer a solution to the shortcomings of convetional titanium alloys. Reinforcing the matrix with ceramic continuous fibres or discontinuous particulates can further enhance the strength and wear resistance immensely, while the matrix can maintain both the ductility and toughness, hence opening the possibility of tailoring composites for many different applications. An in-situ route allows for a chemical reaction to take place between the titanium matrix and ceramic reinforcement particles, resulting in phases formation that are high in strength, thermodynamically stable and exhibiting superior interfacial bonding, hence allowing for an improvement in the mechanical and tribological behaviour of the composite in comparison with ex-situ routes.

II. DESIGN/METHODOLOGY/APPROACH

Argon gas atomised (AGA) Ti6Al4V (Ti64) powder (15-45μm) was used as the metal matrix (LPW Technology, UK). Graphene nanoplatelets (GNPs) with a length of <2μm, 5-20nm thickness and a high surface area of 750m^2/g have been purchased from Sigma aldrich, Germany. Boron (B) (>95% pure) amorphous powder (~<1μm) was also purchased from Sigma aldrich, Germany. Four different powder blends were prepared. Ti64+ 1 vol.% B , Ti64 + 1 vol.% GNP , Ti64 + 2 vol.% GNP, Ti64 + 1 vol.% B + 1 vol.% GNP. Firstly, the GNPs were de-agglomerated via ultrasonication for a time period of 30 min in ethanol with a concentration of roughly 0.1mg/ml. Ti64 was added to the de-agglomeration GNP suspension and ultrasonicated for an additional 30 min. The blended powders were then mechanically alloyed (MA) via low-energy milling (HMK-1901) using ethanol as a process control agent for a duration of 6h, ball to powder ratio (BPR) of 4:1 and a speed of 200 RPM to limit the deformation and overheating of Ti powders. The MA powders were then consolidated by hot isostatic pressing (HIP). Mild steel canisters with an outer diameter of 20.8mm, length of 80mm, wall thickness of 2.03mm were TIG welded, helium leak checked and filled with the MA powders using vibratory table. The powder filled canisters were outgassed and hot crimped. The outgassed operation was performed at 100℃ to remove any trapped air and moisture from the powders until achieving a vacuum level of 10^-5 mbar. The canisters were hot isostatically pressed (HIPped) using EPSI HIP at three different temperatures, 920℃ (sub-transus), 1040℃ and 1160℃ (super-transus) temperature at a constant pressure of 140MPa with 3h dwell time.

III. FINDINGS/RESULTS

Fig.1 shows the influence of GNP vol.% on the phase formation of TiC processed at 1040℃. It can be seen that as the vol.% of GNP increases, there is more retention with a higher amount of TiC precipitates. During the exothermic in-situ reaction, very high heat is released which is enough to convert Ti and C into TiC. TiC phase is feasible as per the reaction shown below due to releasing a highly negative Gibbs free energy:

$$Ti + C \longrightarrow TiC \ (\Delta Go \text{ at } 1000\ K) \ \ -150\ kJmol^{-1} \quad (1)$$

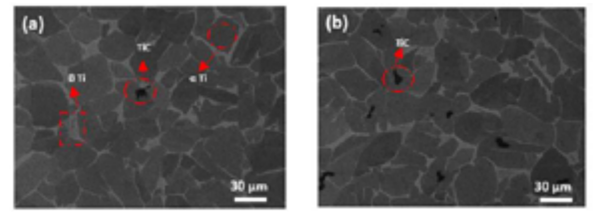

Figure 1. Microstructure of As-HIPped Ti64 with varying vol.% of GNP HIPped at 1040℃ (a) Ti64 + 1 vol.% GNP (b) Ti64 + 2 vol.% GNP

The microhardness of TMCs were measured. As the volume fraction of the reinforcement increases from 1 vol.% to 2 vol.%, there is a clear trend of increase in the microhardness from 350HV1 to 380HV1. The increase in hardness could be attributed to the increase in the formation of the TiC phase. Furthermore, load-transfer mechanism plays an important role in transferring the load from a soft metallic matrix to a harder phase. It is vital to note that the load-transfer mechanism is heavily sensitive to a change in reinforcement volume fraction.

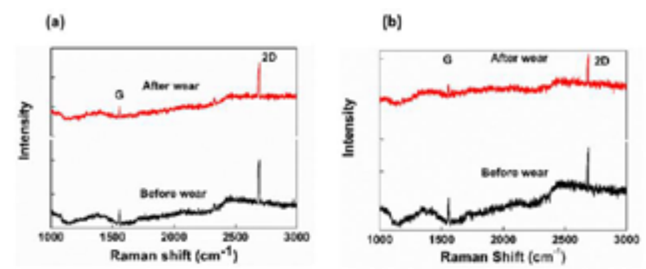

Figure 2. Raman of wear tested track surfaces (a) Ti64 + 1 vol.% GNP (b) Ti64 + 2 vol.% GNP

Fig.2 (a) shows the Raman spectra of Ti64+1 vol.% GNP before and after the wear testing, while Fig.2 (b) shows the Raman spectra of Ti64 + 2 vol.% GNP before and after the wear testing. It can be seen in Fig. 2 (a) that the (2D and G) peaks of graphene are much lower compared to before the wear test. This suggests that the structure of GNP was destroyed during the wear test and since it is known that GNP exhibit extremely high flexural strength, it is anticipated that they will bend and tilt towards the surface of the composite of the track under the contact of a load and help lubricate the surface, hence lowering the coefficient of friction (CoF) values. In addition to that, Fig.2 (b), before the wear testing, exhibits higher (2D and G) peaks in comparison to Fig.2 (a) which suggests that there was a higher retention of GNP due to the higher vol.% used and it can be concluded that not all the GNP has in-situ reaction to produce TiC precipitates. Again, it can be seen that the (2D and G) peaks after wear test is way lower suggesting that the graphene on the surface is acting as a lubricant hence why CoF values are very low for this TMC material.

IV. DISCUSSION/CONCLUSIONS

An attempt was made in this study to understand the formation of hard phases via in-situ reactions during HIP and their influence on the tribological perfomance of the produced TMCs. The aim of the study was to develop TMCs via in-situ reactions using reinforcements such as B and GNP with varying vol.% for high wear resistance applications and tackle the main challenges of fabrication such as the homogeneity of the blended powders and mainly the challenges associated with dispersing the reinforcement in the matrix. Furthermore, an attempt to understand how different HIP temperature conditions above and below the β-transus temperatures were performed in order to see the effect of HIP temperature on the completion of in-situ reactions, consolidation behaviour and the microstructure. Finally, a structure-property modelling was done to see whether it was possible to predict the behaviour of the advanced TMCs using the ROM and test the validity of the equations. The conclusions are as follows:

(a) Increasing the vol.% of GNP increases the microhardness due to the load transfer mechanism and more retention of TiC phase

(b) HIPping at 1160°C ensures full consolidation, however resulting in grain growth, while HIPping at 920°C shows lack of consolidation and no in-situ reaction. HIPping at 1040°C resulted in retention of TiC phase with some unreacted graphene which helps in the tribological perfomance

(c) Increasing the vol.% of GNP reduces the CoF due to an increase in microhardness and an increase in GNP content at the surface of the composite lubricating the surface.

V. FUTURE PLAN/DIRECTION

Compression testing will be carried out for the different TMCs and structure-property modelling will be conducted to see if there is an agreement between theoritical and experimental strength values and validate the equations.

REFERENCES

[1] L.Cai et al., Journal of University of Science and Technology Beijing, vol.13, 2006, pp. 551
[2] C.Cai et al., Journal of Alloys and Compounds, vol.710, 2017, pp. 364-374

Burak Serhat Sakarya

Burak is a Doctoral Researcher of Brunel University London, based at National Structural Integrity Research Centre (NSIRC) of TWI. He achieved an MSc in Structural Integrity with distinction from Brunel University London in collaboration with NSIRC in 2017. His master thesis title was "Numerical Modelling of Damage in Composite Materials for different damage mechanisms". After graduation, he worked as a Mechanical Project Engineer at the General Directorate of State Hydraulic Works as part of his scholarship agreement. Burak is currently pursuing a PhD on the "Design of Composite Pressure Vessels with built-in Leak-Before-Break capability", sponsored by Lloyd's Register Foundation. His research interests lie within the areas of composite materials, numerical modelling, failure analysis, composite pressure vessels.

Design of Composite Pressure Vessels with built-in "Leak-Before-Break" capability

Dr Nenad Djordjevic[1], Dr Mihalis Kazilas[1, 2], Dr Vasiliki Loukodimou[2]
[1]Brunel University London, [2]TWI Ltd
2nd Year of PhD

Keywords: composite pressure vessel, numerical analysis, failure analysis

I. INTRODUCTION

Fibre-reinforced composites play a significant role in the aerospace, automotive, energy and Oil & Gas industries due to their high strength-to-weight ratio, corrosion resistance and crashworthiness. The filament winding technology is used for the manufacturing of composite pressure vessels, namely Type II, III, IV and V for the storage of substances such as hydrogen, compressed natural gas, liquid oxygen, helium and nitrogen. To ensure the safety of these structures cost-effective analytical and numerical simulation tools are developed and used during the design phase. In this research work, this is addressed through the estimation of the Leak-Before-Break (LBB) capability of the composite pressure vessels. The occurrence of leakage before burst enables taking preventative action to avoid catastrophic failure during service life. The aim of this project is the development and proof of a conceptual design enabling inherent LBB capability in composite pressure vessels. To achieve this, three objectives are defined in this project:

- Development of an analytical tool for the rapid investigation of potential fail-safe design patterns.
- Development of a small-scale design concept involving artificial damage by using the Finite Element Method.
- Proof-of-concept with validation of the best scenario coming from the numerical solutions in the vessel and small-scale specimens.

The work presented in this abstract mainly addresses the first objective.

II. DESIGN/METHODOLOGY/APPROACH

An algorithm for the analytical tool was developed by using MATLAB commercial software. Control Volume Approach described in Equations 1-4 was used to estimate the equivalent stiffness and compliance matrix of the laminate-of-interest under linear-elastic material response [1]. Lamé Equations were implemented to relate the applied internal and external pressure with axial, hoop and radial stresses. The fibre failure strain investigated as the first-ply failure was considered for the burst pressure estimation.

$$(i,j = 1,2,3,4,5,6): \quad \sigma_i = C_{ij}\epsilon_j \tag{1}$$

$$(i,j = 1,2,3,6):$$

$$C_{ij} = \sum_{k=1}^{n} V_k \left[C_{ij}^k - \frac{C_{i3}^k C_{3j}^k}{C_{33}^k} + \frac{C_{i3}^k \sum_{l=1}^{n} \frac{V^l C_{3j}^l}{C_{33}^l}}{C_{33}^k \sum_{l=1}^{n} \frac{V^l}{C_{33}^l}} \right] \tag{2}$$

$$(i = 1,2,3,6; j = 4,5): \qquad C_{ij} = C_{ji} = 0 \tag{3}$$

$$(i,j = 4,5)\ and\ \Delta'_{k,l} = \begin{vmatrix} C_{44}^{k,l} & C_{45}^{k,l} \\ C_{54}^{k,l} & C_{55}^{k,l} \end{vmatrix}:$$

$$C_{ij} = \frac{\sum_{k=1}^{n} \frac{V^k}{\Delta'_k} C_{ij}^k}{\sum_{k=1}^{n} \sum_{l=1}^{n} \frac{V^k V^l}{\Delta'_k \Delta'_l}} \left(C_{44}^k C_{55}^l - C_{45}^k C_{54}^l \right) \tag{4}$$

A case study from literature was modelled with the developed tool to demonstrate its accuracy [2]. A four-layered pressure vessel model with 97.4mm inner and 125mm outer diameter, and 690mm length was prepared in ABAQUS commercial finite element software. The vessel consisted of an HDPE80 outer layer of 2mm thickness, and HDPE100 inner layer of 6.3mm thickness and one ±55° aramid fibre-HDPE80 tape layer with 5.5mm thickness. The model was prepared with 3mm-to-3mm four-node shell elements (S4). The internal pressure of 30MPa was applied for both the analytical tool and finite element model. Figure-1 indicates the stress-strain measurement points chosen around the circumference to comply with Saint Venant's principle. The pressure vessel is fixed at X, Y and Z directions on one side; whilst at X and Y directions on the other side. The boundary conditions and shell-edge load to represent the axial structural response were applied as illustrated in Figure-2.

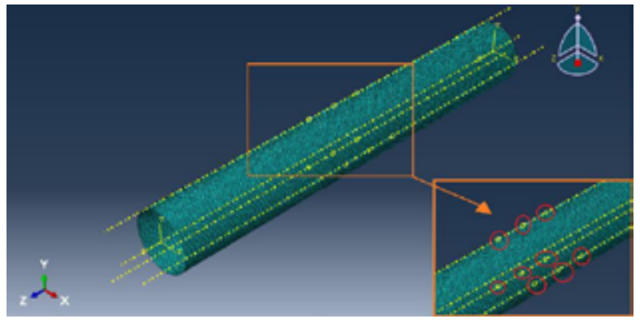

Figure-1 Strain Gauge Positions in FEM

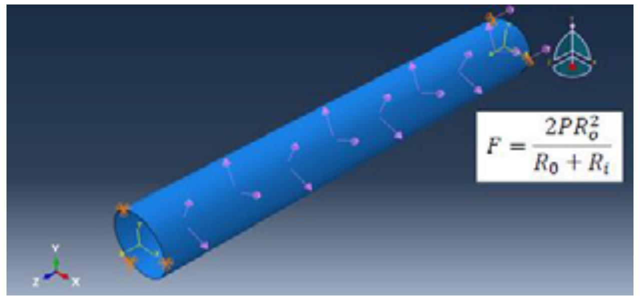

Figure-2 Applied Boundary Conditions, Internal Pressure and shell-edge load

III. FINDINGS/RESULTS

Figure-3 shows that the strain in the fibre direction in both the analytical tool and finite element model has good agreement with those given in the literature. The maximum pressure presented in Figure-3 corresponds to the strain at failure in the fibre direction [3].

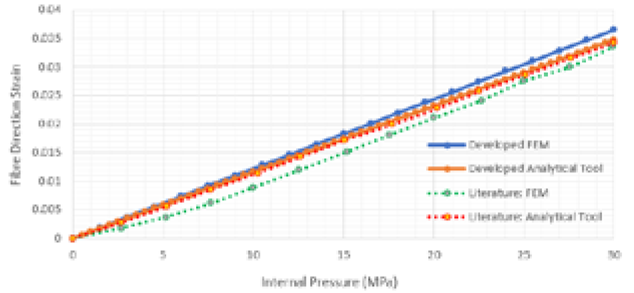

Figure-3 Strain in Fibre Direction at second layer vs Internal Pressure

Table-1 shows that hoop-to-axial stress ratio of 2.1 value was obtained at the outer layer where strain gauges were located, which verify the structural response results obtained in the analytical tool. The greatest deviation from the 2:1 stress ratio was obtained for the inner HDPE layer, which might be due to nonlinear elastic response, experimentally observed at this loading state in [2].

Table-1 Hoop-to-Axial Stress Ratio at 30MPa

Layer-of-Interest	Ratio
HDPE 100 (inner layer)	2.7
-55 Aramid Fibre-HDPE80	2.33
+55 Aramid Fibre-HDPE80	2.2
HDPE 80 (outer layer)	2.1

IV. DISCUSSION/CONCLUSIONS

The tool enables the investigation of various design patterns including different combinations of winding angles, liner and prepregs, geometry, and pressures. It calculates the structural response of an undamaged pressure vessel corresponding to on-axis and off-axis strain and stresses, and burst pressure in thick pressure vessels. The tool can also be used for thin pressure vessels, by neglecting the radial stress calculation in Lamé Equations. More experimental case studies can be investigated to demonstrate the capabilities of the analytical tool.

V. FUTURE PLAN/DIRECTION

The future activities will focus on the conceptual design solution for inherited LBB in composite pressure vessels. Available finite element tools in ABAQUS are being tested at vessel scale with different damage mechanisms such as longitudinal crack as fibre cracking. The aim is to observe crack propagation dominated in the through-the-thickness direction whilst maintaining limited instability during the internal pressure increment. Then, depressurisation of the pressure vessel will prevent catastrophic failure. The simulation programme at the vessel scale aims to assess the actual local stress states in the structure, which will be replicated in the small-scale testing for cost-effective validation. The experiments will provide validation for both the simulation models and the analytical tool.

VI. ACKNOWLEDGEMENTS

This publication was made possible by the sponsorship and support of Lloyd’s Register Foundation*. The work was enabled through, and undertaken at, the National Structural Integrity Research Centre (NSIRC), a postgraduate engineering facility for industry-led research into structural integrity established and managed by TWI through a network of both national and international Universities.

VII. REFERENCES

[1] P. C. Chou, J. Carleone, and C. M. Hsu, “Elastic Constants of Layered Media,” J. Compos. Mater., vol. 6, no. 1, pp. 80–93, 1972, doi: https://doi.org/10.1177/002199837200600107

[2] M. Bai, Young; Xu, Fan; Cheng, Peng; Badaruddin, Mohd Fauzi;Ashri, “Burst Capacity of Reinforced Thermoplastic Pipe (RTP) Under Internal Pressure,” in OMAE2011-49325, 2011, pp. 281–288, doi: https://doi.org/10.1115/OMAE2011-49325

[3] I. P. Giannopoulos and C. J. Burgoyne, “Stress limits for aramid fibres,” Proc. Inst. Civ. Eng. Struct. Build., vol. 162, no. 4, pp. 221–232, 2009, doi: 10.1680/stbu.2009.162.4.221.

* A charitable foundation, helping to protect life and property by supporting engineering-related education, public engagement and the application of research. www.lrfoundation.org.uk

Maciej Gierulski

Maciej graduated with a MEng Aerospace Engineering from University of Sheffield in 2019. His research experience includes a year internship in Nuclear Advanced Manufacturing Research Centre in Rotherham and an extensive MEng project of building a high pressure combustion testing rig for measuring emissions from various aviation fuels. Maciej is currently pursuing a PhD in electrofusion welding of thermoplastic composite pipes funded by the Non-metallic Innovation Centre at University of Sheffield, but based in TWI.

Electrofusion Welding of Thermoplastic Composite Pipes

Mike Troughton[1],Rachel Tomlinson[2], Anthony Ryan[2], Matt Smith[3]
[1]TWI, [2]University of Sheffield, [3]AMRC
2nd Year of PhD

Keywords: electrofusion welding, thermoplastic composite pipes, polyethylene composites

I. INTRODUCTION

Oil and gas producers have been struggling with the maintenance of their steel pipelines, as crude oil greatly promotes corrosion. Also, the bolted joints between individual pipes are relatively complex and vulnerable to environmental conditions. Thermoplastic pipes connected with electrofusion (EF) joints are an attractive solution: they do not suffer from corrosion and are flexible, which, in combination with excellent end-load resistance of joints, can guarantee a maintenance-free service life of 50 years or more. Thermoplastic pipelines can even endure earthquakes.

Therefore, to reduce maintenance costs and the risk to the environment, oil and gas operators are looking to change some of their pipelines to fully non-metallic. Recently, thermoplastic composite pipes (TCPs) have been developed that have pressure capacities comparable to that of the metallic solutions, but they still are connected with steel joints. The aim of this project is to design a thermoplastic connector for polyethylene (PE)TCPs that utilises EFwelding technology.

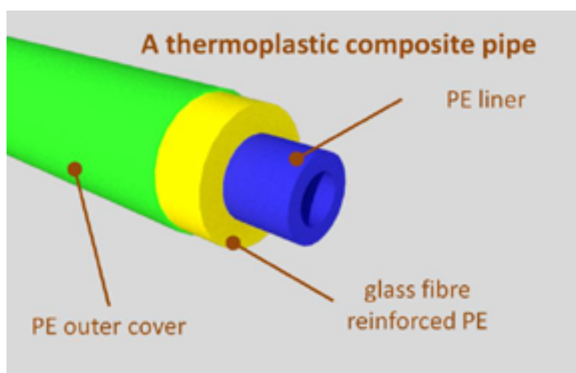

Fig. 1 Schematic of a TCP.

II. DESIGN/METHODOLOGY/APPROACH

The project is to design a bespoke EF coupler specifically for joining TCPs. In order to do this a finite element (FE) model of a joint between a conventional EF coupler and TCPs was developed and will be validated by whole joint mechanical testing (hydrostatic pressure test and axial tension test) with strain gauges attached to both the EF coupler and the TCPs. The model will then be used to optimise the geometry and structure of the EF coupler.

A challenge of the project is that the material investigated, glass fibre reinforced PE, is a novel one and there is little literature and data on the mechanical properties required as input data for modelling. Consequently, the properties of each of the three layers of TCP have to be established in the course of the PhD. Due to the production process typical for spirally wound composite pipes, the material is only available in curved form, which makes the use of traditional methods for determining composite properties difficult. As an arrangement to solve this problem, a custom set of three specimen tests was chosen:

- ISO 527-2 to determine Young's modulus in the axial direction
- ASTM D2290 (modified) to determine Young's modulus in hoop direction
- ASTM D5379 (Iosipescu test) to determine shear modulus.

These tests have been modelled to assess whether the curvature of the composite layer affects the measurements.

Another issue is that, due to the way they are stored and transported, TCPs are not perfectly straight or round. To prevent this from having an adverse effect on the results of the whole joint mechanical tests, a straightening jig has been made and trials will be carried out to attempt to straighten and re-round the pipes.

III. FINDINGS/RESULTS

The typical failure mode for EF joints between conventional unreinforced PE pipes under pressure is by slow crack growth through the coupler wall from the stress concentration area at the inner cold zone notch, and in axial tension they usually fail through the pipe wall starting at the outer cold zone notch (see fig.2).

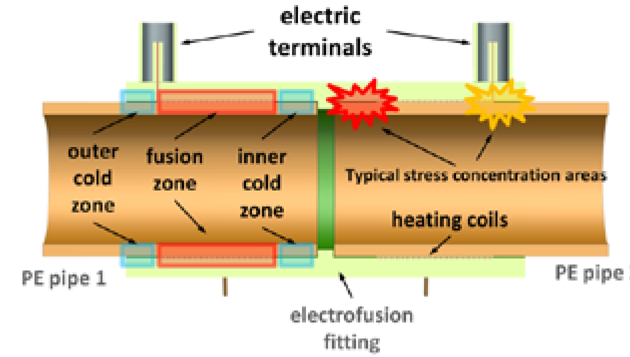

Fig. 2 A cut through of an EF joint in conventional unreinforced PE pipes with two typical stress concentration areas indicated.

One question investigated while modelling was whether the stress concentrations change their positions if the conventional PE pipes are replaced by TCPs. So far, the simulation results suggest that the areas of highest stress concentration are the same for both pipe types (compare figures 2 and 3), the actual stress values are yet to be confirmed.

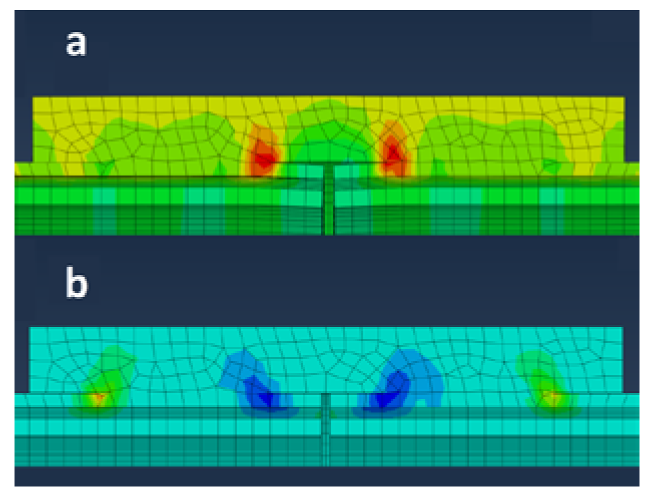

Fig. 3 Simulated stress concentrations in a TCP electrofusion joint for a) hydrostatic pressure and b) tensile test.

The modelling of the specimen tests suggests that results from the two tensile tests will not be affected by the curvature of the composite layer. However, there is a risk that the shear test, if the curvature axis of the coupon is perpendicular to the test load direction might be invalidated because the strains on the concave side are larger than on the convex side due to buckling (fig.4).

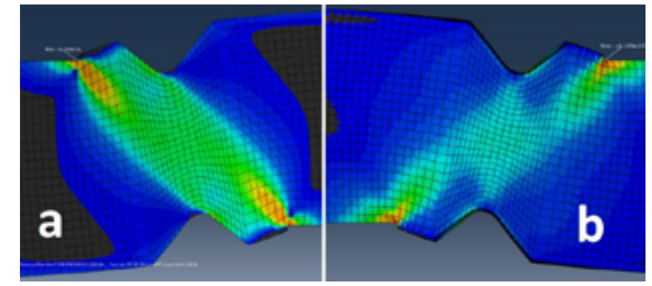

Fig. 4 Simulated strains of a Iosipescu test of a curved specimen, a) concave and b) convex side.

IV. DISCUSSION/CONCLUSIONS

Looking at the result of the shear test simulation, changing the orientation in which the specimen is cut, such that the composite layer is flat in the direction of the test load and less likely to buckle, is worth considering.

The results of the simulations of the whole pipe tests suggest that the stress concentration areas do not relocate when reinforcement is introduced into EF welded pipes. Designing the coupler will, therefore, most likely require only reinforcing it so that it can match the high pressure capabilities of the reinforced pipes.

V. FUTURE PLAN/DIRECTION

Once the required mechanical properties of the liner, reinforced layer and jacket of the TCP have been determined from specimen tests, the models will be verified against strain measurements in experimental tests on TCP electrofusion joints using commercially available couplers. The verified models will subsequently be used to design a prototype, dedicated EF coupler for TCPs.

Corentin Penot
Corentin is a 3rd year PhD student at the University of Southampton. He obtained his Master's degree in Material Science at the National Institute for Applied Sciences in Lyon, France. His PhD focuses on understanding the corrosion performances of WAAM deposited 316L corrosion resistant alloy and is founded by the Lloyd's Register Foundation.

Investigation of the Corrosion Performance of a WAAM Deposited 316L Alloy in NaCl Environment

Adrian Addison[1], Qing Lu[1], Julian Wharton[2], Yikun Wang[2]
[1]TWI, [2]University of Southampton
3rd Year of PhD

Keywords: Wire arc additive manufacturing, 316L, Corrosion

I. INTRODUCTION

Material properties resulting from additive manufacturing builds are currently under intensive research, driven by the possible economic gains these techniques may offer. Wire and Arc Additive Manufacturing (WAAM), a Direct Energy Deposition process, is particularly suitable for the manufacturing of large metallic structures of several meters in size. In recent years, the mechanical performance of WAAM manufactured parts have been extensively studied [1]. However, the corrosion performance of such parts has only received limited attention and needs further investigation. Especially corrosion resistance alloys, since the maritime sector would greatly benefit from this type of new manufacturing process. To that purpose, the corrosion properties of WAAM deposited AISI 316L specimens were investigated in different conditions; including no-inter-pass cooling, inter-pass cooled, and after a stress relief heat treatment.

II. METHODOLOGY

A. Specimen preparation

WAAM walls were deposited using a robotic arc welding system with a Fronius TPS 4000 CMT Advanced MIG/MAG welding equipment. The welding wire used for all the depositions was a Lincoln LNM ER316L-Si.

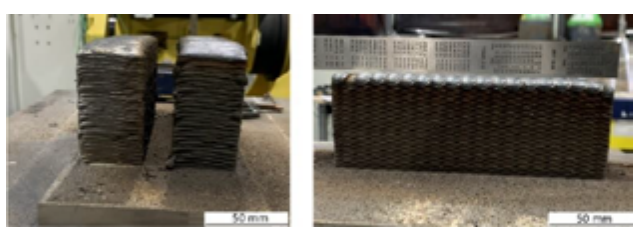

Figure 1: WAAM walls B1 (left) and B2 (right) after the deposition.

Wall B1 was deposited without inter-pass cooling and had an inter-pass temperature of 400 °C. Wall B2 was deposited with a pulsed-air cooling stage, i.e. the inter-pass temperature was maintained below 70°C between each pass. Specimens were extracted from the walls and several specimens from wall B1 underwent a stress relief heat treatment (900 °C for 2 h, air-cooled).

B. Corrosion testing

Electrochemical tests were carried out on WAAM specimens, as well as on conventional (wrought) AISI 316L specimens. Potentiodynamic polarisation (PDP) scans were performed using a Gamry potentiostat and a three-electrode cell with a carbon graphite rod as counter electrode and Ag/AgCl as the reference electrode. The electrolyte used was a 3.5 wt.% NaCl solution at ambient laboratory conditions.

Critical pitting Temperature (CPT) and pitting corrosion tests were carried out in accordance with ASTM G150 standard using an ACM potentiostat and a three-electrode Avesta cell. Finally, pitting corrosion tests by immersion in a 6% ferric chloride solution were undertaken in accordance with ASTM G48 standard.

C. Surface characterization

The microstructure and post-test surface condition were analysed using Optical Microscopy (OM), Scanning Electron Microscopy and Energy Dispersive X-Ray spectroscopy (SEM/EDX).

III. FINDINGS/RESULTS

A. Microstructure

The WAAM 316L build microstructure is closer to a welded 316L than that of a conventional wrought 316L. The microstructure is vertically oriented along the thermal gradient because of the high cooling rate due to a rapid heat dissipation through the substrate. Columnar dendrites grow epitaxially across several layers with typical size of 1-2 mm. The dendrites are significantly finer at the root of a layer (remelted zone) and become coarser closer to the top until the next layer is reached. Ferrite phase (white in Figure 2) is present at the inter-dendritic space following the columnar dendrites. Sigma phase was detected at the inter-dendritic region among the ferrite phase. The proportion of sigma phase was greater in the heat-treated specimens and the lowest within the inter-pass cooled specimens. The presence of micro-sized Si-oxides has been observed as illustrated in Figure 2 and no MnS inclusions was detected.

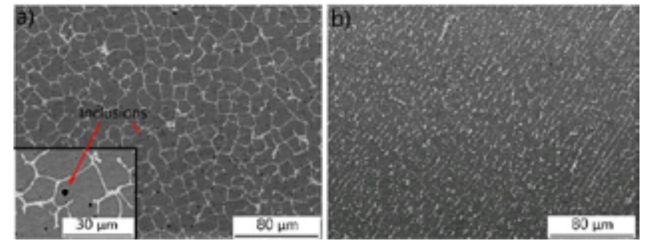

Figure 2: BSE image of a WAAM specimen from wall B1. a) horizontal and b) vertical to the build direction.

B. Corrosion testing

WAAM 316L had higher pitting potential and CPT than its wrought counterpart as shown in Figure 3 and

Table 1. Pitting tests showed higher mass losses for the WAAM 316L revealing a weaker passivity.

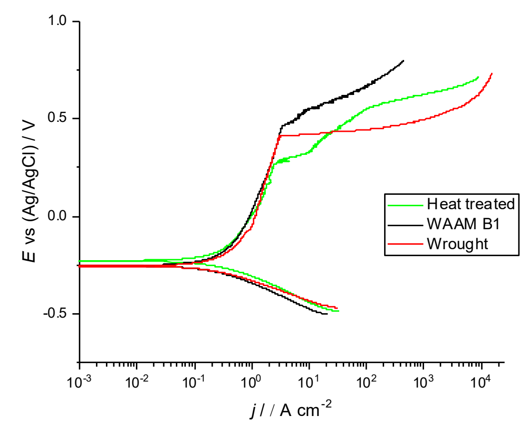

Figure 3: PDP scans in 3.5 wt.% NaCl solution.

The stress relief heat treatment leads to a degradation of the WAAM 316 corrosion resistance as the pitting potential dropped significantly.

Table 1: CPT values and weight loss from ASTM G48 pitting test.

	CPT / °C	G48 Weight loss / g m-2
WAAM B1	29.4 ± 3.9	37 ± 5
WAAM B2	26.9 ± 0.5	36 ± 11
Wrought	19.5 ± 1.3	<1

IV. DISCUSSION/CONCLUSIONS

It is evident the pitting potential and higher CPT of the WAAM 316L is due to the absence of MnS inclusions within the WAAM microstructure that act as initiation sites for the stable pit development and propagation in traditional 316L.

A de-alloying of Mo and Cr elements was observed between the ferrite and the austenite phase using EDX analysis. The ferrite phase was richer in Cr and Mo and a Mo depleted zone was observed at the phase boundary. The de-alloying effect is likely to weaken the passive film stability and to promote the initiation of pits at the phase boundary as shown in Figure 4.

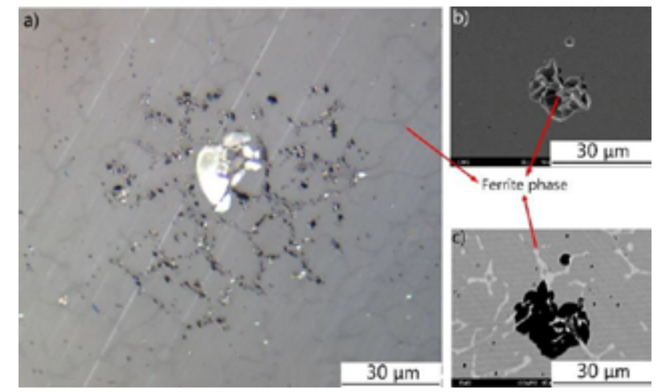

Figure 4: a) OM, b) SE and c) BSI observation of post-PDP test pits on the heat treated WAAM specimen.

This phenomenon would explain the high mass loss from WAAM B1 and WAAM B2 specimens recorded during the pitting test in ferric chloride solution.

V. FUTURE PLAN/DIRECTION

Elucidate the pit initiation mechanism at the interphase boundary by:

- Determining the passive film chemical state and composition developing on top of each phase using XPS analysis;
- Studying the pit initiation sites using Pulsed Potentiostatic Testing (PPT).

Additionally, testing of a new feed wire chemical composition to lower the content of ferrite and inter-metallic phase within the deposit.

REFERENCES

[1] S. W. Williams et al. "Wire plus Arc Additive Manufacturing,", Mater Sci Tech-Lond, vol. 32, no. 7, pp. 641-647, 2016.

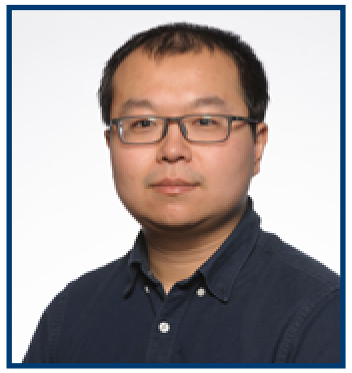

Yi Yin
3rd Year PhD student of Engineering Department, Lancaster University. Yi's PhD research is funded by Lloyd's Register Foundation and Lancaster University. His research is to enable a 'smarter' electron beam welding process and reduce the inconsistent human factor. Yi earned his master's degree from University of Bath in 2014 and his bachelor's degree from Ocean University of China in 2013. Yi has four-years working experience as engineer at Qilu University of Technology and SIASUN Robot & Automation CO.,LTD.

Electron Beam Weld Penetration Depth Prediction Based on Artificial Neural Network and Numerical Modelling

Tim Mitchell[1], Darren Williams[1], Andrew Kennedy[2], Yingtao Tian[2]
[1]TWI, [2]Lancaster University
3rd Year of PhD

Keywords: electron beam welding, computational fluid dynamics, artificial neural network, electron beam probing

I. INTRODUCTION

The quality of electron beam welds is largely determined by the weld shape and penetration depth. In practice, a trial-and-error approach is usually adopted to tune the electron beam parameters against the desired penetration depth before moving to the final production. This trial-and-error step can be very time consuming and costly, especially in the case of welding of expensive high-grade materials, which makes the EBW process very hard to be standardised and fully automated. Therefore, a reliable method is demanded to enable machine operators to predict EBW penetration depth before conducting weld. It is hoped the real-time electron beam probing combining with CFD-ANN model will increase the accuracy of weld bead shape prediction and enable a fully automated electron beam welding without relying on the operator's experiences.

II. DESIGN/METHODOLOGY/APPROACH

- Several different methods are applied to predict the EBW penetration depth of S275JR plates. These methods are illustrated in Figure 1.

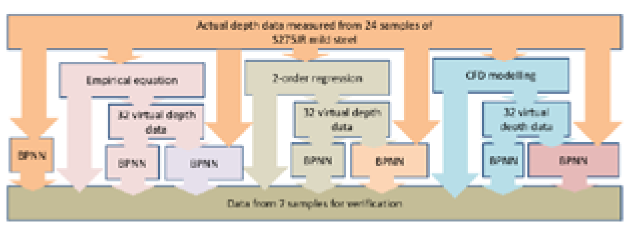

Figure 1. An Overview of Methods for Penetration Depth Prediction

- By using an EB machine developed by Cambridge Vacuum Engineering (serial no. CVE 661, maximum power 4kW and maximum voltage 60kV), the welding experiments were carried out at 40 - 60 kV accelerating voltage and 25 - 45 mA beam current at a speed of 500 - 700 mm/min in a vacuum level of 10-3 mbar. S275JR mild steel was used as the sample material in a dimension of 100*75*20 mm. A sketch of the weld trail is shown in Figure 2.
- Electron beam is characterized by a four-slit probe developed by TWI, shown in Figure. 3.
- Computational fluid dynamics modelling was carried out by using ANSYS Fluent 2020R2 with user-defined functions (UDF) written in C++ to generated virtual data. An example of simulated molten pool results is shown in Figure 4.
- The back propagation neural network was written by python keras based on training data from experiments and CFD modelling. The schematic view of the neural network is depicted in Figure 5.
- The empirical equation for penetration depth prediction is tuned by experimental data based on the method introduced by J. Elmer et al [1], shown in Equation 1.

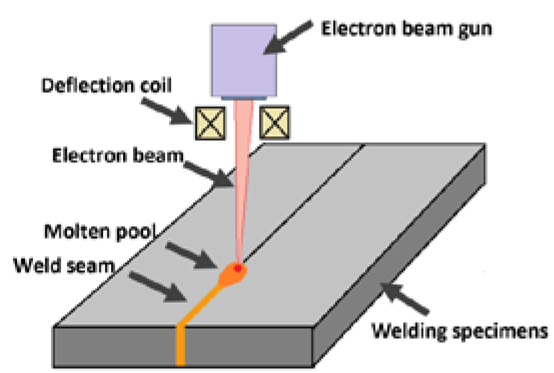

Figure 2. Design Sketch of S275JR Mild Steel Plate Welds

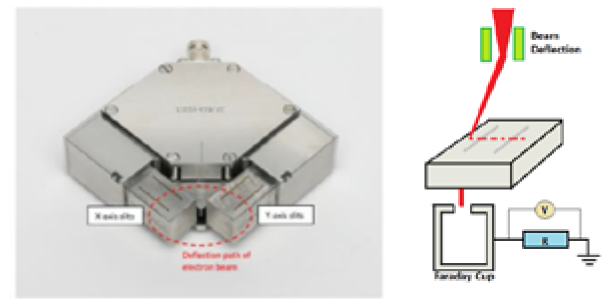

Figure 3. The Structure of BeamAssure Four-Slit Probe and the Composition Diagram of Slit Probes

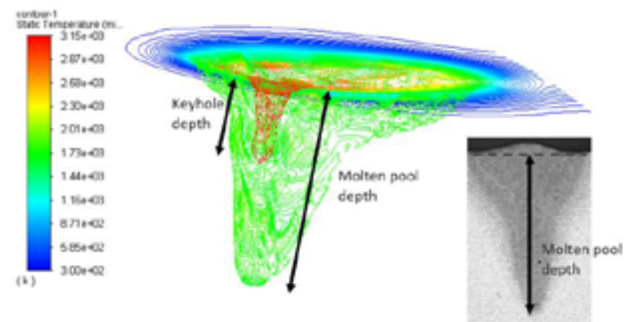

Figure 4. An Example of Molten Pool Penetration Depth Prediction by CFD Method

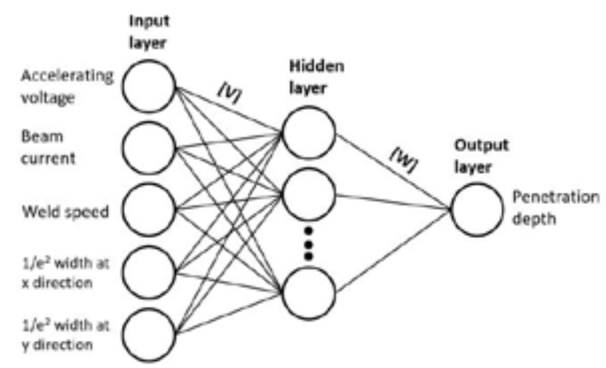

Figure 6. Schematic View of the Neural Network

$$D_p = \frac{1}{\delta} \cdot \frac{\alpha^{\varepsilon}}{k \cdot \theta_M} \cdot \frac{Q_{in}}{(V \cdot B)^{\varepsilon}} \qquad (1)$$

III. FINDINGS/RESULTS

The prediction results of each method and the average depth prediction errors are shown in Figure 6. The prediction results show that applying virtual data generated by CFD model is promising to train the neural network and remedy the defects caused by outliers of experimental data. The predicted depth error is about 7%, which is contributed by both the algorithm and the beam probing technology.

IV. DISCUSSION/CONCLUSIONS

In real production of electron beam welding, the quality prediction can be achieved by the following methods:

- For extremely limited quantity of experimental data, prediction can be made directly by CFD modelling. This method is most economic, but the modelling experience is strongly required and the prediction error is slightly high.
- For a few experimental data, CFD-ANN method introduced in this study can be applied.
- For enough experimental data, ANN can be applied directly. However, acquiring adequate data is usually expensive and time-consuming.

V. FUTURE PLAN/DIRECTION

The following work is to adopt the CFD-ANN method to predict not only weld bead dimensions but also weld quality. Besides, there can be some other measures to improve the predicted results. A more complex CFD model or more detailed beam intensity distribution may enhance the prediction accuracy.

REFERENCES

[1] W. H. Giedt and L. N. Tallerico, "Prediction of electron beam depth of penetration," Welding journal, vol. 67, no. 12, pp. 299-305, 1988.

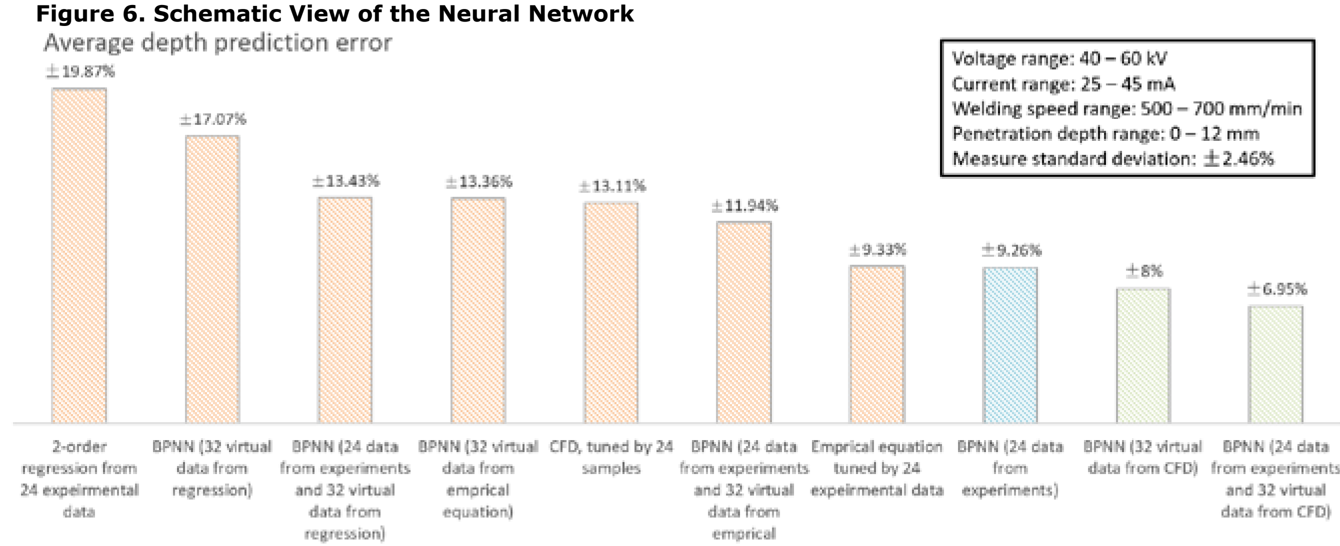

Figure 5 Average Depth Prediction Errors of Ten Methods for Weld Penetration Prediction

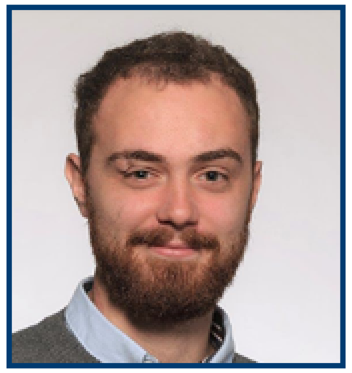

Marco Berchiolli
Marco obtained his masters' degree with first class honours in Mechanical Engineering from Brunel University. He joined Brunel Innovation Centre in 2018 as a Research Fellow in the Analytics team. His work and research lie within applied deep learning. He is responsible for the development of "small data" applications, leveraging advanced techniques to deliver deep learning models from minimal data quantities. He is sponsored by Brunel Innovation Centre.

Deep Learning Based Chest Cavity Segmentation in T1-Weighted Contrast-Enhanced Breast MRI

Professor Tat-Hean Gan[1], Professor Wamadeva Balachandran[2]
[1]TWI, [2]Brunel University London
3rd Year of PhD

Keywords: MRI, Breast, Segmentation, Convolutional Neural Networks, Deep Learning, Cancer

I. INTRODUCTION

Breast cancer is the most frequent cancer among females, consisting of 24% of all occurrences in 2018 [1]. The World Health Organisation (WHO) indicates screening programmes aimed at early detection as one of the key factors in reducing mortality [2]. While not the reference screening tool, Magnetic Resonance Imaging (MRI) is an increasingly popular procedure for the assessment of screening and treatment response [3] of high-risk groups [4]. MRI has several benefits over X-ray mammography; it is a non-ionising radiation and generates high resolution images and contains dynamic information. Moreover, recent developments in MRI image processing [5] indicate that MRI is gaining popularity even with its major drawbacks (time consuming, stressful and costly), and are actively being targeted by the research community.

The Dynamic Contrast Enhanced MRI (DCE-MRI) outputs 4D data (3D spatial + 1D temporal), consisting of images acquired before and after the intravenous injection of a contrast agent. The anomalous response of the tissues to such agent is indicative of the presence of lesions [6]. Such patterns, unfortunately, are extremely similar to the ones of the internal organs such as the heart. Therefore, the automatic removal of the internal organs from the images is instrumental to the development of an automatic lesion detection methodology, as manual delineation of the chest wall is an extremely time-consuming activity.

This paper proposes a novel, deep learning-based methodology for the segmentation of the inner portion of the chest from DCE-MRI scans.

II. DESIGN/METHODOLOGY/APPROACH

The segmentation model is based on a Dynamic UNet with a pre-trained ResNet encoder. A transfer learning approach was utilised with a pre-trained ResNet encoder to address the challenge of insufficient training data. Transfer learning [7] is a widely used technique in computer vision tasks outside of medical image segmentation [8-9]. In order to leverage transfer learning, the technique employed in the proposed solution is the Dynamic UNet [10], based on the original Unet proposed by Ronneberger et al. [11]. A UNet architecture was chosen as it is the best methodology in terms of overall performance in medical imaging applications [12]. The flexibility derived from using custom encoders provided by Dynamic UNet allows for a much greater degree of exploitation of transfer learning.

The original UNet architecture can be divided into an encoding part, or "downsampling", and a decoding part, or "upsampling". The encoding side performs a similar task to a conventional convolutional neural network, with regular downsampling steps, performed through the maxpool operation. At the same time, the decoding path follows a symmetrical structure, with the upsampling steps performed through a fractionally-strided convolution layer. The symmetry allows for the activations of the downsampling layers to be concatenated to the activations of the upsampling layers, thus better retaining spatial information throughout the upsampling path.

The Dynamic UNet architecture was originally presented by Iglovikov and Shvets [13]. It follows the same basic architecture as the original UNet but adds a pre-trained model as the encoder. The approach not only achieves considerable improvements over the traditional UNet, but it also allows to experiment with a variety of pre-trained

encoders [13]. In this study, the use of ResNet encoders were used , as it has been demonstrated that they reduce the reliance on regularisation techniques [14].

ResNets were first introduced in 2015 [15] as a way to counteract the vanishing/exploding gradient problem in deeper networks, which had been a mainstay challenge in the deep learning research field since the inception of ConvNets [16]. The fundamental component of a ResNet is the residual block, which is also known as "skip-connection". The input to the block is passed through an identity mapping and is summed to the activation of a series of convolutional layers. ResNets are able to reach theoretically infinite depths, due to the self-regularisation method provided by the identity mapping [17]. The flexibility of ResNets allows to train for longer (more epochs), thus reducing the likelihood of overfitting [18].

The experiments included adding a self-attention layer [19], featuring a skip connection in the form of:

$$y_i = \gamma o_i + x_i$$

Where γ is a learnable parameter which scales the output of a self-attention layer and x_i is the input of the layer.

III. FINDINGS/RESULTS

The best performing configuration was found using a ResNet34 backbone, with a blurring mechnism inserted in the upsampling path of the network, in the form of an average pooling layer after each activation.

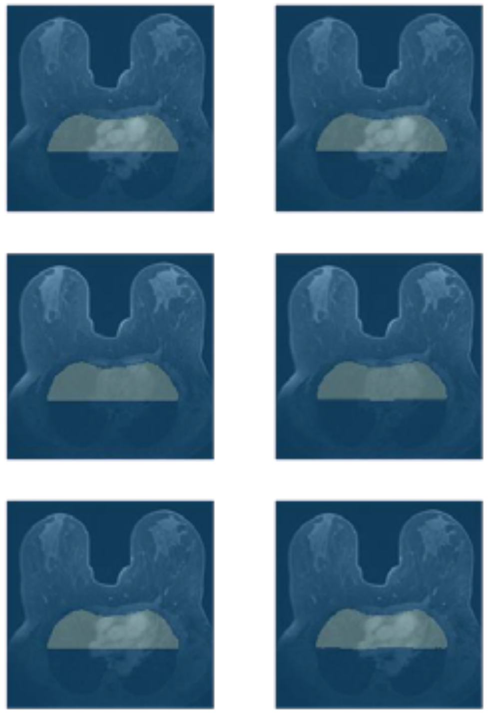

Figure 1. Ground truth (left) vs output of the best performing network configuration (right).

The results shown above are taken from the validation set. On the left, the manually labelled image. On the right, the output of the network.

The average Dice Similarity Coefficient (DSC) on the validation set was 0.936. The average Jaccard Similarity Coefficient (JSC) was 0.887. Applying a simple algorithm to correct the artifacts at the bottom boundary of the mask (consequence of an aggressive data augmentation strategy) brought the DSC and JSC to 0.961 and 0.979 respectively.

IV. DISCUSSION/CONCLUSIONS

The results dramatically improve on the current state of the art [20], and could be further improved by having access to more data. Experiments showed the amount of data to be insufficient to train a ResNet50 backbone.

V. FUTURE PLAN/DIRECTION

Future research should be focused to improve inference and postprocessing timings (10 ms/image at the moment, 127 s for a whole case). Desireable timings would be below 1 minute/case.

REFERENCES

[1] https://pubmed.ncbi.nlm.nih.gov/30207593/
[2] https://pubmed.ncbi.nlm.nih.gov/25220842/
[3] https://pubmed.ncbi.nlm.nih.gov/24738612/
[4] https://www.ncbi.nlm.nih.gov/pmc/articles/PMC4960688/
[5] https://arxiv.org/abs/1811.08839
[6] https://pubmed.ncbi.nlm.nih.gov/22245697/
[7] https://ieeexplore.ieee.org/document/7333916
[8] https://link.springer.com/chapter/10.1007/978-3-030-01424-7_27
[9] https://papers.nips.cc/paper/2019/file/eb1e78328c46506b46a4ac4a1e378b91-Paper.pdf
[10] https://arxiv.org/abs/1801.05746
[11] https://link.springer.com/chapter/10.1007%2F978-3-319-24574-4_28
[12] https://www.ncbi.nlm.nih.gov/pmc/articles/PMC7327346/
[13] https://arxiv.org/abs/1801.05746
[14] https://arxiv.org/abs/1901.09321
[15] https://arxiv.org/pdf/1512.03385
[16] https://papers.nips.cc/paper/2012/file/c399862d3b9d6b76c8436e924a68c45b-Paper.pdf
[17] https://arxiv.org/pdf/1512.03385.pdf
[18] https://arxiv.org/pdf/1512.03385.pdf
[19] https://arxiv.org/pdf/1409.0473.pdf
[20] https://www.sciencedirect.com/science/article/pii/S0933365718306985

Norbert Sieczkiewicz

Norbert received his education in Mechanical Engineering (BSc) and Materials Science (MSc) from the West Pomeranian University of Technology in Poland. He also undertook the Erasmus+ programme studying at Técnico Lisboa in Portugal, where he did freelance work for ISQ related to Microbond and FSW-TECH projects. He did an International Welding Engineer diploma and his previous work was related to resistance welding, 3D printing and optical metrology. He joined the NSIRC PhD programme in March 2019 with the University of Lancaster and sponsored by Lloyds Register Foundation. His research examines the electron beam quality assurance and he is currently in the 3rd year of his studies.

Electron Beam Characterisation Using Time Series Imaging and Deep Learning

Dr Colin Ribton[1], Prof. Andrew Kennedy[2], Dr Yingtao Tian[2] and Dr Darren Williams[2]
[1]TWI, [2]Lancaster University
3rd Year of PhD

Keywords: Industry 4.0, electron beam welding, computer vision, artificial intelligence, smart manufacturing, multisensor fusion

I. INTRODUCTION

The electron beam powder bed and wire-feed additive manufacturing (EBAM) processes have the potential for small-batch productions of full-density metallic parts with excellent integrity. It is used for high-value components in biomedical and aerospace, with prospects for other applications. Solidification microstructure and mechanical properties are affected by various processing parameters, but to ensure the highest process stability the beam focus needs to be precisely monitored. This parameter needs to be precisely monitored as it affects melt pool shape, energy deposition, microstructure and temperature gradients. The objective of this study was to develop an automated segmentation and classification model to distinguish between various focus states and predict focus location based on a deep learning approach. As Industry 4.0 is based on machine learning and multisensor data fusion, which combines information from several sources to find a robust process window, our focus detection model can be used with additional sources of data. These include, but are not limited to: a high dynamic range (HDR) camera, backscattered electron detector and white light interferometry to measuring the weld pool depth, width and bead profile. AI tools will be used to correlate the data streams from these sensors with weld quality in a controlled experiment, designed to be relevant to the aerospace and nuclear industries. The output from this work when applied in production manufacture is expected to provide high confidence quality assurance in real time for the electron beam process.

II. DESIGN/METHODOLOGY/APPROACH

A. Beam probing using BeamAssure™

A BeamAssure probe head was used in this work to provide signals representing the beam current distribution over the beam spot.

The automatic segmentation and classification developed in this work comprises three parts:

- signal segmentation,
- encoding the electron beam pulses as images,
- usage of a convolutional neural network for image classification.

In this work the accuracy of classification of time-series images obtained from different encoding methods such as Recurrence Plots (RP), Gramian Angular Fields (GAF), and Markov Transition Fields (MTF) [1] were compared and concatenation of images from these different methods was explored.

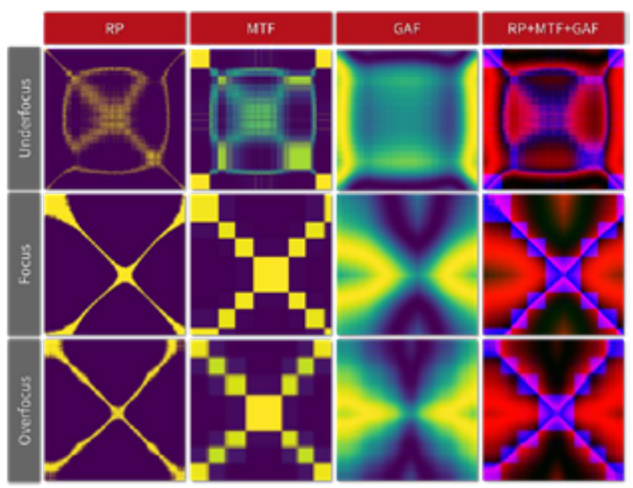

Figure 1. Different encoding methods revealed distinguishable patterns of the BeamAssure signal

B. Backscattered electrons collector plate

When electrons hit a workpiece various scattering processes occur in the material [2]. Those backscattered electrons are detected using a ring-shaped aluminium detector plate mounted on the top of the vacuum chamber, so the beam can pass through it freely. Electrons hitting the detector plate are guided through a 100Ω resistor to a USB oscilloscope (PicoScope 3203D). The signal is currently analysed using the same time-series imaging techniques as described in Part A.

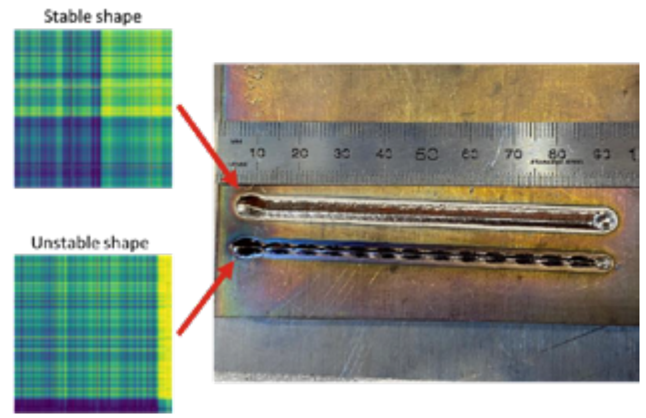

Figure 2. GAF images (left) and corresponding meltruns shapes

C. Multisensor fusion preparatory actions

In order to develop correctly timestamped measurement system synchronization, it is required to trigger all devices at the same time. This is done by a combination of software and hardware triggers commanded by a programmable logic controller (PLC) for actions such as the welding process start and stop. Additionally, to make the raw output of the sensors straightforward to analyse, data is organized and formatted to create structured data labels.

III. FINDINGS/RESULTS

A.

Markov Transition Field images, generated from probe signal and classified by ResNet models, give the lowest accuracy results (80.3%) between four described encoding methods. The Gramian Angular Field encoding increases the accuracy to 94.56% and Recurrence Plots can increase the score slightly up to 94.64%. The highest accuracy was obtained using concatenated images. The combined effect of all RGB layers connected allows neural network to correctly classify beam focus conditions with an accuracy as high as 98.66%.

Deep and complex neural networks are not needed to classify BeamAssure signals encoded as images. It was proven, for BeamAssure signal dataset, that smaller ResNet architectures like ResNet-34 achieved the same accuracy as deeper ones such as ResNet-50 and ResNet-101. Such models require less storage for their model parameters, so they can be used in embedded industrial systems

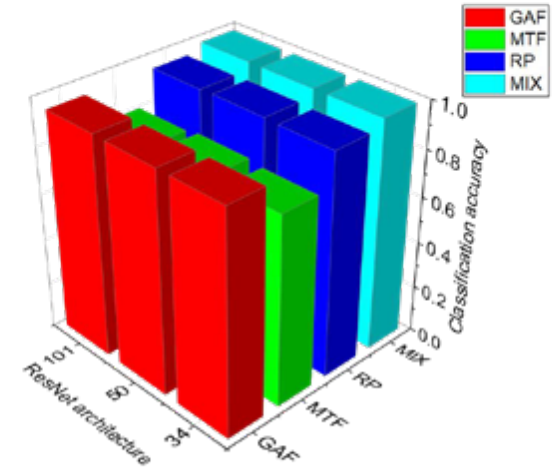

Figure 3. The classification accuracy on unseen data, including different ResNet deep learning architectures and encoding method

B.

First preliminary trials showed, that the stability of meltruns can be detected by analysing the Gramian Angular Field encoded images. Meltrun welds with higher shape instability are described by GAFs with characteristic bars and lines around the edges of the image, as opposed to stable process images which are more evenly distributed.

IV. DISCUSSION/CONCLUSIONS

- Results obtained from the beam focus detection model and preliminary signal analysis from the backscattered electrons collector plate are promising solutions for quality assurance.
- Supporting BeamAssure signal processing with time-series imaging allows using just one beam probe signal, instead of multiple focus current measurements.
- The backscattered electron collector plate outputs a signal, which can be used to differentiate between stable and unstable meltruns.

V. FUTURE PLAN/DIRECTION

As future work, a multisensor fusion experiment will be conducted with additional data sources such as an HDR camera and white light interferometry. It is anticipated that a complex neural network model will be able to predict the quality of the weld with greater accuracy than separate sensors.

REFERENCES

[1] Sánchez, Sara Hernández, Rubén Fernández Pozo, and Luis Alfonso Hernández Gómez. „Deep Neural Networks for Driver Identification Using Accelerometer Signals from Smartphones." International Conference on Business Information Systems. Springer, Cham, 2019.
[2] Reisgen, U., et al. "Determination of the influence of welding parameters on the efficiency of electron beam welding by measurement of backscattered electrons." Vacuum 159 (2019): 182-185.

Mohammad Khairy
Mohammad firstly joined NSIRC in 2017 where he received an MSc degree in Structural Integrity from Brunel University London. He started his PhD in 2019 with Brunel University London and sponsored by TWI. His research examines the influence of the addition of hydrogen to vacuum furnace during brazing of stainless steel, on the quality of the brazed joints.

Effect of Partial Pressure of Hydrogen on Vacuum Brazing of 316L Stainless Steel

Paul Brooker [1], Nick Ludford[1], Hari Babu Nadendla [2]
[1]TWI, [2] Brunel University London
3rd Year of PhD

Keywords: Vacuum brazing, hydrogen, wetting stainless steel, 316L

I. INTRODUCTION

Brazing is a thermal joining process where the filler metal melts and flows into a gap between the parts to be joined, driven by capillary action (Fig.1).

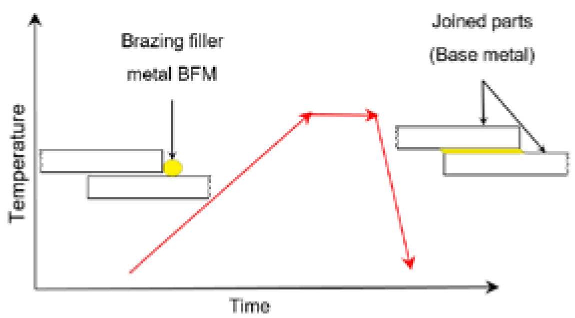

Figure 1: Typical brazing cycle

For quality joints, the filler must completely wet the faying surfaces, therefore, the brazing atmosphere is adapted so that any surface Oxides, which impede wetting, are reduced and do not re-form during the brazing cycle, an example of poor wetting is shown in Figure 2.

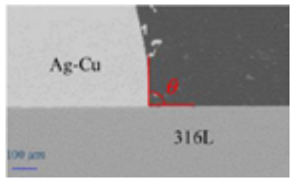

Figure 2: Cross-sectional image of Ag-Cu filler on 316L stainless steel substrate showing a typical a non-wetting ($\theta \approx 90^o$) condition.

Vacuum is widely used as brazing atmosphere; however, for materials with stable oxide film such as stainless steels, the brazing is performed at a relatively high temperature [1], which deteriorates the tensile properties. The introduction of partial pressure of hydrogen, as a reducing agent, could help reduce the processing temperature.

II. THEORETICAL BASIS

The surface energy of liquid metal/vapour and liquid metal/Oxides interface are high, compared to low temperature liquids such as water; which leads to non-wetting conditions; therefore, the removal of the thin protective oxide film on the stainless steels surface is prerequisite to achieve good wetting.

The formation or dissociation of metal (M) oxides may be represented by the following reversible reactions:

$$a\mathrm{M} + {}^{1}/_{2}\, b\mathrm{O}_2 \Leftrightarrow \mathrm{M}_a\mathrm{O}_b \qquad \text{Eq.1}$$

The driving force for the reaction at a temperature T is the change in Gibbs energy $\Delta \boldsymbol{G}$, which is given by:

$$\Delta G_1 = \Delta G^0_{\mathrm{M}_a\mathrm{O}_b} + RT\ln\left(P_{O_2}\right)^{-0.5b} \qquad \text{Eq.2}$$

Where,

$\Delta G^0_{M_aO_b}$ The standard Gibbs energy of the formation of the metallic oxide $\mathrm{M}_a\mathrm{O}_b$

R Gas constant

P_{O_2} partial pressure of Oxygen

Accordingly, below a specific partial pressure of Oxygen (known as dissociation pressure), the backward reaction is favoured. i.e. the oxide dissociates. Similarly, the amount of Oxygen in a hydrogen-containing atmosphere is maintained through the following reaction:

$$\mathrm{H}_2 + {}^{1}/_{2}\, \mathrm{O}_2 \Leftrightarrow \mathrm{H}_2\mathrm{O} \qquad \text{Eq.3}$$

$$\Delta G_2 = \Delta G^0_{H_2O} + RT\ln\frac{1}{(P_{O_2})^{0.5}} \times \left(\frac{P_{H_2O}}{P_{H_2}}\right) \qquad \text{Eq.4}$$

Given that $\Delta G^0_{M_aO_b}$ and $\Delta G^0_{H_2O}$ are obtainable from the available thermodynamic data [2], at a given temperature, P_{O_2} is only controlled by $\frac{(P_{H_2O})}{(P_{H_2})}$ ratio [3].

To ensure that the hydrogen concentration remains below the flammability limit, the gas is supplied as a mixture of $\mathrm{H_2}$ and $\mathrm{N_2}$ or Ar. Accordingly, $\frac{(P_{H_2O})}{(P_{H_2})}$ratio is limited by the concentration of $\mathrm{H_2}$ and the water content.

III. METHODOLOGY AND EXPERIMENTAL APPROACH

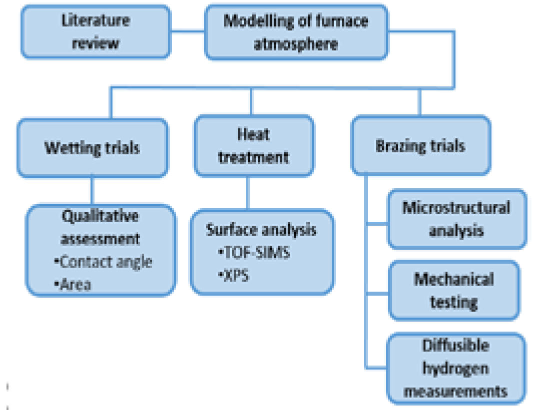

Figure 3: Methodology and experimental approch

Wetting and brazing trials are conducted in a vacuum furnace (Figure 4). The brazing filler metal is made of 72%Ag 28%Cu eutectic alloy. At the full vacuum mode, the pressure is maintained through the diffusion pump; the roughing pump maintains the pressure after the introduction of ($\mathrm{N_2/H_2}$) gas mixture.

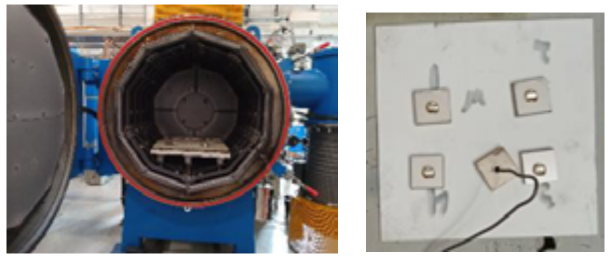

(a) (b)

Figure 4: (a) Vacuum furnace. (b) Disc-shaped Ag-Cu brazing filler placed on 316L steel substrate for wetting trials.

A typical pressure and temperature cycle that applied to wetting trials are shown in Figure 5.

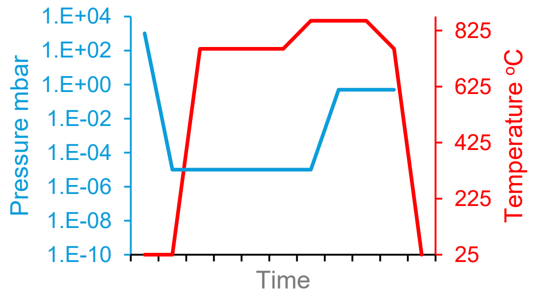

Figure 5: Pressure and temperature cycle for wetting trials of 72%Ag-28%Cu eutectic brazing filler on 316L stainless steel.

IV. RESULTS AND FINDINGS

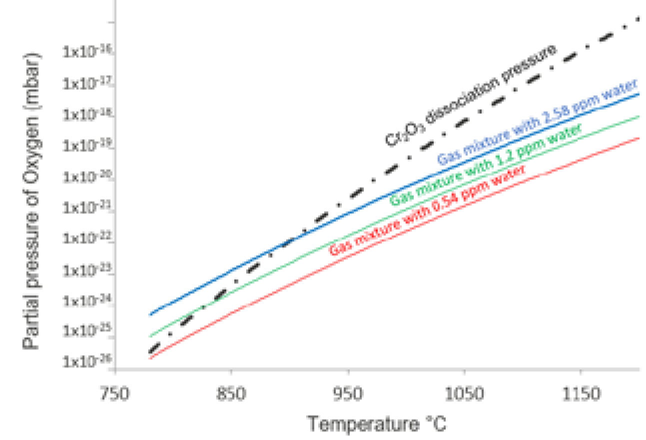

Figure 6: The partial pressure of Oxygen in 95/5 $\mathrm{N_2/H_2}$ mixture; compared to the dissociation pressure of $\mathrm{Cr_2O_3}$.

Figure 6 shows the dissociation pressure of $\mathrm{Cr_2O_3}$ compared to the oxygen content in a vacuum furnace filled with a mixture of $\mathrm{N_2/H_2}$. The figure indicates that in order to reduce $\mathrm{Cr_2O_3}$, the water content of the supplied gas shall be below 1.2 ppm, it is worth noting that $\mathrm{Cr_2O_3}$ is the most stable oxide within the 316L oxide film, therefore, such conditions should effectively remove the oxide film from 316L stainless steel surface.

Figure 7: Results of wetting trial performed at 860 °C, the contact angle $\theta \approx 63^o$

The preliminary wetting trials results (Figure 7) indicates poor wetting, no conclusions have been drawn yet, one of the factors being considered is the increasing the purity of the gas mixture.

V. FUTURE PLAN

To carry on the proposed experimental approach using a gas mixture with less than 0.6 ppm water content.

REFERENCES

[1] Brazing handbook. Fifth Edit. AWS. Miami: American Welding Society; 2007.
[2] Haynes WM, editor. CRC Handbook of Chemistry and Physics. 97th Editi. London: CRC Press; 2017.
[3] MOORE JJ. Chemical Metallurgy. Second Edi. Butterworth & Co. (Publishers) Ltd; 1990.

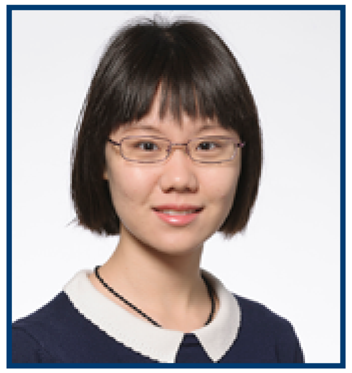

Tianmiao Li

Tianmiao completed her BSc in Polymer Science and Engineering at Beijing University of Chemical Technology (China) and MSc at Loughborough University. After her MSc, she continued her PhD study in TWI as an NSIRC student of Loughborough University. She thought research based in an industry/company environment could shape one's thinking of both theoretical and practical. Tianmiao's PhD project is to study how good cold atmospheric plasma (CAP) surface treatment can be on different materials. She is now in the second year of her PhD focusing on the effectivness of CAP on the surface treatment of Aluminium alloy.

The Using of Cold Atmospheric Plasma to Enhance Adhesive Bonding

E. J. C. Kellar[1], G.W. Critchlow[2]
[1]TWI, [2]Loughborough university
3rd Year of PhD

Keywords: Plasma, surface treatment

I. INTRODUCTION

Atmospheric plasma is a popular technology for effective surface treatment of many substrates. For adhesive bonding of low surface energy materials in particular, surface treatment is crucial. It is usually conducted just prior to the adhesive bonding process to enhance the adhesion properties of the adherend surfaces. Atmospheric plasma has been shown to provide an effective surface treatment for polymers such as polyethylene (PE). In recent years, it has also been investigated as a surface treatment for metals as an alternative to wet etching processes. In the case of stainless steel (316 grade), it has been demonstrated that atmospheric plasma surface pre-treatment can achieve bond strengths equivalent to that obtained with an acid etching process [1]. As chemical etching for different metals requires different chemistries, production flexibility can be limited to certain classes of materials. In contrast, atmospheric plasma has the potential to become a universal treatment technology, with the same equipment being able to treat many different types of materials, including polymers and metals, with the only variables being easily adjustable equipment settings such as exposure type, power and feed gas composition.

II. DESIGN/METHODOLOGY/APPROACH

The cold plasma generating system used in this project is shown in Figure 1. It includes a microwave plasma generator, a mass flow controller, an XYZ stage with the plasma torch attached, and a computer. The plasma generator was an AdTec-Europe PlasmaTact. The maximum output power of the plasma generator is 30W.

Figure 1. The main components of the plasma generating system used in this work.

The material used in the first stage was Al2024 T3, which is widely used in aircraft. The adhesive was Redux 319 provided by Hexcel. It is a high strength single part epoxy film adhesive designed for aluminium bondings. The material for the second stage of the project was 62%wt glass fibre reinforced PE provided by Hive Composit Ltd. The adhesive used for the glass-PE composit was Araldite 2021-1.

This work investigated the relationship between the treatment effect, including surface free energy and lap shear strength, and different plasma settings i.e. exposure time, generation power and working distance. Surface analysis technologies including FTIR, XPS, contact angle, and SEM were used to study the mechanism of the plasma treatment.

III. FINDINGS/RESULTS

The mechanical test result showed that the bond strength of both aluminium alloy and glass-PE composite was increased significantly after a plasma treatment. The strength of the plasma treated aluminium alloy joints reached ~90% of that of chromic acid etched (CAE) ones (Figure 2) and an effective plasma treatment can double the bond strength of a glass-PE composite joint (Figure 3).

The surface free energy results, shown in Figures 4 and 5 indicated that after plasma treatment, the surface free energy of both aluminium and glass-PE were increased.

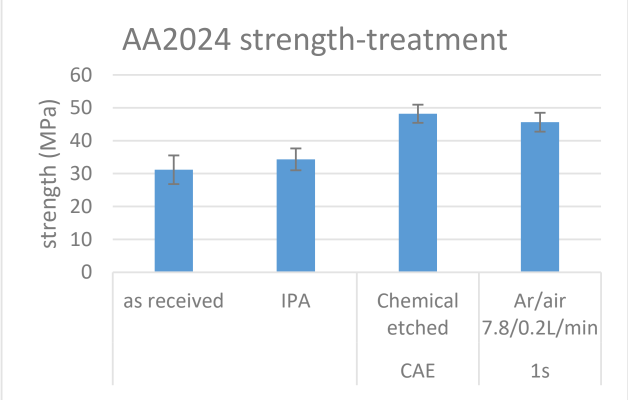

Figure 2. lap shear strength of aluminium bonds with different surface treatments.

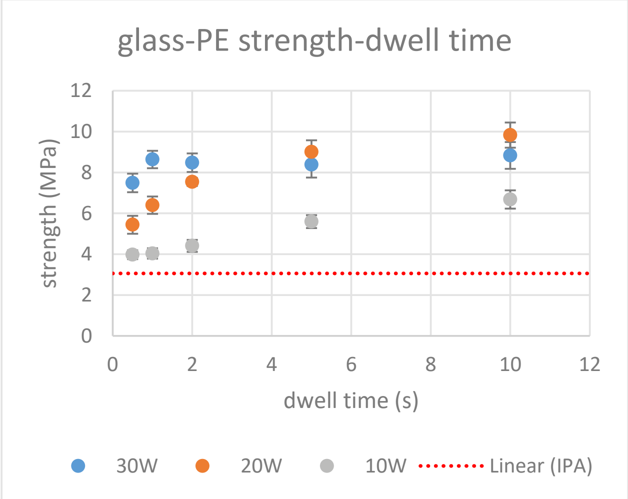

Figure 3. lap shear strength of glass-PE joints with different plasma power and dwell time.

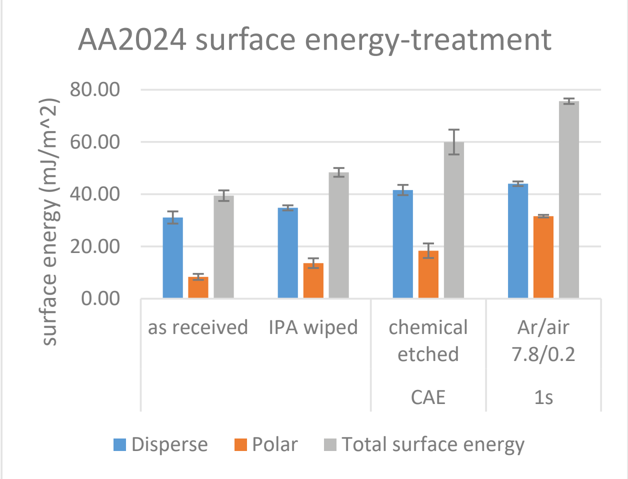

Figure 4. Surface free energy results of aluminium with different surface treatments.

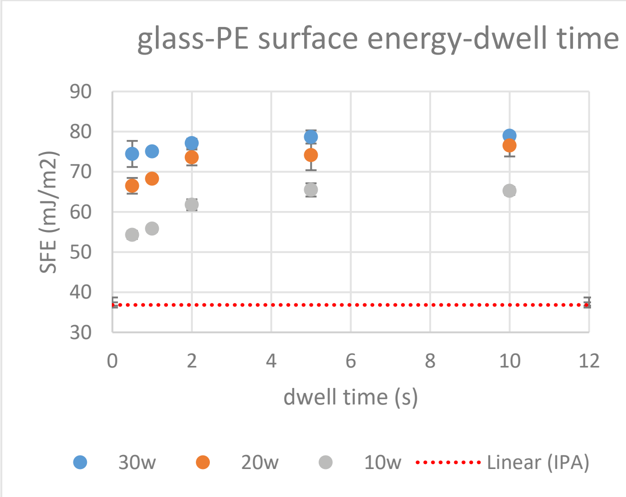

Figure 5. Surface free energy results of glass-PE with different plasma power and dwell time.

IV. DISCUSSION/CONCLUSIONS

In the contact angle test, the disperse part of surface free energy can reflect to the roughness of a surface, and the polar part can reflect to the surface chemistry. From the results, it can be known that plasma treatment is likely to increase the wetablity of an aluminium surface by enhancing the polar distribution of the surface energy and then improve the bond strength.

For achieving an appropriate treatment, it usually requires iterative adjustments of the plasma parameters. The surface energy of plasma treated glass-PE surfaces are in the same trend of their lap shear strength. Therefore, for glass-PE composite, surface energy could be a way to predict the effect of a plasma treatment for adhesive bonding.

V. FUTURE PLAN/DIRECTION

Future work will focus on analysing the chemical and physical changes of the aluminium and glass-PE surface after different plasma treatments. XPS, SEM and FTIR will be used. In addition, the durability of plasma treated aluminium bonds will be studied by doing the Boeing wedge test.

VI. ACKNOWLEDGEMENTS

I would like to acknowledge my supervisors and colleagues at TWI and Loughborough University. I am very grateful for funding provided by NSIRC, TWI Ltd and Loughborough University for this project.

REFERENCES

[1] Williams, D.F. et al., 2017. Surface analysis of 316 stainless steel treated with cold atmospheric plasma. Applied surface science, 403, pp.240-247.

Chiamaka Emilia Mbanusi

Chiamaka received BEng in Mechanical Engineering degree (first class honours) from University of Benin, Edo State Nigeria in 2016, and MSc in Advanced Mechanical Engineering (distinction) at Cranfield University funded by Commonwealth Scholarship Commission. She started Emilia Science /Mathematics Project which was a volunteering project to educate and encourage young students in embracing STEM subjects. She joined the NSIRC programme in May 2019 with Lancaster University and sponsored by Lloyd's Register Foundation. Her research is based on development of methods for the evaluation of material properties at high strain rate loading conditions and presently in the 3rd year of her studies.

Dynamic Fracture Toughness of Metallic Materials at Very High Loading Rates

Dr Yin Jin Janin[1], Prof Pedro Rivera-Diaz-Del-Castillo[2]
[1]TWI, [2] Lancaster University
3rd Year of PhD

Keywords: High strain rate loading; Johnson-Cook; dynamic test; controlled drop weigh; dislocation evolution

I. INTRODUCTION

Testing of materials at high strain rates introduces some technical challenges e.g. huge oscillations which could mask the true response of the material under dynamic loading. Quasi-static fracture toughness testing procedures are well defined within various British Standards (BS) and American Society for Testing and Materials (ASTM), but there is currently no comprehensive standard for high strain rate tests.

Strain gauges are fit for tesile test and clip gauges for fracture toughness test under quasi-static loading to monitor and record the displacement during deformation, making it easy to derive the strain for material properties determination. The procedure is significantly different when determining dynamic tensile and fracture toughness properties as they do not allow recording of test data using strain and clip gauges easily. The only testing procedure for dynamic fracture toughness is BS 7448-3[1], which is rather outdated and inconsistent with modern testing equipment and measurement techniques. In addition, very little guidance on the treatment of oscillations (or ringing effects) in the experimental load-displacement curve is available.

A possible technique to supplement this type of testing is digital image correlation (DIC) which utilizes high speed camera to capture the deformation, thereby providing the strain to determine the material properties at high loading rates. This study was carried out to determine how material properties would be affected under dynamic loading by means of various testing at both static and high strain rates. The investigation included tests such as quasi-static tensile, dynamic tensile, and controlled drop weight on a well characterised pipeline grade material API 5L X65.

To describe the behaviour of the material at high strain rate, Johnson-Cook (JC) model was applied. The model takes into account three major effects which are; strain hardening, strain rate dependence and temperature. The constants used in JC plasticity and damage models were derived from experimental data. These were then incorporated in finite element method (FEM) to simulate the effect of strain rates.

II. WORK CARRIED OUT

Tests were carried out to characterise the material properties at high strain rate loading. Quasi-static tensile tests were conducted at room temperature in accordance with BS EN ISO 6892-1[2] under displacement control mode to determine the mechanical properties at room temperature.

Table 1: Mechanical properties of API 5L X65 steel

Strain Rate	Young Modulus (GPa)	0.2% proof strength (MPa)	Ultimate tensile stress (MPa)	Elongation (%)
Static	210	486	600	27
Dynamic	240-460	640-688	740-856	27-30

The tensile tests at high strain rate were performed in accordance with BS EN ISO 26203-1 using B1003 INSTRON VHS machine. The machine comprises of the high rate actuator with maximum velocity up to 20 m/s. Specimen geometry is shown in Figure 1 and test setup in Figure 2.

High strain tensile tests results (shown in Table 1) were analysed and strain rate-dependent parameters were subsequently determined. A conventional approach such as Levenberg-Marquardt algorithm (in MATLAB) was used to fit the damage parameters D_1 to D_3 from the plot of fracture strain against triaxiality.

Figure 1: Specimen geometry for the high strain rate tensile testing (All dimensions in mm)

Figure 2: B1003 INSTRON VHS machine with a mounted flat tensile specimen sprayed with speckles ready for high-strain ratetesting

Quasi-static fracture toughness tests were carried out on EDM notched specimens (with different crack depths) to determine the resistance curve using ISO 12135 [3] procedure on the Instron 8801 B910 machine at room temperature with a_0/W of 0.2 and 0.5.

To define the relationship between stress and strain at high strain rate, JC model in Equation 1 was employed. Flow stress behaviour in terms of strain hardening, strain rate dependence and an effective temperature components can be defined:

$$\sigma = (A + B\varepsilon^n)(1 + C\ \ln \dot{\varepsilon}_p^{\,*})(1 - \ T^{*m}) \quad \text{Eqn 1}$$

Where A, B, n, and C are yield stress at reference conditions, strain hardening constant, strain hardening coefficient and strengthening coefficient of strain rate respectively. σ is the effective stress, ε is the equivalent plastic strain [4] , $\dot{\varepsilon}_p^{\,*} = \dot{\varepsilon}_p/\dot{\varepsilon}_0$, $\dot{\varepsilon}_p$ is the plastic strain rate, $\dot{\varepsilon}_0$ reference strain rate taken as $1\,s^{-1}$, $T^* = \frac{T-T_R}{T_m-T_R}$, where T is deformation temperature, T_R is reference temperature, and T_m is melting temperature. Also, JC damage model is given as:

$$\varepsilon_f \ = [D_1 + \ D_2 \exp(D_3\, \sigma^*)][1 + \ D_4 \ln(\ \dot{\varepsilon}_p^{\,*})]\ [1 + \ D_5\, T^*] \quad \text{Eqn 2}$$

where ε_f is the equivalent strain at failure, $D_1 - D_5$ are damage coefficients/parameters, $\sigma^* = \frac{\sigma_m}{\sigma_{eq}}$ is the triaxiality factor, σ_m mean stress, σ_{eq} equivalent stress.

III. FINDINGS/RESULTS

It was found that the EDM notched specimens were not suitable to construct resistance curves as the points were mostly invalid according to BS ISO 12135 [3]. Hence, fatigue pre-cracked specimens are being prepared.

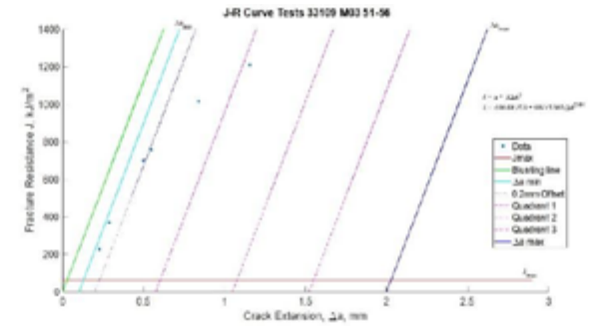

Figure 3: J-R Curve for multi-specimen at a/W=0.2

The JC-constants determined from experimental analysis were implemented in a dynamic explicit FEA. It was observed that FEA did not predict crack propagation (as seen in experiments) therefore machine learning will be used to find the best fit JC constants.

IV. DISCUSSION/CONCLUSIONS

Investigations on SENB fracture test were carried out on EDM notched sub-sized specimen with a_0/W of 0.2 and 0.5, and both were not fit for J R-curves and CTOD R-curves. Experimental and numerical models obtained with JC constants does not show good agreement. The high strain rate tensile result showed to be higher than the static counterpart.

V. FUTURE PLAN/DIRECTION

Machine learning will be implemented to optimise best fit JC constants to apply in FEM model of 3-point bend fracture toughness. In addition, a dislocation evolution model will be applied to analyze the flow stress at high strain rate thereby characterising the material behaviour at room temperature.

REFERENCES

[1] BS 7448-3:2005 "Fracture mechanics toughness tests. Method for determination of fracture toughness of metallic materials at rates of increase in stress intensity factor greater than 3.0 MPam$^{0.5}$ s^{-1}".

[2] BS EN ISO 6892-1:2019 "Metallic materials. Tensile testing. Method of test at room temperature".

[3] ISO 12135:2016 "Metallic materials. Unified method of test for the determination of quasistatic fracture toughness".

[4] M. A. Meyers, Dynamic Behaviour of Materials. 1994.

Zeng Chen

Zeng is currently a 2nd year PhD student and a member of the Solid Mechanics Research Group at the University of Bristol. He graduated with his Bachelor and Master degrees at the Hefei University of Technology in China. With the sponsorships of TWI Ltd and China Scholarship Council, Zeng started his PhD programme in 2019. His research focuses on improving the approach of assessing the apparent fracture toughness caused by a change in crack-tip constraint, which can assist with making less conservative structural integrity assessment to potentially reduce costly repair and replacement decisions for plant operators.

Evaluation of Applicability of Different Constraint Parameters in Brittle SEN(B) Specimens

Rob Kulka[1], Mahmoud Mostafavi[2]
[1]TWI, [2]University of Bristol
2nd Year of PhD

Keywords: Constraint, Parameter Q, Plastic zone, SEN(B) specimen

I. INTRODUCTION

The crack-tip constraint is defined as the resistance of a structure against crack-tip plastic deformation [1]. It is found that the constraint has a significant relationship with fracture toughness. A high constraint component has a lower fracture toughness, while a low constraint component shows a higher stress intensity factor at fracture. Thus, to make a less conservative structural integrity assessment to potentially reduce costly repair and replacement decisions for plant operators, it is necessary to study an approach of quantifying the level of crack-tip constraint and evaluating the apparent fracture toughness caused by the change in crack-tip constraint.

Crack-tip constraint can be divided into in-plane and out-of-plane components. In real industry projects, these two constraints mix at the same time. For those complicated cases, single constraint parameters, such as T-stress and T_z, which can characterize only one constraint, are no longer applicable. Thus, a unified parameter φ is proposed with the crack-tip plastic zone area. It is validated that φ is sensitive to both constraints [2]. However, recent research shows in-plane constraint parameter Q can also partially quantify two constraints [3]. Therefore, in this abstract, the applicability of φ and Q are compared by using the test data of Al7075 T651 steel and a number of numerical results.

II. METHODOLOGY

Parameter Q is defined as the deviation between the crack-tip stress field and a reference stress field at a point ahead of the crack tip:

$$Q = \frac{\sigma_{\theta\theta} - \sigma_{\theta\theta}^{ref}}{\sigma_{\theta\theta}}, at\ r = \frac{2J}{\sigma_0}\ and\ \theta = 0 \qquad (1)$$

Where $\sigma_{\theta\theta}$ is the opening stress.

φ is defined as the crack-tip plastic zone area ratio [2]:

$$\varphi = \frac{A_c}{A_{ref}} \qquad (2)$$

where A_c is the area of the plastic region at fracture and A_{ref} is the reference plastic region at fracture for a standard specimen.

To evaluate the effectiveness of these two parameters to both constraints, a series of experiments and simulations were done. The experiments were conducted by Simon Tonge, my colleague in the Solid Mechanics Research Group at the University of Bristol. Nine different geometries of SEN(B) specimens were tested, that present nine different mixed constraint levels. All specimens were cut from a Al7075 T651 steel plate (Young's Modulus = 71.7GPa, Poisson's ratio = 0.33, Yield Stress = 450MPa).

The numerical modelling was conducted with ABAQUS 6.14. Due to the SEN(B) specimen's symmetry, one-quarter model was adopted which can be seen in Figure 1. 8-noded quadratic elements with reduced integration (C3D8R) were applied. An initial blunted notch with a radius of 2.5 µm was introduced to model the EDM wire seam. The load roller and a support roller were created as rigid bodies, and the contact condition between them and the specimen was defined as surface-to-surface contact with a finite-sliding formulation. The modelling was conducted by applying a load-line displacement (VLL) to the load roller in the Y direction. All simulation outputs were extracted at the midplane. The contour output, J-integral, was considered to use the results at the 10th contour.

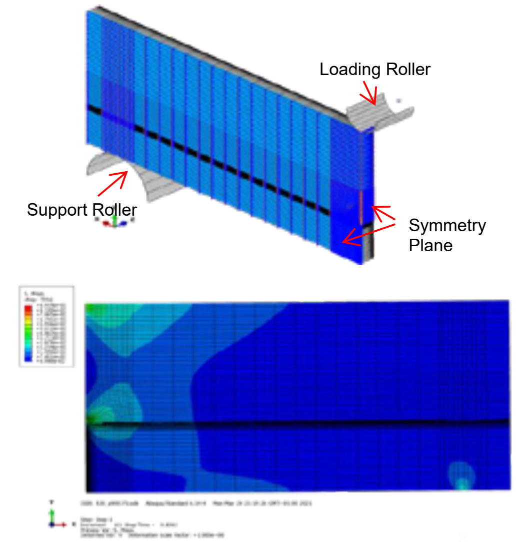

Figure 1 Finite element model for the SEN(B) specimen and one of the FEA result diagrams

III. RESULTS

According to the Load-CMOD curves from experiments, the specimens all show a very brittle condition. There are almost no plastic components in the curves. Therefore, the stress intensity factors K are calculated by the tested fracture loads and then are compared with the results converted from simulated J-integral. The comparison shows two results are very close, which proves the simulations are correct.

After the essential data was extracted from simulation results, the parameters Q and φ, corresponding to each specimen's critical J-integral value, were calculated with equation (1) and (2), respectively. The relationships between them and the critical J-integral are shown in Figure 2 and Figure 3.

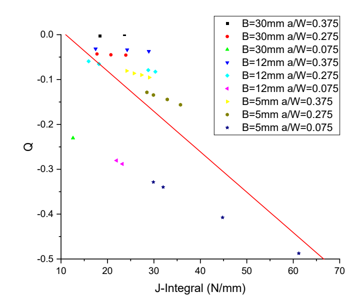

Figure 2 Correlations between Q and J-integral

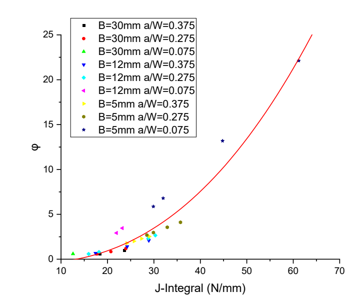

Figure 3 Correlations between φ and J-integral

IV. DISCUSSION

From Figure 2 and Figure 3, it is found that Q and φ can be sensitive to both constraints. Q reduces with the constraint levels decreasing, while φ shows a contrary trend. Comparing two diagrams, Q scatters so significantly that it is hard to establish a good correlation between it and the J-integral. On the other hand, it can be seen that there is a high order relationship between φ and J-integral. Moreover, if we square root φ, a good linear correlation with J-integral can be obtained as shown in Figure 4. Such monotonic correlation is much better to help engineers to assess a more accurate fracture toughness of a low constraint component.

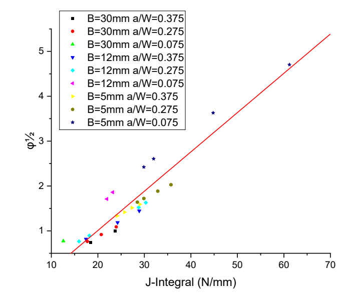

Figure 4 Correlations between $\varphi^{1/2}$ and J-integral

V. FUTURE PLAN

The next works for this programme are as follows:

1. Conduct the fracture toughness test with ASTM A516 Grade 70 steel. SEN(B) specimen is expected to be tested first.

2. Once the test is completed, a series of finite element analyses will be conducted to extract simulation results to validate the applicability of a novel method of mine.

3. Other supplementary experiments with different specimens will be considered to extend my approach's applicability.

REFERENCES

[1] W. Brocks and W. Schmitt,, "The Second Parameter in J-R Curves: Constraint or Triaxiality ?." In STP1244-EB Constraint Effects in Fracture Theory and Applicatons: Second Volume, ed. M. Kirk and A. Bakker, (pp. 209-231). West Conshohocken, PA: ASTM International, 1995.

[2] Mostafavi, M., Smith, D.J. and Pavier, M.J., 2011. A micromechanical fracture criterion accounting for in-plane and out-of-plane constraint. Computational materials science, 50(10), pp.2759-2770..

[3] Hebel, J., Hohe, J., Friedmann, V. and Siegele, D., 2007. Experimental and numerical analysis of in-plane and out-of-plane crack tip constraint characterization by secondary fracture parameters. International journal of fracture, 146(3), pp.173-188.

Hanwei Zhou

Hanwei is an NSIRC PhD student of Brunel University London, based at TWI. She received her master's degree from Wuhan University of Technology in China in 2019, majoring in Engineering Structures of Ship and Offshores. After graduation, she was sponsored by the Lloyd's Register Foundation to study 'Fatigue Propagation from Short Cracks in Thick Welded Steels' at TWI.

Fatigue Propagation from Short Cracks in Thick Welded Steels

Yin Jin Janin[1], Kuveshni Govender[1], Bin Wang[2]
[1]TWI, [2]Brunel University London
2nd Year of PhD

Keywords: SENB, fatigue crack growth,extended finite element, stress intensity factors

I. INTRODUCTION

Fatigue is the most common cause of failures in mechanical structures. Cracks propogate under cylic loading when the fatigue crack growth (FCG) threshold, ΔK_{thres} is exceeded. Hanbook solutions offer ΔK_{thres} for a range of environments but these values were determined using through-thickness nothced specimens. The shipping industry, in particular, has found them to be penalising when used to predict fatigue life. This research examines the effect of semi-elliptical short cracks on ΔK_{thres}. The experimental findings are complemented by numerical simulations. The findings from modelling are to be validated using experimental data. The work presented here describes prediction of the fatigue crack growth using finite element analysis (FEA). The reference geometry for this study is single edge notch bend (SENB) specimens with different crack sizes manufactured from X65 steel. FCG tests were carried out at room temperature. A numerical model based on XFEM (ABAQUS) was constructed. The relationship between crack length and number of cycles from both experimental and numerical analyses were compared. In the numerical model, the Paris Law equation was implemented in ABAQUS to define the growth rate of a fatigue crack, in which the strain energy release rate, ΔG, was employed (instead of the stress intensity factor range, ΔK). Though the relationship between crack length, a, and the number of cycles, N, can be readily determined from FEA model, it was not the case for the determination of the stress intensity factors or the strain energy release rate [1]. To establish the relationship between crack growth rate and stress intensity factor range, a program was developed to analyze fatigue crack growth using ABAQUS scripting interface.

II. METHODOLOGY

The methodology employed in this work involved the FCG tests and FEA.

A. Experimental details

A pipe made of X65 steel was selected. The material properties are yield strength of 519MPa and the ultimate tensile strength of 591MPa. The width of the SENB specimen was 27mm, the thickness 13.5mm, and the length 200mm. A fatigue pre-crack was introduced into the machined specimens. The intention of introducing a fatigue pre-crack into the specimen is to replicate a sharp crack tip which resembles those in actual structures. Experimental tests were carried out in accordance with BS ISO 12108:2018 procedure[2], which specifies the test conditions to determine crack growth rates in fatigue tests. The direct current potential drop (DCPD) method is recommended to measure the average crack length across the thickness of the specimen. Three short surface crack sizes have been selected in this test and used as the calibration specimens. The constant ΔK method was used for these tests. The results of the through-thickness notched specimens and the existing measurement method were compared to determine the most suitable measurement method for the remaining specimens. A stress ratio of 0.1 was used and all tests were conducted in air at room temperature. The load-controlled tests were performed with a constant sinusoidal fluctuating stress at a frequency of 5Hz. The setup of the three-point bending test is shown in Figure 1.

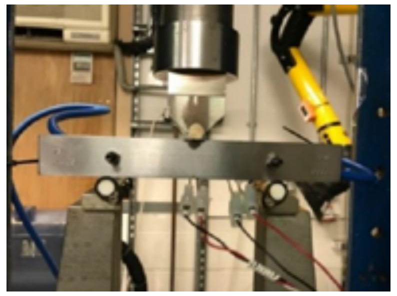

Figure 1. Pre-cracked specimen undergoing fatigue testing

B. Numerical model

ABAQUS/Standard offers the low cycle fatigue criterion in its components for the simulation of crack propagation phenomenon subjected to sub-critical cyclic loadings. In this work, the onset and fatigue crack propagation are characterized by Paris law, which relates the crack growth rate, da/dN, to the range of energy release rate, ΔG, at the crack tip. The energy release rate ΔG is the derivation of the maximum energy release rate G_{max} and minimum energy release rate G_{min}, which corresponds to the maximum force P_{max} and minimum force P_{min} loaded on the structures, respectively. The Paris regime is bounded by G_{thres} and G_{pl}. Below G_{thres}, there is no fatigue crack growth. Above G_{pl}, the fatigue crack will grow at an accelerated rate. G_c is the fracture energy of the material.

III. RESULTS

From the fatigue propagation tests, the material constants C and m (material parameters in the Paris law, concerned with fatigue crack growth rate) can be obtained and implemented into ABAQUS for the specific specimen. The observed crack growth rates versus the range of stress intensity factors, from which the values of C and m are derived, are shown in Figure 2.

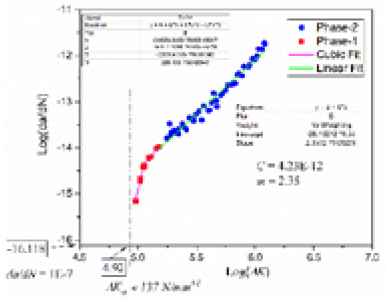

Figure 2. Characteristic Paris law of the specimen

As seen in Figure 1, a curve was fitted in the Paris Regime, and C =4.23E-12 and m =2.35 can be obtained. Therefore, the parameters to define the characteristic of fatigue crack growth in ABAQUS could be determined, and the FEA results are shown in Figure 3.

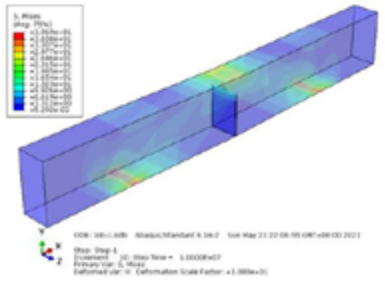

Figure 3. Crack shape at the end of cycles

The comparisons between the experimental and numerical results have been made based for a given crack length subject to a number of fatigue cycles, as shown in Figure 4. Minor derivation in crack growth has been observed in FEA prediction (compared to experiment), there is a reasonable correlation between the experimental and numerical results.

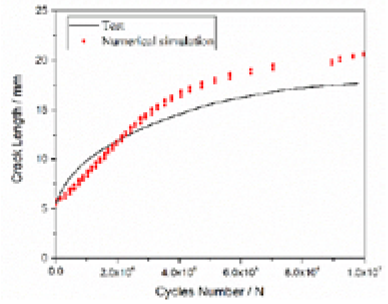

Figure 4. Comparison of average crack length of the specimens versus the number of cycles.

IV. DISCUSSION AND CONCLUSIONS

The parameters C and m determined from tests were implemented into ABAQUS. The FCG predictions from FEA are considered satisfactory and acceptable. This demonstrates that the use of XFEM based LEFM approach is sufficiently adequate to simulate fatigue crack growth in SENB specimens.

V. FUTURE WORK

The XFEM formulation in the ABAQUS software does not take into account enrichment functions at the ctip of propagating cracks, therefore it is unable to predict the stress intensity factors (SIFs) or energy release rates at the crack front during propagation. Further tests will be performed to examine different crack sizes. Prediction of FCG threshold from FEA will be validated once experimental results become available.

REFERENCES

[1] Bergara, A., Dorado, J. I., Martin-Meizoso, A., & Martínez-Esnaola, J. M. (2017). Fatigue crack propagation in complex stress fields: Experiments and numerical simulations using the Extended Finite Element Method (XFEM). International Journal of Fatigue, 103, 112-121.
[2] BS ISO 12108:2018, Metallic materials. Fatigue testing. Fatigue crack growth method

Vishal Vats

I am a materials engineer, currently working on my PhD project 'hexavalent chromium in welding fumes'. I am in my third year of PhD at Teesside University and sponsored by TWI. I obtained my bachelor's degree in mechanical engineering from Annamalai University (India) in 2014 and then earned a scholarship from the Government of India, to pursue my Master's in materials engineering from the National Institute of Technology Karnataka, Surathkal (India) in 2015. After completing my Master's in 2017 I joined the Indian Institute of Technology, Gandhinagar as a Junior Research Fellow for the project titled 'Nanocrystalline substituted cobalt based metal oxides for oxygen evolution reaction'. My interests are electrochemistry, corrosion science and welding engineering.

Characterization of arc welding fume samples by FT-IR spectroscopy

Geoff Melton[1], Dr Venkatesan V. Krishnanr[2] , Prof Meez Islam[2]
[1]TWI, [2]Teesside university
3rd Year of PhD

Keywords: FT-IR, Welding fumes, Cr (VI), Hexavalent chromium, Arc Welding

I. INTRODUCTION

Welders are exposed to welding fumes and although their exposure is minimized by fume extraction and RPE, the risk of getting lung cancer increases compared to people working in other industries [1,2,3]. Exposure to hexavalent chromium [Cr (VI)] depends on the type of welding and the way it is carried out since different welding processes generate a different amount of welding fumes and have different amounts of Cr (VI) present in them[1,2]. Cr (VI) is produced in the arc when Cr (III) converts to Cr (VI). Therefore, it becomes more important to analyse welding fume composition and keep a close look on the exposure of welders to the welding fumes and Cr (VI).

Airborne hexavalent chromium compounds, generated during arc welding is a known human carcinogen [highly toxic due to its ability to oxidize biomolecules, notably DNA] whilst Cr (III) which is not harmful, is usually in condensed phase [1,2,3]. The Na^+ and K^+ ions present in welding electrodes are known for forming Cr (VI) compounds during welding via the following reaction pathways.

$$2Na + Cr + 2O_2 \rightarrow Na_2CrO_4$$

$$2K + Cr + 2O_2 \rightarrow K_2CrO_4$$

The presence of both $^+3$ and $^+6$ oxidation stage of chromium in welding fumes makes it difficult to analyse the correct amount of Cr (VI) in welding fumes [3,4]. The current analytical methods used to determine Cr (VI) percentage in welding fumes are always being challenged as these methods involve wet chemistry, and are pH dependant, thus introducing errors in analysis due to Cr-redox chemistry [3]. To avoid these redox reactions during the analysis of Cr (VI) new methods to analyse Cr (VI) in welding fumes are being sought after and continually explored.

Direct usage of Fourier Transform Infrared Spectrometry (FT-IR) is a promising technique to resolve some of these problems. FT-IR does not involve any wet chemistry so redox reactions do not occur, and the sample can be analysed as-received.

Fourier Transform Infrared Spectroscopy (FT-IR) is a well-established analytical technique for qualitative analysis, with the mid-IR region (4000 cm^{-1} to 400 cm^{-1}) being rich in information about the structure of the functional groups [4,6]. FT-IR can be used quantitatively, as the energy absorbed at a particular wavelength is in proportion to the number of bonds absorbing the associated quanta of energy, so with larger concentrations to analyse more of the energy will be absorbed.

II. DESIGN/METHODOLOGY/APPROACH

Welding fumes which were generated through different types of welding process were investigated. Welding fumes were collected on cellulose filters and then brushed off and stored in glass vessels. The fume samples were analysed for bulk composition using inductively coupled plasma mass spectrometry (ICP-MS) by HSL Buxton and for analysis Cr (VI) in welding fumes Ion chromatography was implemented. The fume samples were then studied under Scanning Electron Microscopy (SEM) along with Energy Dispersive X-ray Spectroscopy (EDX) for particle size analysis and elemental composition of welding fumes. The fume samples then were analysed by Perkin Elmer FT-IR which had an ATR (Attenuated Total Reflection) probe attached. Along with the fume sample, FT-IR was also performed on a reference Cr (VI) sample, viz., potassium dichromate, potassium chromates and sodium chromates, to establish a clear peak location for the absorption bands for Cr (VI). To get clear peaks, fumes were tested with different parameters of FT-IR and finally optimized at a probe resolution of $2cm^{-1}$. Most of the important peaks in welding fume samples are present between $400cm^{-1}$ to $2000cm^{-1}$ wavenumber, hence 128 scans for each sample were recorded in this range.

III. FINDINGS/RESULTS

Chemical grade chromium compounds and metal oxides such as manganese, iron and silica were analysed using FT-IR and then the welding fume samples from different welding processes were analysed too. Fig (1) shows the obtained FT-IR spectra of compounds which are found in welding fumes. Fig (2) shows the FT-IR spectra of different welding fumes generated during various arc welding processes. Sample M3 represents the welding fumes generated during welding from basic metal manual arc (MMA) electrodes and M5 from rutile electrode. Sample FC4 represents the welding fumes generated during fluxed cored wire welding (FCAW). SW2, SW4, SW5 represents the fumes generated by solid wire welding. SW2 are mild steel welding fumes and SW4 and SW5 are from stainless steel welding electrodes.

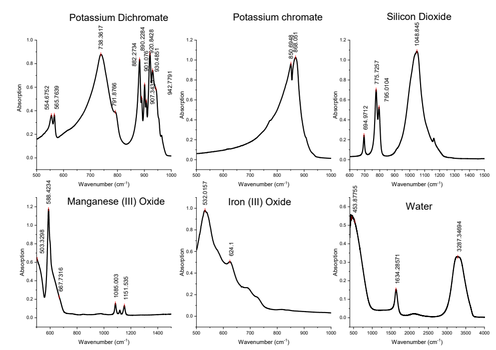

Fig (1) FT-IR spectra of compounds found in welding fumes.

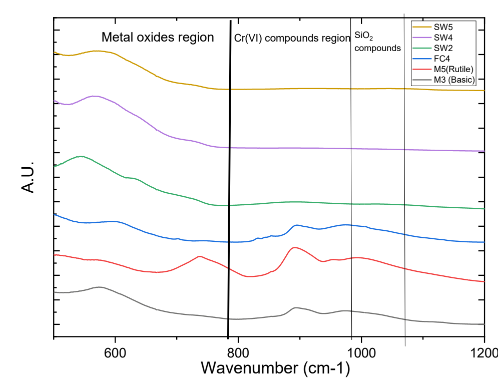

Fig (2) FT-IR spectra of welding fumes

IV. DISCUSSION/CONCLUSIONS

Welding fumes generated during MMA and FCW arc welding shows the clear presence of Cr (VI) compounds in the form of chromates, dichromats and chromium trioxide. Other elements which are seen in welding fumes during FT-IR are SiO_2, Fe_2O_3, Mn_2O_3, moisture.

Chromates were observed around wavenumber 851 and 868, dichromats were observed around wavenumber 738, 792 and 890. The most interesting observations made in these results is the presence of chromium trioxide peak which is observed around 964 wavenumbers. Chromium trioxide has not been reported in the literature since there is a concern that it cannot exist in welding fumes because it usually dissociates at high temperatures. Welding fumes from solid mild steel stainless wires only show the presence of Fe_2O_3 and whereas fumes from stainless steel wire electrodes show a broad peak around 800 wavenumbers due to the overlapping and interferences of the peaks of hexavalent chromium compounds and iron compounds. The moisture content was seen more in the MMA electrode fume samples which is believed to be due the presence of cellulose and also show presence of C-C compounds due to evolution of carbon dioxide during the MMA welding process.

FTIR results were also semi quantitative as when they are compared to each other with Cr (VI) absorption intensities, welding fumes from the MMA welding process shows the highest percentage of Cr (VI) compounds than FCW and solid wire absorption intensities at the same wavenumber. It is also mentioned in other literature that MMA produces the highest amount of Cr (VI) in welding fumes when compared to FCW and solid stainless steel wires [5,7].

V. FUTURE PLAN/DIRECTION

Plans include carrying out electrochemical analysis to understand more about the chemical structure of welding fumes. There are also plans to analyse more welding fumes generated by varying shielding gases.

REFERENCES

[1] Arc welding and the risk of airways and cardiovascular diseases: WELSHIP study by Andrea Marongiu; 2015; imperial college London.
[2] Antonini, James M. "Health effects of welding." Critical reviews in toxicology 33.1 (2003): 61-103
[3] Ashley, Kevin, et al. "Sampling and analysis considerations for the determination of hexavalent chromium in workplace air." Journal of Environmental Monitoring 5.5 (2003): 707-716.
[4] Blair, A. J., and D. A. Pantony. "Inorganic analysis in organic solvents: Spectrophotometric determination of chromium following a chromatographic separation." Analytica Chimica Acta 14 (1956): 545-552.
[5] Floros, Nicolas. "Welding fume main compounds and structure." Welding in the World 62.2 (2018): 311-316.
[6] Kimura, S., et al. "Investigations on chromium in stainless steel welding fumes." Welding journal 58.7 (1979): 195.
[7] Hedberg, Yolanda S., et al. "Welding fume nanoparticles from solid and flux-cored wires: Solubility, toxicity, and role of fluorides." Journal of Hazardous Materials 413 (2021): 125273.

CORE RESEARCH PROGRAMME

DAY 1 ABSTRACTS

Chris Worrall

Chris is a Consultant at TWI responsible for providing composites joining, manufacture, processing and testing services to both members and through public funded projects. His 35 years of composites expertise covers; composite-metal joining, thermoplastic composite welding, microstructure characterisation, mechanical testing of composite materials (including impact, fracture and toughness), finite element analysis (FEA) of composites, design of composite structures, and manufacturing technology for composite materials. Chris holds a PhD in the field of impact of composite sandwich structures in addition to a BSc in metallurgy and materials science, and spent 10 years working in Japan before returning to the UK and joining TWI.

Preliminary Mechanical Properties of Thermoplastic Composites Containing Multiple Pierced Perforations

Author: C Worrall and F Bahrami

Download **Available to TWI Industrial Members**

Industrial Need

Perforated metal panels are currently used in many industries and applications including sound absorbing engine components, leading edge de-icing, and blast protection systems. Due to the increased demand for ever more lightweight components, the aerospace industry in particular is trying to exploit composite materials. Composite parts can be manufactured to near-net-shape with minimum wastage of material; however, there is often a need for further machining. Creating holes for assembly account for approximately 90% of the aerospace industry's requirements for composite machining.

Perforation of composite materials is currently carried out using conventional machining techniques, such as drilling or abrasive water jet cutting. However, these techniques cut the load-bearing fibres and reduce the efficiency of the composite around the holes. The work described in this report aims to exploit the benefits of thermoplastic composite materials for perforated structures.

The approach investigated in this project is a development of thermally assisted piercing (TAP). The thermoplastic composite is heated to its melting point and a metal pin is pushed into the material. Since the matrix is molten, the fibres are free to move around the pin allowing a hole to be made without cutting the fibres. In previous work strength improvements of up to 11% and 21% were found for pierced specimens compared with drilled specimens for open-hole tension and compression loading, respectively.

Although offering several advantages over drilling as a means of making holes for mechanical fastening, the TAP process may offer a greater potential as a process for making multiple small diameter holes. The volume of material heated per hole is reduced for smaller holes, making it more energy efficient. Furthermore, if multiple holes can be made in a single TAP process then there could be significant time savings to be exploited when making a large number of small holes in a composite (perforating). Therefore, this work was carried out in order to determine what applications could benefit from using perforated composites, and whether the strength improvements seen with the larger TAP holes were preserved with multiple small holes.

Key Findings

- Mechanical tests and microstructural analysis show that pierced composite coupons have superior tensile properties but inferior compressive properties, compared with drilled composite coupons.
- These findings will determine those applications that can benefit from the TAP perforation process in the future and those for which the process is not suited.
- Microstructural analysis of pierced coupons showed that the reinforcing fibres create a path around the holes that results in the tensile strength increase, but also the formation of local kink bands that cause the reduction in compressive strength.
- Numerical modelling of the process is challenging, and a validated model has not yet been achieved. A suitable model does not need to include the flow of a molten matrix and the displacement of every individual fibre; assumptions can be made to simplify the computation while still generating volume fraction and orientation distributions for the perforated composite.

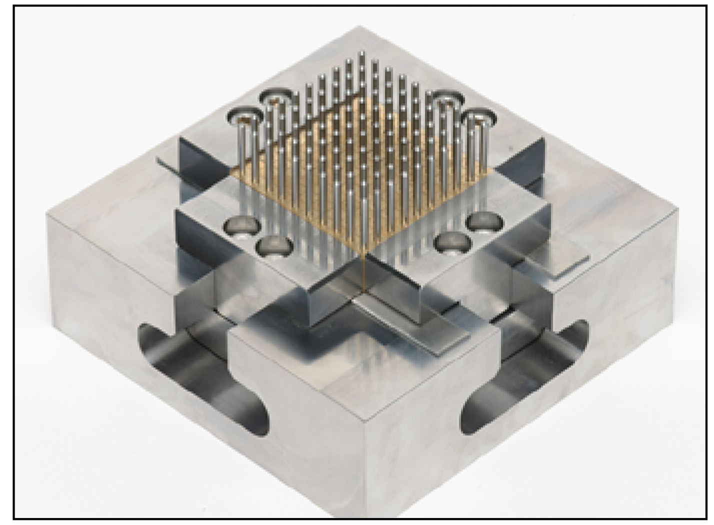

Figure 1: Multiple piercing head, with 100 pin blocks attached

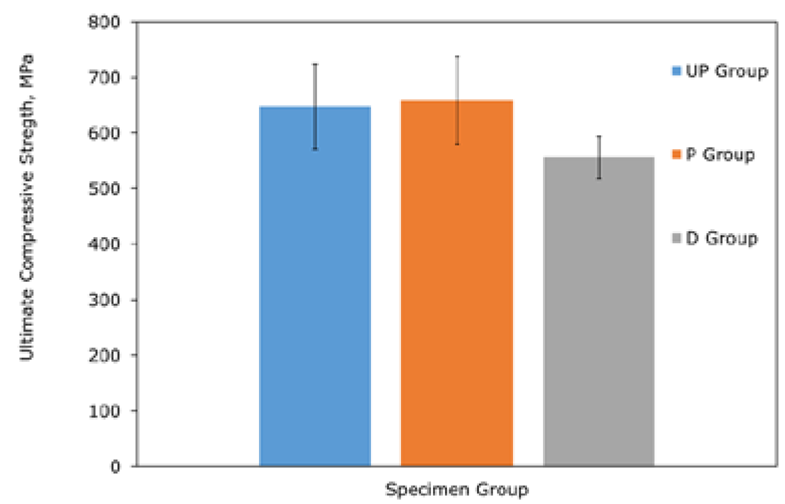

Figure 2: Average open-hole tensile strength of the composite for unperforated (UP), pierced (P), and drilled (D) group. Error bars indicate plus/minus one standard deviation

Adrian Addison

Adrian works in the Arc Processes and Welding Engineering Section at TWI. He has been working in research and development of additive manufacturing primarily with Directed energy Deposition with Arc (DED-arc) often known as Wire Arc Additive Manufacturing (WAAM) since 2014.

He has coordinated several collaborative projects with diverse sponsor groups, managed focussed research for individual clients, coordinated many of TWI's cross cutting research internal research efforts and mentored post-graduate students and researchers. His long-term aim is to ensure maximum value and progress is made across the additive manufacturing technology spectrum and adoption into industry spreads as quickly and widely as possible.

Areas of research at TWI currently include active process development, deposited material properties and performance, in-process and post-process non-destructive evaluation and advanced numerical modelling. In addition to active research, Adrian contributes to BS, EN, ISO/ASTM and ASME committees developing standards for safe application, qualification and coordination of additive manufacturing and associated processes as an industrial process.

Prior to Additive Manufacturing, Adrian gained extensive experience in developing and applying emerging joining technology in applications ranging from below the sea floor to outer space. He also has 20 years' experience in industrial and series manufacture for aerospace, automotive, oil and gas and general engineering applications.

Welding of Additively Manufactured Materials: Preliminary Assessment

Author: A Addison and A Allison

Download **Available to TWI Industrial Members**

Industrial Need

Parts manufactured by additive manufacturing (AM) processes often have microstructures that are different from 'conventional' materials, such as cast or wrought products. It may be necessary to join such parts to other AM parts or to cast or wrought materials using conventional arc welding processes. In such circumstances, the effect of the microstructure of the AM part on the weld is of interest.

This report describes work carried out to prepare a limited number of illustrative examples to assist decisions about future development work in this area. The parts to be welded were fabricated by laser powder bed fusion (PBF) or directed energy deposition-arc (DED-Arc), sometimes referred to as wire plus arc additive manufacture (WAAM)

Key Findings

- Welding of most AM materials by conventional means is both possible and relatively insensitive to the configuration of the AM material relative to the weld interface.
- At the macro scale, the structures in the HAZ and weld metal of the joints were entirely conventional in their nature and no unusual or unexpected microstructure was seen to form as a result of the incorporation of AM material into the joint.
- It was noted that significant porosity occurred adjacent to the fusion boundaries of the joints between aluminium PBF specimens. It is felt that the most likely cause of this is dissolved gas being released from the PBF microstructure and boiling out through the weld metal.

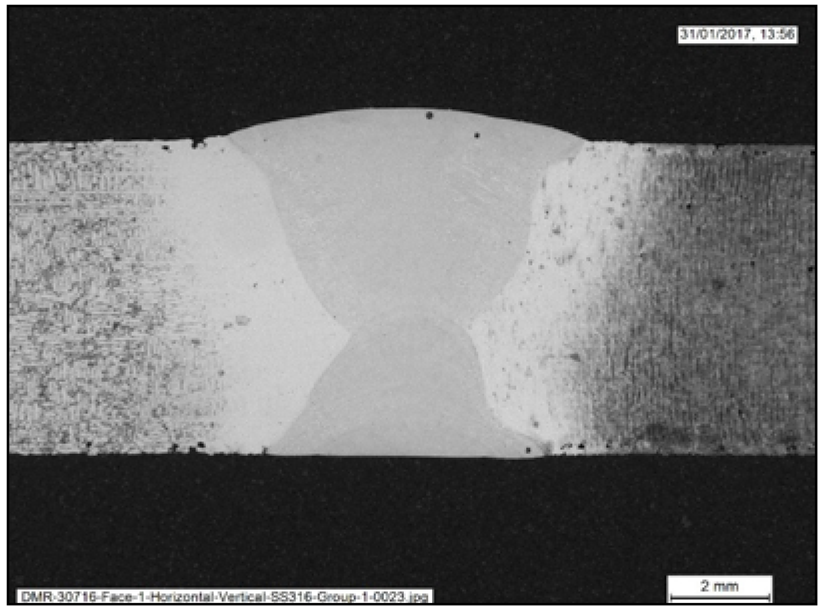

Stainless steel PBF weld macro cross-section.

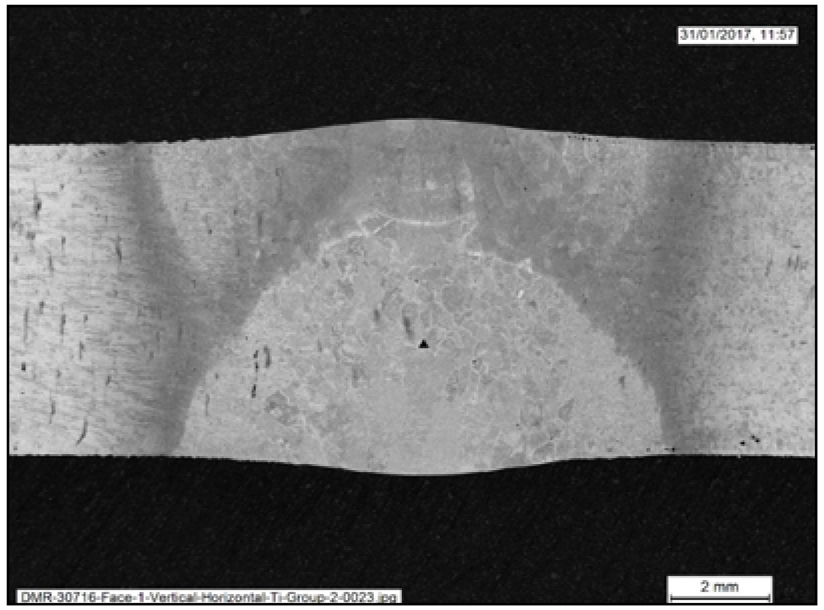

Ti-6Al-4V PBF weld macro cross-section.

Michael Dodge

Mike is a Principal Project Leader within TWI's Materials Performance and Characterisation section. His role involves managing confidential single-client projects, joint industry research programmes, and CRPs for TWI's members and collaborators. Mike still has a particular interest in hydrogen embrittlement, and has authored a number of journal articles and TWI reports on this topic. Mike has been involved in over 50 failure investigations, ranging from 1" corrosion resistant alloy tubes to catastrophic rupture of large bore carbon steel and clad pipelines. The failure mechanisms encountered during these investigations include fatigue, sulphide stress cracking, stress corrosion cracking, hydrogen embrittlement, mechanical overload, buckling, liquid metal embrittlement, etc. Mike enjoys sharing experiences gained from these investigations with colleagues, and is a lecturer on TWI's Failure Investigation Course.

Hydrogen Embrittlement of High Strength Precipitation Hardenable Nickel Alloys

Author: M Dodge and M Gittos

Download **Available to TWI Industrial Members**

Industrial Need

The high strength and corrosion resistance of nickel-chromium-iron alloys, such as Alloys 718 (UNS N07718), 945 (UNS N09945) and 945X (UNS N09946), make them particularly good candidates for use in demanding environments in the upstream oil and gas industry. These materials generally perform well where resistance to sulphide stress cracking and chloride stress corrosion cracking is required. However, while these alloys are considered 'NACE compliant', environmentally-assisted failures can still occur.

It is generally accepted that for hydrogen cracks to initiate, threshold conditions of stress, susceptible microstructure and hydrogen concentration must be exceeded. It stands to reason that complete eradication of any of these variables would prevent failure altogether. Of course this is not always practicable in the field, and a simpler approach is often to understand how these variables interact such that the risk of failure can be managed.

The effect of stress, hydrogen concentration and microstructure has been explored in isolation by a number of authors; however, there does not appear to be a unified source of information on the interaction between each variable. In this project, the effect of microstructure is explored by heat treating Alloys 718, 945 and 945X to standard and non-standard conditions. Tensile specimens were slow-strain-rate-tested in air and under cathodic protection (CP) to explore sensitivity to hydrogen embrittlement. Finally, the effect of a severe stress concentration, in the form of a sharp notch, was used to determine whether there is an enhanced susceptibility to hydrogen embrittlement due to the presence of local stress raisers. The results are compared with tests undertaken by other authors under various hydrogen-charging conditions.

Key Findings

- Testing of specimens under CP did not result in significant reductions in proof strength. However, there was a clear relationship between increasing material strength in air and reduced ultimate tensile strength (UTS) and elongation when tested under CP.
- The materials revealed an increased notch sensitivity when tested in the presence of hydrogen, particularly for the higher strength materials, such as Alloy 945X. Notch sensitivity in hydrogen was manifested mainly by reduced UTS. The increased notch UTS sensitivity in hydrogen is attributed to the interplay between strain localisation within the notch and the propensity for hydrogen to diffuse towards highly strained and plastically deformed regions.
- Macroscopically, the fracture morphology of the hydrogen-charged specimens consisted of a ring of brittle faceted fracture which corresponds to the area into which hydrogen has diffused during pre-charging and testing. Towards the centre of the specimen the fracture morphology became increasingly ductile;
- High magnification inspection of the embrittled portions of the fracture surface revealed the 'brittle' intragranular facets to be populated by slip band traces, the intersections of which were shown to be nucleation sites for micro- and nano-void formation. At high strains it is anticipated these voids will coalesce, resulting in hydrogen crack propagation. Most importantly, these results show that hydrogen embrittlement of these alloys, while macroscopically brittle, is fundamentally a high strain and dislocation activated plastic process.

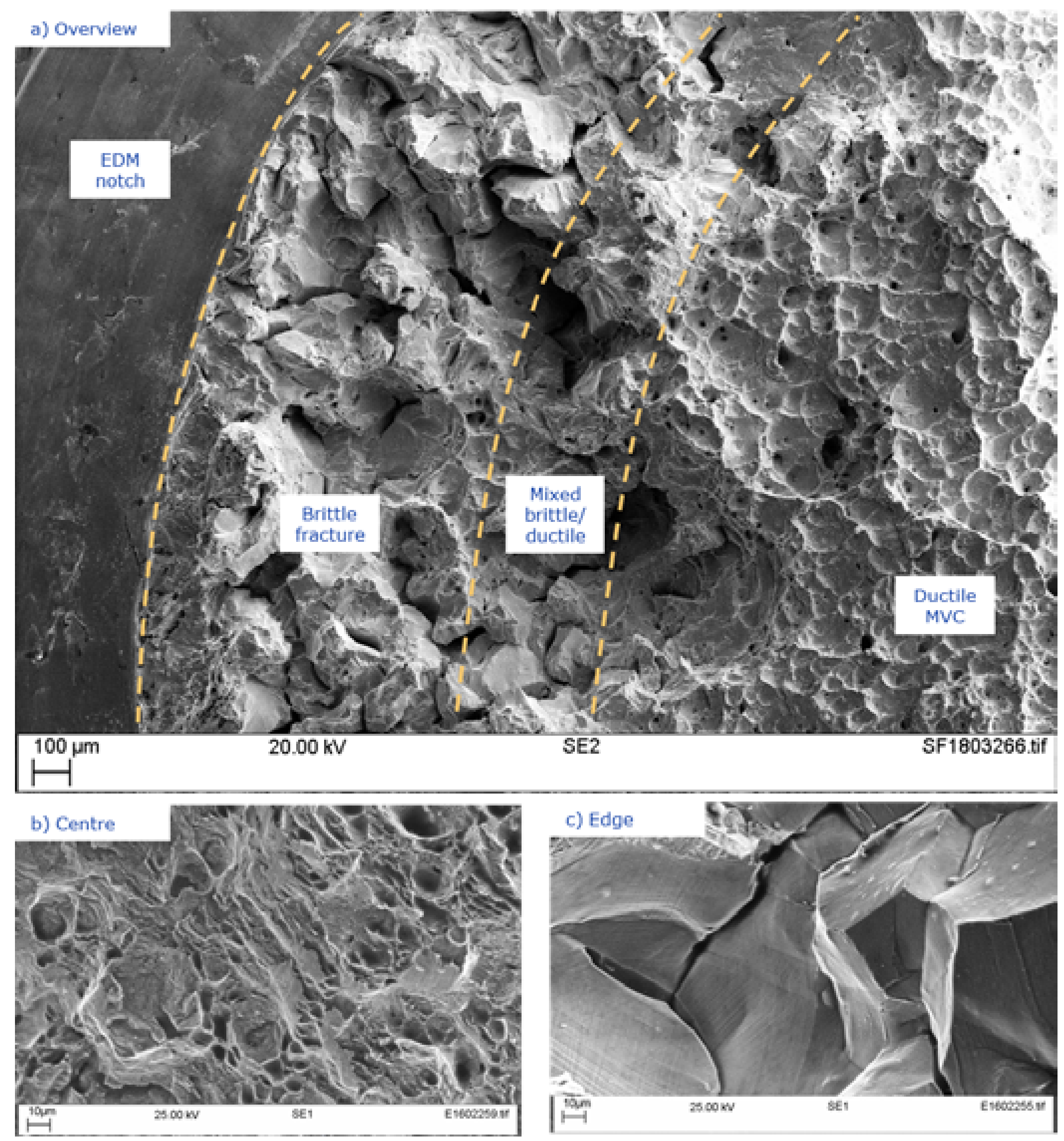

EM images of Alloy 945X specimen, solution treated condition, notched, tested under CP:

a) Low magnification overview of the specimen's fracture surface and notch;

b) Higher magnification image of the centre of the specimen showing microvoid coalescence (MVC);

c) Higher magnification image of the edge of the specimen.

DAY 2 ABSTRACTS

Rukhshinda Wasif

Rukhshinda has obtained an MSc in Structural Integrity from Brunel University London. She is a civil engineer who has worked on non-destructive testing and maintenance of buildings and roads in Pakistan. She is a 3rd year PhD student with London South Bank University. Her research focuses on the reliability based design of a magnetic sensor for corrosion monitoring of oil and gas pipelines. Her project involves finite element modelling and experimental investigations on the capability of the sensor to detect and quantify corrosion in mild carbon steel pipelines or other steel structures.

Development of Permanently Installed Magnetic Eddy Current Sensor for Corrosion Monitoring

Ryan Marks[1], John Rudlin[2], Mohammad Osman Tokhi[3]
[1,2]TWI, [2]London South Bank University
3rd Year of PhD

Keywords: Magnetic, eddy current, corrosion monitoring, ferromagnetic structures.

I. INTRODUCTION

Corrosion costs almost 3-4% of GDP of each nation. In 2016, the global cost of corrosion was estimated to be US $2.5 trillion [1]. Corrosion is a serious issue especially in oil and gas pipelines where undetected corrosion may result in catastrophic failures causing economic, environmental and human losses. Therefore, there is an industrial demand to develop and apply continuous corrosion monitoring.

In recent years, the use of wireless permanently installed sensors has become popular because of their advantages, such as less human interaction, low cost and continuous data acquisition [2]. Electrical resistance (ER) probes, ultrasonic thickness (UT) gauges and capacitance based corrosion sensors are discussed in literature for remote corrosion monitoring [3-4]. However, they have some drawbacks. ER probes are intrusive, UT gauges require couplants for their installation and capacitance sensors are used for detecting near side corrosion only. The magnetic eddy current (MEC) method presented can be used over insulation, differentiate between internal and external corrosion and requires less magnetisation level in the test material.

The development of a low power and low cost wireless sensor based on the magnetic eddy current method is presented. Finite element modelling was carried out to optimise the design of the sensor. The sensor was tested on mild steel plates and a corroded pipe sample. The results were compared with an ultrasonic thickness test. Additionally, an accelerated corrosion test was conducted to simulate the in-service environment for the sensor. The results are presented and discussed in this paper.

II. DESIGN/METHODOLOGY/APPROACH

Eddy currents have limited penetration in the ferromagnetic materials due to their high permeability. The penetration depth of the eddy currents can be increased by magnetising the material under test. In the magnetic eddy current technique, the material under test is magnetised using static magnetic field such as rare earth magnets or electromagnets.

The coil is excited with a sinusoidal voltage and is placed above the sample. As corrosion results in the wall loss, the flux lines inside the material under test are squeezed resulting in changing the permeability. This variation in permeability causes perturbance in the coil impedance as shown in Figure 1.

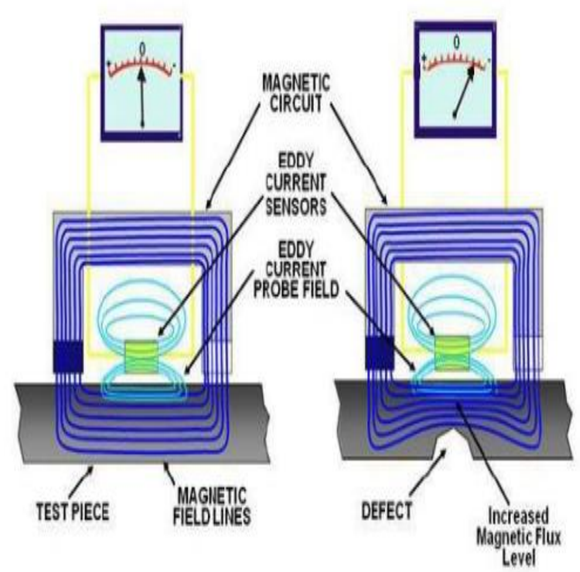

Figure 1. The working principle of MEC [5]

The finite element modelling was carried out in two steps. A static magnetic field physics was used to evaluate the flux density in the plate under tests using Maxwell equation as presented in Equation 1;

$$\nabla \times H = \left(J + \frac{\partial D}{\partial t}\right) \qquad \text{Equation 1}$$

The alternating current module was used for computing and optimising the coil sensor using Faraday's law presented in Equation 2;

$$\nabla \times E = -\frac{\partial B}{\partial t} \qquad \text{Equation 2}$$

The finite element model for optimisation of the sensor is shown in Figure 2.

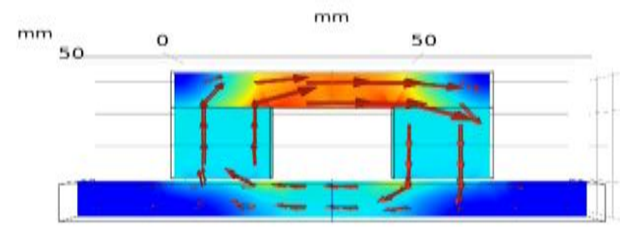

Figure 2. The finite element model for optimisation of the sensor

III. FINDINGS/RESULTS

The sensor was tested on mild carbon steel plates with different thicknesses. The sensor was also tested on a corroded pipe sample and the results were compared with the ultrasonic thickness gauge test as shown in Figure 3.

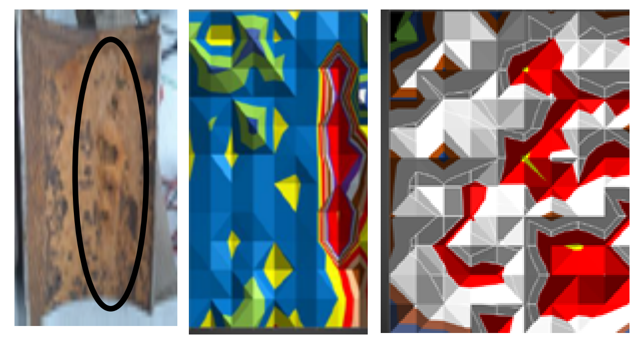

Figure 3. The corroded pipe sample (Left), The UT results (Middle), The MEC sensor results (Right)

An accelerated corrosion test was conducted to simulate the real application environment of the sensor. An 8mm thick S275 mild steel plate was corroded using 25% v/v concentrated sulphuric acid. The test was carried out for 48 hours in a controlled laboratory environment. The sensor was sampled every minute using a data cloud. Three parameters, reactance, resistance and impedance were recorded from the sensor data. The reactance was found to be more sensitive to corrosion than other parameters.

A moving average filter was used to de-noise the reactance signals obtained from the sensor. The window size of 10 readings was used to average the signals. The original data obtained from the sensor and the filtered signals after application of the moving average filter are shown in Figure 4.

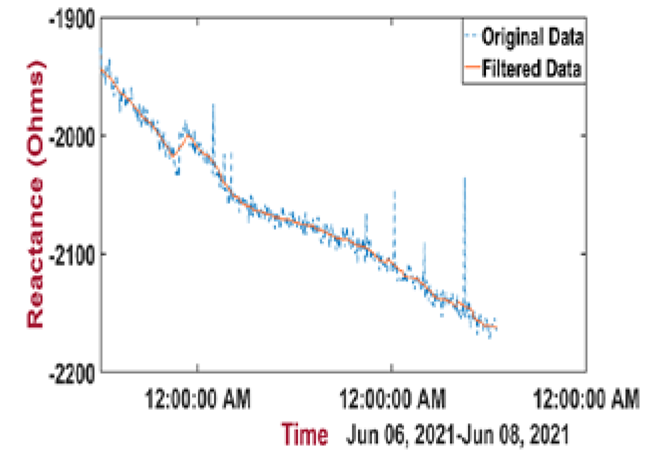

Figure 4. The recorded reactance signals for 48 hours.

IV. DISCUSSION/CONCLUSIONS

The test results show that the sensor is capable of detecting corrosion remotely. The noise in the measurement of the sensor was mainly due to the electronics and can be removed with a moving average filter. The signal to noise ratio is high and the sensor can potentially be used in long term monitoring of corrosion.

V. FUTURE PLAN/DIRECTION

These studies on corrosion sensors show that it has the capability to detect corrosion under controlled environments. However, to predict the life of sensor in service environments, reliability studies are required. In future, the reliability of the senor will be evaluated through extreme, accelerated and real life ageing tests.

REFERENCES

[1] NACE International, 2016. International Measures of Prevention, Application and Economics of Corrosion Technology (IMPACT). [online] Houston, Texas.
[2] Vujic, D., 2015. Wireless sensor networks applications in aircraft structural health monitoring. Istrazivanja i projektovanja za privredu, 13(2), pp.79-86.
[3] Vujic, D., 2015. Wireless sensor networks applications in aircraft structural health monitoring. Istrazivanja i projektovanja za privredu, 13(2), pp.79-86.
[4] Jarvis, R., Cawley, P. and Nagy, P., 2017. Permanently installed corrosion monitoring using magnetic measurement of current deflection. Structural Health Monitoring, 17(2), pp.227-239.
[5] Kim, Y., Jung, S., Song, H. and Lee, S., 2007. Application of steel thin film electrical resistance sensor for in situ corrosion monitoring. Sensors and Actuators B: Chemical, 120(2), pp.368-377.
[6] Innospection Limited, 2017. Magnetic Eddy Current (MEC) Inspection Technique. [online] Aberdeen.

Dandan Liu AWeldI

Dandan graduated from the Xi'an University of Science and Technology, China in Mechanical Manufacturing and Automation in 2019 (MSc). She joined NSIRC PhD programme in January 2020 with Brunel University London and sponsored by Lloyd's Register Foundation. Dandan is currently pursuing a PhD on the "Hydrogen Induced Cracking in Oil and Gas Pipelines and Its Monitoring" and she is in the 2nd year of her study.

Hydrogen Induced Cracking in Oil and Gas Pipelines and its Monitoring

Dr. Ryan Marks[1], Dr. Bin Wang[2]
[1]TWI, [2]Brunel university
2nd Year of PhD

Keywords: hydrogen induced cracking,acoustic emission, data filter, signal analysis

I. INTRODUCTION

Hydrogen induced cracking (HIC) is a phenomenon in which the material's mechanical properties are severely degraded due to hydrogen absorption or hydrogen penetration, resulting in brittle fracture. Steels used in harsh environments, such as oil and gas pipeline steels, have a higher susceptibility to HIC. HIC cannot be eliminated once it initiates within a material, thus after HIC occurs, the state and development of the crack is required to be detected and the remaining life of the structure needs to be assessed through regular monitoring. Acoustic Emission (AE) monitoring is a Non-Destructive Testing (NDT) method which can detect the transient elastic wave generated when the material or structure is damaged and convert it into an electrical signal with AE equipment for further analysis.

This research work focuses on developing models of AE wave propagation and HIC propagation. Therefore, it is necessary to quantitatively analyse the relationship between hydrogen penetration, crack growth, and the AE signals. Based on crack growth, a model between HIC and wave propagation can be established.

II. DESIGN/METHODOLOGY/APPROACH

In order to analyse the relationship between HIC and AE signals, a HIC test monitored by AE is required. However, due to the complex mechanism of HIC, a pre-test was conducted to verify the feasibility of the method. Thus, the single edge notched tension (SENT) test was conducted.

In order to avoid rapid brittle fracture of the material during the tensile loading, S275 mild steel (square bar) was chosen in this experiment because of the lower yield stress. Four specimens were prepared: two were allocated for monotonic tension loading and two for unloading compliance loading. The dimension of sample is shown as Figure 1.

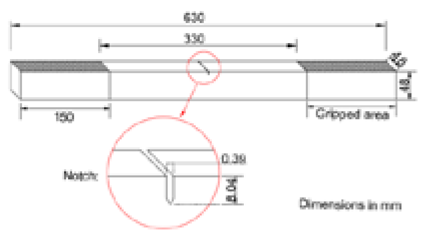

Figure 1. the dimension of sample

Figure 2 shows the experimental setup. Four Vallen VS150-RIC sensors were placed on two adjacent faces (the red circle indicates the notch location). Two clip gauge were used to monitor the crack mouth opening displacement (CMOD). The test was conducted in line with BS8571:2018.

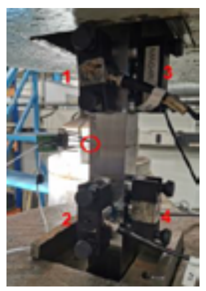

Figure 2. Set up of SENT test

III. FINDINGS/RESULTS

The results of one unloading compliance SENT test and associated AE signals are presented here. The test generated a large amount of background AE from movement in the loading attachments and the environment. This was first required to be filtered out.

A Self-Organizing Map (SOM) is a clustering method based on artificial neural networks (ANN) [1]. A SOM was built using the MATLAB neural network toolbox. The input data chosen were peak amplitude, signal rise time, duration, counts and energy. By using a SOM, signal clusters were established to filter noise from damage signals. The signal waveforms from noise and crack propagation are shown in Figure 3 and Figure 4, respectively. Compared with the 'crack' waveform, the short duration and low amplitude of the 'noise' waveform clear to differentiate.

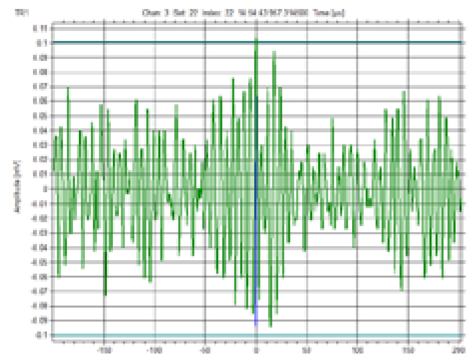

Figure 3. Signal waveforms from noise

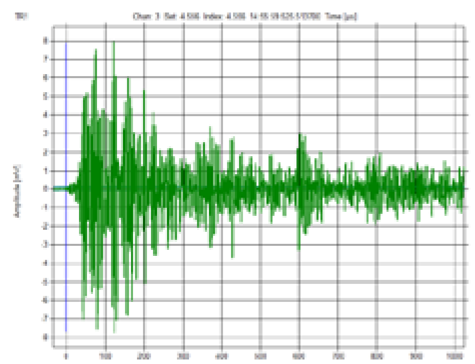

Figure 4. Signal waveforms from crack

In addition, AE events that were located outside the gauge length were discarded as they were considered as grip noise. Figure 5. shows the peak amplitude distribution before (a) and after (b) filtering. It can be seen that the AE signals from background noise predominantly have lower peak amplitudes.

Based on filtered data, the felicity ratio was also calculated to evaluate the failure severity of steel, shown as Figure 6. It indicates possible plastic deformation when the value is reduced to below 1[2].

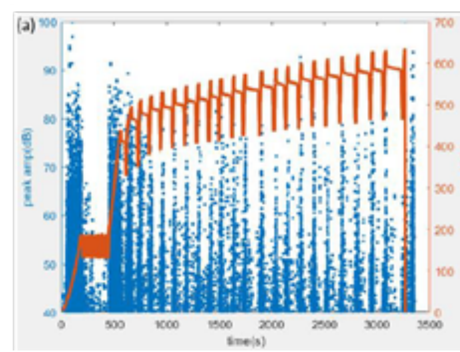

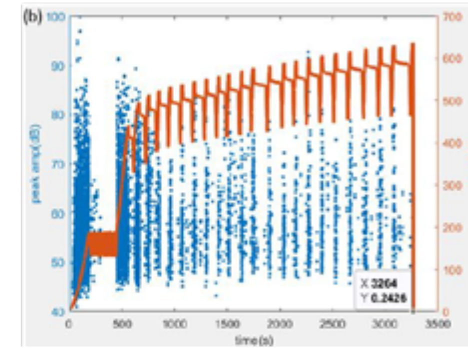

Figure 5. Peak amplitude distribution for raw data (a) and filtered data (b)

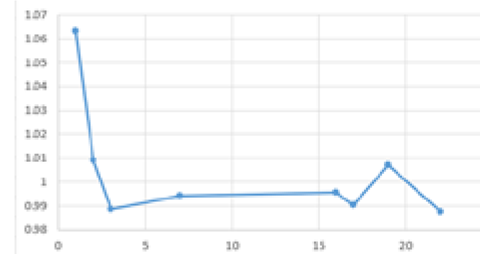

Figure 6. The Felicity ratio of different cycles

IV. DISCUSSION/CONCLUSIONS

It was demonstrated that the SOM was effective in removing background noise from the AE test data however the clustering results need further evaluation. Performance indices, like Davies-Bouldin, may provide more information to automate the clustering process. This work combines AE signal and fracture data for analysis, therefore the process of crack propagation and the fracture severity of the material can be inferred from the signals. This laid the foundation for the subsequent quantitative analysis of the HIC propagation.

V. FUTURE PLAN/DIRECTION

The next step in this study is to combine mechanical data to analyse the trend of AE by counts, energy and other features, and to compare individual signal characteristics from different mechanical stages. In addition, to establish a model of AE signal and tensile crack propagation, and to make an analogy about the model of AE signal from HIC propagation.

REFERENCES

[1] Davide Crivelli, Mario Guagliano, Alberto Monici. Development of an artificial neural network processing technique for the analysis of damage evolution in pultruded composites with acoustic emission[J]. Composites: Part B, 2014, 56: 948-959.

[2] Mingwei Zhang, Qingbin Meng, Shengdong Liu, et al. Impacts of Cyclic Loading and Unloading Rates on Acoustic Emission Evolution and Felicity Effect of Instable Rock Mass[J]. Advances in Materials Science and Engineering, 2018, Article ID 8365396, 16 pages.

Faris Nafiah

Faris attained his Bachelor's degree in Electrical Engineering from the University of Auckland, New Zealand before joining International Islamic University Malaysia where he completed his Msc in Mechatronics Engineering in eddy current NDT. Sponsored by Lloyd's Register Foundation, his PhD with London South Bank University aims at developing a pulsed eddy current instrument that is capable of carrying out inspections for corrosion under insulation in pipelines. The key interest is to establish methods for fast pipe scanning while compensating for variations in parameters during inspection.

In-situ Inspection of Corrosion Under Insulation using Pulsed Eddy Current

Faris Nafiah[1], Owen Rees-Lloyd[2]
[1]London South Bank University, [2]TWI
3rd Year of PhD

Keywords: pulsed eddy current, corrosion under insulation, signal processing

I. INTRODUCTION

Corrosion may develop and grow on steel pipes under layers of insulation and cladding. The multi-layered structure of a pipe, as visualised in Figure 1, complicates the inspection process of a corrosion under insulation. Unlike the conventional non-destructive testing (NDT) techniques that require removal of the insulation, pulsed eddy current (PEC) offers the capability of non-contacting inspection, which consequently enables an in-situ technique to be devised. However, responses from a PEC system are highly influenced by variations in the cladding and insulation thicknesses. Although recent works have established different approaches in compensating for these adverse effects on PEC responses [1], none of the techniques present an approach for in-situ measurement. The aim here is to utilise a novel signal processing technique to overcome the variability in PEC signals due to variations in the cladding and thickness variations. The results, validated by experiments, prove that the approach is effective in quantifying corrosion on pipes independent of confounding cladding and insulation thicknesses variations.

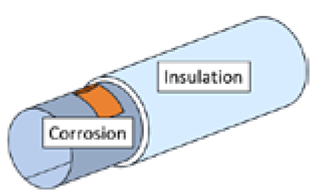

Figure 1. Corrosion on multi-layered pipe structure.

II. NOVEL SIGNAL PROCESSING

The previous work [2] has established the functional relationship of a new feature, namely $|\nabla|^{-1}$, with pipe wall thickness d, as

$$d^2 \propto \left|\frac{\mathrm{d}\,t}{\mathrm{d}\,\ln[V(t)]|_{t\gg 0}}\right|_{t\gg 0} \tag{1}$$

$$d^2 \propto |\nabla|^{-1}, \tag{2}$$

where t is the time and $V(t)$ is the time-dependent induced voltage in the detector coil. With the known relationship of the proposed feature, $|\nabla|^{-1}$, with the squared of the sample thickness, d^2, the calibration curve can be established by taking one (or multiple) reference signals from the inspected area. This can later be compared with the signals taken in air (without the presence of any pipe), and a straight line can be drawn crossing the $|\nabla|^{-1}$ values obtained from these measurements. This slope of the straight line indicates the functional relationship of $|\nabla|^{-1}$ with d^2.

In the context of the PEC responses from the developed PEC system, $|\nabla|^{-1}$ is extracted by computing the gradient of the signals within a specified thresholds. Figure 2 demonstrates the extraction of the feature from a set of PEC signals of different wall thicknesses.

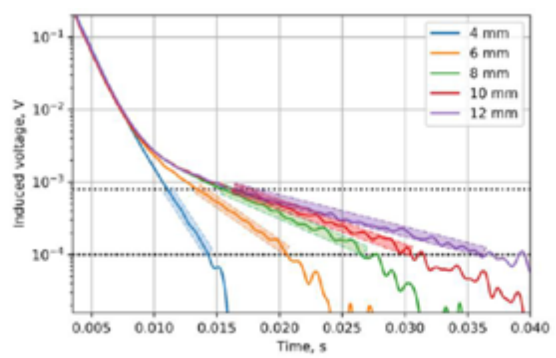

Figure 2. $|\nabla|^{-1}$ features extracted from PEC signals.

As equation (2) suggests, the linearity of the $|\nabla|^{-1}$ feature with thicknesses is demonstrated in Figure 3.

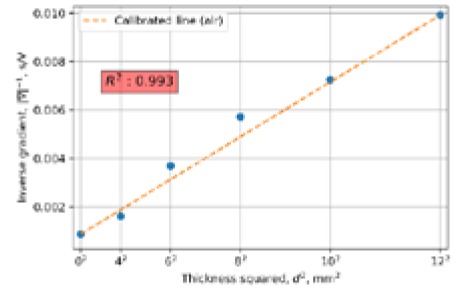

Figure 3. Plot of extracted $|\nabla|^{-1}$ against d^2

III. COMPENSATING FOR INSULATION AND CLADDING THICKNESS VARIATIONS

For validation purposes, a PEC system has been developed consisting of a transmit-receive coil, excitation circuit and a LabVIEW data acquisition program. Carbon steel plates of S275 grade were used, with thicknesses of 4 mm to 12 mm, at increments of 2 mm. Plastic plates were used as a non-conductive insulation of 40 mm. A 0.5 mm thick aluminium sheet was placed on top of the plastic plates to simulate cladding. The excitation voltage was 10 V with 8 Hz excitation frequency. Data was acquired at the rising edge, and 16 pulse signals were averaged for each test for the purpose of white noise reduction.

The effects contributed by different thicknesses of insulation are demonstrated in Figure 4. As can be seen, for each wall thickness, despite the difference in the lift-off values, the PEC signals still decay at similar rates. This shows up as a generally parallel shift in time.

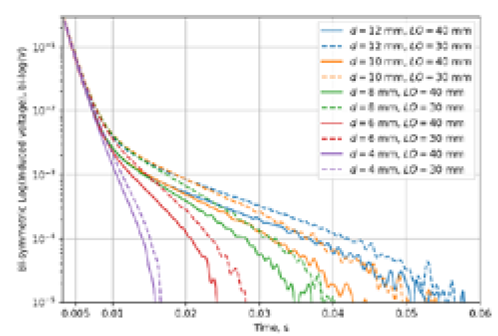

Figure 4. PEC signals for different pipe wall and insulation thicknesses.

The effects of cladding thickness variations is demonstrated in Figure 5. Cladding thickness variations affect the early part of the signals, but can be said to diminish at the later part. The signal gradients during this time range are also consistent corresponding to their thicknesses.

Figure 6 shows the extracted $|\nabla|^{-1}$ values corresponding to different aluminium cladding and wall thicknesses. The extracted $|\nabla|^{-1}$ values, in general, can be said to be almost linear with the value of d^2. Although the aluminium cladding thickness is proven to affect the PEC signals, the linearity of $|\nabla|^{-1}$ with respect to d^2 is still maintained. Moreover, the values of each $|\nabla|^{-1}$ corresponding to respective wall thicknesses (irrespective of aluminium cladding thicknesses) are profoundly consistent, suggesting the immunity of the proposed $|\nabla|^{-1}$ technique to the presence of aluminium cladding.

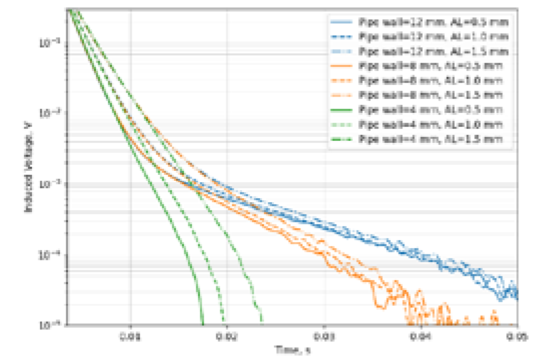

Figure 5. PEC signals for different pipe wall and cladding thicknesses.

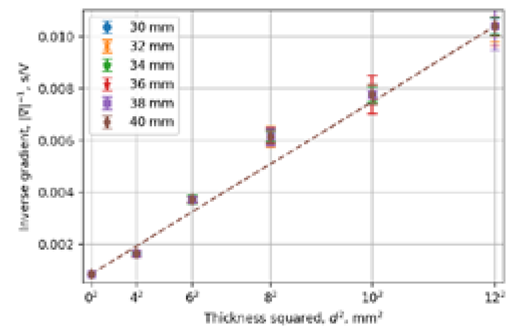

Figure 6. Extracted $|\nabla|^{-1}$ for different aluminium cladding thickness over different wall thicknesses.

IV. CONCLUSION

A novel signal processing technique based on $|\nabla|^{-1}$ feature to enable in-situ measurement of wall thinning without insulation removals in oil and gas pipelines has been demonstrated. The proposed feature, inspired by analysing the physical phenomenon governing the PEC working principle, makes use of the gradient of the received PEC signals within a certain thresholds. The outlined in-situ calibration procedure has been demonstrated to be immune to insulation and cladding thickness variations, which will contribute largely to enable pipe profiling for corrosion under insulation detection.

V. ACKNOWLEDGEMENTS

This publication was made possible by the sponsorship and support of Lloyd’s Register Foundation. Lloyd’s Register Foundation helps to protect life and property by supporting engineering-related education, public engagement and the application of research.

REFERENCES

[1] Ulapane, N. et al. (2017). Pulsed eddy current sensing for critical pipe condition assessment. Sensors, 17(10):2208.

[2] Nafiah F. et al. (2020). Pulsed eddy current: Feature Extraction Enabling In-situ Calibration and Improved Estimation for Ferromagnetic Application.

Paul Ukpaayedo Sukpe

Paul joined the NSIRC PhD programme in February 2020 after graduating from Brunel University London with MSc Structural Integrity (Asset Reliability Management) in 2019 at NSIRC, TWI. He also holds BSc Mechanical Engineering from the Kwame Nkrumah University of Science and Technology, Ghana. Paul's PhD topic aims at providing suitable guidance that can be incorporated into existing fracture mechanics assessment procedures, primarily, BS 7910 to minimise the conservatism inherent in these standards. His research interests lie in structural integrity of offshore structures, particularly, pipelines.

Crack Tip Constraint in Typical High Strength Steel Components in Arctic Conditions

TWI Supervisor: Dr Rob Kulka
Academic Supervisors: Prof. Rade Vignjevic, Dr Kevin Hughes, Brunel University London
2nd Year of PhD

Keywords: crack-tip constraint; low temperature; brittle fracture; thickness; integrity assessment

I. INTRODUCTION

Crack-tip constraint has been an issue in the fracture toughness testing of offshore structures that rely on deeply bend cracked specimens to guarantee high levels of stress triaxiality which drive the fracture process. However, structural defects in pipelines are often surface cracks that generally develop low levels of crack-tip constraint associated predominantly with tensile loading. Moreover, high grade pipeline steel exhibits much higher cleavage fracture resistance resulting in the development of extensive plastic deformation at the crack tip prior to failure. Assessment of defects in low constraint structural components based on procedures such as BS 7910 [1] give safe (conservative) predictions of failure conditions, since fracture toughness is measured under conditions of high crack tip constraint.

This work is aimed at presenting more refined defect assessment procedures to include the effects of in-plane and out-of-plane constraint variation on fracture toughness so that crack-tip constraint in the test specimen closely matches the crack-tip constraint of the structural component.

II. METHODOLOGY/APPROACH

The robustness of the current assessment methods available in literature have been studied comparing published tests data and analytical solutions. The levels of constraint and crack driving force defined by the J-integral in the vicinity of the crack are fundamental to the estimation of the effective crack driving force for fracture initiation for any chosen configuration. A substantial test programme involving low temperature fracture toughness tests of single-edge notched bend (SENB) and single-edge notched tension (SENT) with different specimen configurations would be presented. It is proposed for the current plan to use digital image/volume correlation (DIC/DVC) to determine the crack strain energy release rate (J-integral) from measured displacement fields by examining the deformations near the crack tip. The results from the experiment would be used to validate the finite element (FE) analyses that use different constitutive models. FE analyses of full-scale pipes containing surface breaking defects will also be conducted. The triaxiality or crack-tip constraint would be quantified based on the two-parameter framework (J-T or J-Q). The stress field in front of the crack tip is written by the first two terms of the Williams' series expression as [2]:

$$\sigma_{ij} = \frac{K_I}{\sqrt{2\pi r}} f_{ij}(\theta) + T\delta_{1i}\delta_{1j}$$

where the first term of the above equation is the singular elastic K field with K_I as the stress intensity factor (SIF), the second term is the non-singular with magnitude denoted by a parameter T and δ_{ij} is the Kronecker delta.

The Q parameter is defined by O'Dowd and Shih when they performed a series of detailed elastic-plastic FE calculations for various geometries based on the theory of deformation plasticity and developed the J-Q theory as a numerical solution to describe the elastic-plastic crack tip field. Q is computed as [2]:

$$Q = \frac{(\sigma_{\theta\theta})_{FEA} - (\sigma_{\theta\theta})_{HRR}}{\sigma_o}; \ at \ r = \frac{2J}{\sigma_o} \ \ and \ \theta = 0$$

where $(\sigma_{\theta\theta})_{FEA}$ is acutal crack opening stress at distance $r = \frac{2J}{\sigma_o}$, $(\sigma_{\theta\theta})_{HRR}$ is Hutchinson-Rice-Rosengren (HRR) field for small-scale yielding (SSY) and σ_o is the yield stress.

III. FINDINGS

Much theoretical and numerical work has been done to quantify crack tip constraint effects on fracture toughness in both two- and three-dimensional specimens and structural configurations. However, due to the loss of single-parameter J-dominance, several two-parameter fracture theories have been proposed. The J-T approach effectively quantifies crack tip stress fields for low constraint conditions such as shallow cracked structures or specimens. This method however, becomes less meaningful as the plastic zone expands at the crack tip since the T-stress is an elastic parameter. In order to address these limitations, O'Dowd and Shih introduced the Q-parameter for elastic-plastic materials under SSY and large-scale yielding (LSY) to account for the parametric evaluation of the crack front stress triaxiality. Further, there seems not to be a robust method to account for constraint effects on the fracture toughness of offshore high-grade steel pipelines at low temperatures particularly on the parent material. Figure 1 demonstrates the development process of fracture analyses from 1-dimension to 3-dimension in order to account for in-plane and out-of-plane constraint effects.

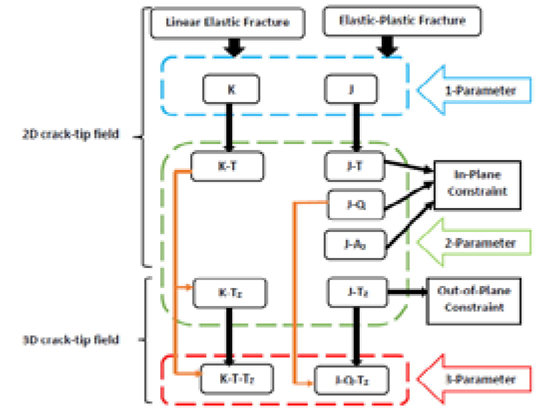

Figure 1: Development of crack-tip fields estimation by considering in-plane and out-of-plane constraint parameters

IV. CONCLUSIONS

Due to the importance of constraint effects on fracture mechanics, three-dimensional FE method is used to study the effects of in-plane and out-of-plane constraint parameters for high strength steel grade pipe. Crack driving force of cracked pipe is underestimated in current assessment procedures for constraint effects. Shallow notched SENB and SENT specimens are deemed suitable for fracture toughness measurement in circumferentially flawed pipe as they provide less conservative crack-tip conditions. At present, there are no solutions for the normalised structural constraint parameter (β_Q) for the Q-parameter and out-of-plane solutions in BS 7910.

The study in progress showed that J-integral is independent of path where it is calculated and it can be computed even further away from the crack tip due to its path independent characteristics. The J-integral is an effective approach in fracture mechanics to calculate the stress intensity factor (SIF) around the crack tip. As no real structural material is linear-elastic and will always have a plastic zone near the crack tip, the J-integral gives appropriate values of SIF in elasto-plastic fracture mechanics. The geometry behaviour studied in this current work is consistent for other planar crack front geometries.

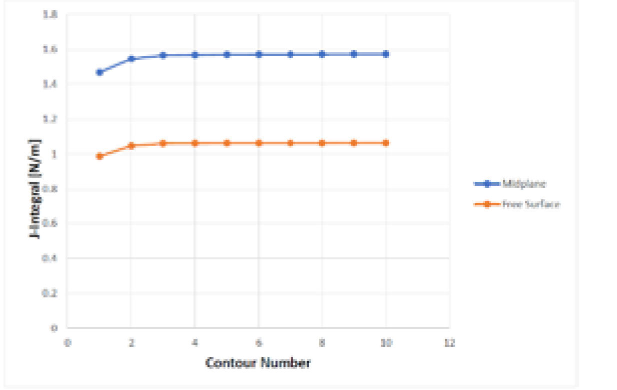

Figure 2: Linear elastic analysis – J-integral vs. Contour Number, mid-plane and surface of through-thickness crack, a=10 mm for applied load of 1000 N

V. FUTURE PLAN

The transferability of fracture toughness data obtained from laboratory specimens to a full-scale cracked structure is key in integrity assessment of engineering structures. Both in-plane and out-of-plane constraint effects would be considered under different constraint conditions. We would also be looking closely at the deformations that occur at the crack tip with multiple SENB and SENT specimen configurations, with DVC/DIC techniques planned for measuring the deformations. A detailed and refined FE analyses using different steel pipe material constitutive models would also be performed to validate suitable models used in simulating cracked pipe exhibiting different levels of crack tip constraint. Parametric FE analyses of cracked pipes subjected to tensile loading and internal pressure will further be performed at varying crack tip constraint conditions.

A novel modified constraint-based fracture assessment for the steel with surface flaws at low temperature will be examined in conjunction with Annex N of BS 7910 to study the influence of constraint level correction on the allowable applied stress.

REFERENCES

[1] BS 7910 2019, "BSI Standards Publication Guide to methods for assessing the acceptability of flaws in metallic structures," 2019.
[2] N. P. O'Dowd and C. F. Shih, "Family of crack-tip fields characterized by a triaxiality parameter-II. Fracture applications," J. Mech. Phys. Solids, vol. 40, no. 5, pp. 939–963, 1992

Xuening Zou

I graduated from Loughborough Universtiy with BEng degree. I am continuing studying in the Material department at Loughborough University for my PhD. My project is about fault diagnosis in stainless steel. I have been focused on faulty simulation modelling and automatic defect detection and localization.

Simulation-Based Training of CNN for Detection of Cracking

Channa Nageswaran[1], YauYau Tse[2]
[1]TWI, [2]Loughborough University
3rd Year of PhD

Keywords: FMC, CNN, stress corrosion crack

I. INTRODUCTION

After initiation, cracks in metallic materials may grow but may not become critical for the structural performance unless a critical size is reached. Health monitoring systems are therefore required to monitor and inspect flaws over time. A major difficulty for health monitoring systems is the uncertainty in the inspection result: cracks may be missed due to unreliable interpretation of complex signals by human inspectors. To overcome this challenge, machine learning (ML) techniques are being increasingly applied in the field of structural health monitoring for a more reliable assessment of the condition of materials and structures. The recent advances in various ML algorithms have solved many difficult detection problems that were previously considered intractable. The proposed ML method is convolutional neural network (CNN) to detect cracks before reaching the critical crack length. A generative ML model was obtained through training datasets generated from simulation of the inspection scenario.

The results show good performance, with 98% accuracy in classifying the presence of a crack

II. DESIGN/METHODOLOGY/APPROACH

The CIVA model was used as the primary platform to simulate the ultrasonic inspection and collect the output results as data for training the ML model. The semi-analytical methods of CIVA to model ultrasonic wave propagation and interactions with cracks are cost effective for industrial studies. It is capable of simulating the experimental pulse-echo technique to obtain A-scan data. The data pairs were collected from the features of surface responses based on the analytically generated waveforms and the corresponding parameters of cracks.

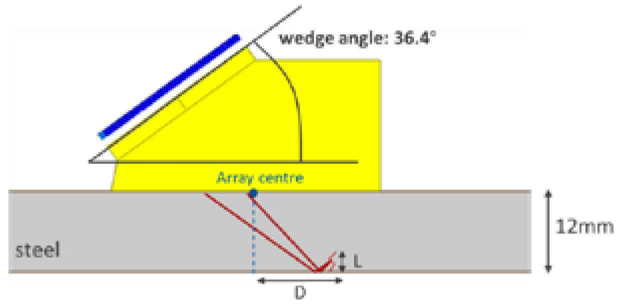

Figure 1 An illustration of the inspection scenario using a phased array ultrasonic probe with wedge transmitting shear wave into the sample, where L represents the crack length into the plate from the back wall and D represent its position with respect to the wedge.

The CNN is good at finding spatial relationships in the data, because weight kernels are shared across the image position so that local feature patterns are learned and correlated. Image pixels have a relationship with each other that is spatially distributed in each image dimension. Similarly in FMC data, not only does a single sample in an A-scan have a spatial relationship with its previous and next sample, but also each elementary A-scan in an FMC dataset has a spatial relationship with its previous and next elementary A-scan. This distinct feature of FMC data enables it to be effectively learned by CNN model. Hence, an automatic SHM framework based on CNN model in Figure 3 trained using FMC data generated by simulation is proposed in Figure 2.

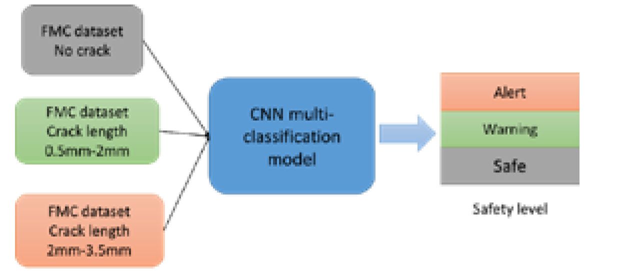

Figure 2 CNN assisted automated SHM framework

The approach is to collect FMC data from the simulation model as a first step. A 32-element array is used to collect the FMC data matrix of size 32 x 32. The front wall echo is removed from each A-scan primarily to reduce the data size to ease the computation load. In this case, each A-scan is downsized to contain 1600 sample points. To train a CNN classifier, FMC data is re-arranged before input to a CNN.

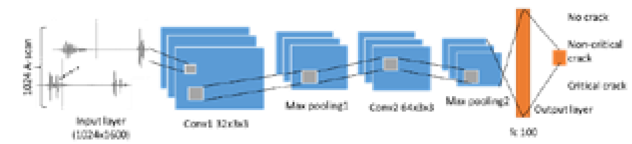

Figure 3 illustration of the proposed CNN architecture

III. FINDINGS/RESULTS

CNN model was initialized with random weights, the assignment of training, validation and test data are random but evenly selected from each crack length datasets to avoid bias. Feature extraction was not needed for the CNN - it learned features automatically by updating the weights. Figure 8 shows the evolution of the training and validation accuracies. The training accuracy was calculated from 280 samples containing evenly distributed crack lengths from 0.5 to 3.5mm, and no crack condition. Validation accuracy was calculated from 70 samples.

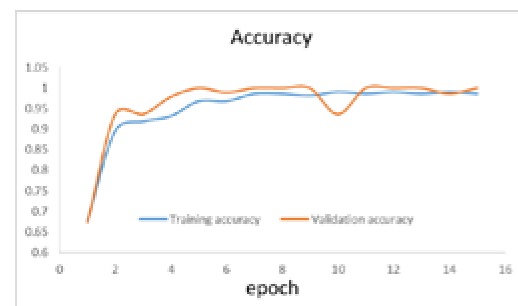

Figure 4 Training and validation accuracy for 16 epochs

The learning curve in Figure 4 showed that CNN starts with approximately 67% training accuracy and reached a saturation point after 8 epochs. It was possible to achieve a training accuracy of 98.5% and a validation accuracy of 100%.

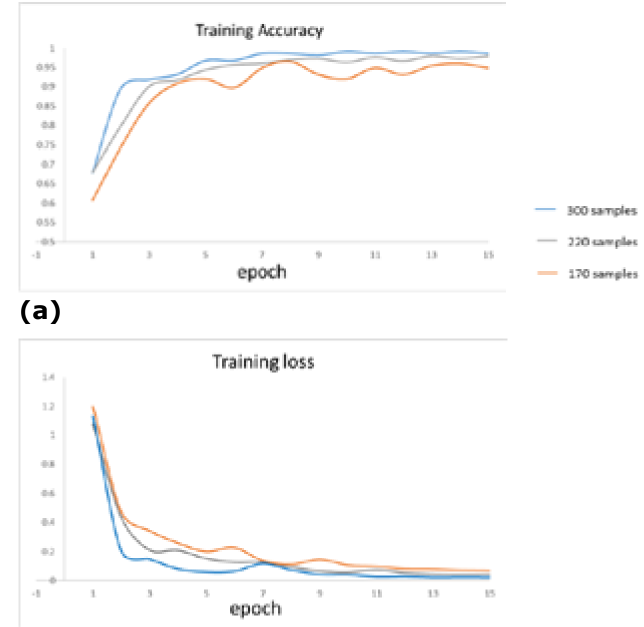

(b)

Figure 5 (a) Training accuracy and (b) loss of parametric study of 300 samples, 220 samples and 170 samples

To understand the effect of the number of training datasets on training accuracy, a parametric study using training datasets comprising 170, 220 and 300 samples was conducted. The architecture used was the same as in Figure 5. This parametric study demonstrates that with the increasing number of samples comprised of different crack lengths, the model learning was producing more results that are accurate.

IV. DISCUSSION/CONCLUSIONS

The present work may have some limitations because the training and validation data were generated by simulation. Although Gaussian noise was added to mimic real world noisy material, it cannot account for all kinds of variations that could exist in the real crack growth environment.

V. FUTURE PLAN/DIRECTION

The next stage of work will be training the model on experimentally created stress corrosion cracking in the equivalent scenario, and study the performance between experimentally trained CNN models and the model trained by simulation as described in this paper.

REFERENCES

[1] Imagenet classification with deep convolutional neural networks, Alex Krizhevsky, Geoffrey E Hinton,2012
[2] C. Holmes, B. W. Drinkwater, and P. D. Wilcox, 'Post-processing of the full matrix of ultrasonic transmit–receive array data for non-destructive evaluation'

Nagu Sathappan

Nagu Sathappan AWeldI is a final year NSIRC PhD student of London South Bank University, based at TWI. She graduated from Anna University, India with a Bachelor's in Production Engineering & Master's in Engineering Design. Having research experience in the field of non-destructive testing (NDT) from IITM motivated her to make this contribution to society. She still takes great pride in serving the teaching profession and empowering young minds. She is incredibly proud in submitting this abstract with the aid of four men who have been her strong pillars of support, including her father and supervisors.

Application of RFID Device for Underwater GMR Sensor Data Storage

Liam Penaluna[1], Mohammad Osman Tokhi[2], Zhanfang Zhao[2], Fang Duan[2], Gholamhossein Shirkoohi[2]
[1]VAL Section, TWI Technology Centre, Port Talbot, UK,[2] London South Bank University, London, UK

3rd Year of PhD

Keywords: Corrosion monitoring ,Magnetic Flux Leakage,GMR sensor,Radio-Frequency Identification

I. INTRODUCTION

In the underwater sector, the use of wireless sensors offers a lot of potential for monitoring the health of rivers and oceans [1]. Humans find it difficult and expensive to detect corrosion in pipes under water: A Remotely Operated Vehicle (ROV) may carry a variety of inspection instruments and record a vast amount of data from on-board sensors [2]. Existing terrestrial wireless sensor network solutions have relied on electromagnetic waves for communication. RFID readers can scan many tags at once and it is omnidirectional whereas Fibre optics is unidirectional [2]. RFID tags are mostly used to identify physical things, and they contain an Electronic Product Code (EPC) [2]. A unique technological solution was investigated in this situation in order to allow the device to function effectively even when submerged.

A Non Destructive Testing tecnique, Magnetic Flux Leakage Testing, involves the use of magnetic circuit (AlNiCo magnet,pipe sample and GMR sensor) where magnetic flux flows through the sample. MFL is widely used in NDT for corrosion monitoring. This paper presents the development of a device to collect and store data from a giant magnetoresistance (GMR) sensor for underwater corrosion monitoring using RFID. The findings show that RFID systems can be used to store data at near ranges regardless of frequency. This paper also provides an investigation into RFID, transponders, and reader classification, as well as existing applications underwater and their benefits.

II. DESIGN/METHODOLOGY/APPROACH

RFID technology is more efficient than other RF approaches when a greater read range, rapid scanning, and diverse data carrying capability are required. An RFID system consists of a transponder and a reader. There are three types of transponders: active, semi-active, and passive tags.

The two main frequencies used by active RFID systems are 433 MHz and 2.5 GHz. Semi active tags combine the advantages of both active and

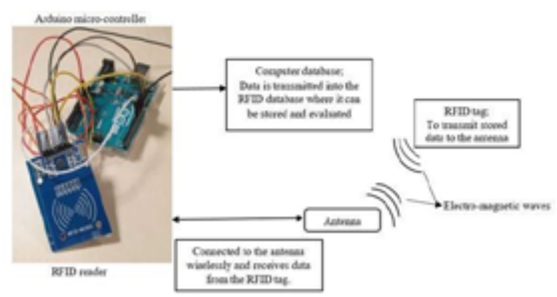

Figure 1. RFID system

passive tags [3]. Unlike active tags, an RFID reader sends a signal to passive tags. The reader sends energy to the transponder's antenna, which transforms it into an RF wave that is sent into the reader's range. A passive tag is powered by the reader, whereas active and semi-passive tags require battery charging [1].

It gives the tag its strength, which fuels the tag's circuits. When the coiled antenna inside a passive RFID tag comes into contact with radio waves from the RFID reader, it generates a magnetic field, and the reader controls the tag [1].

The correspondence between an RFID reader and a tag is controlled by these requirements.

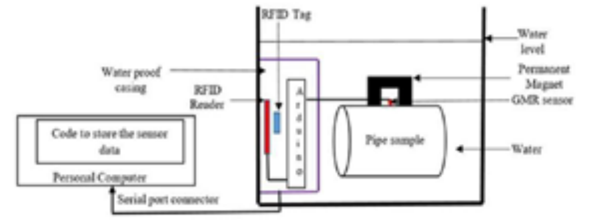

Figure 2: Experimental setup for storing the sensor data in the RFID rewritable tag

III. FINDINGS/RESULTS

The specifications of the equipment used are RFID Reader/writer, Tag – MFRC 522. Frequencies used in RFID applications includes 125 KHz, 13.56 MHz and 860-930 MHz for passive RFID [3];

Because of the reduced reading range, high-frequency systems operating at 13.56 MHz have certain drawbacks.

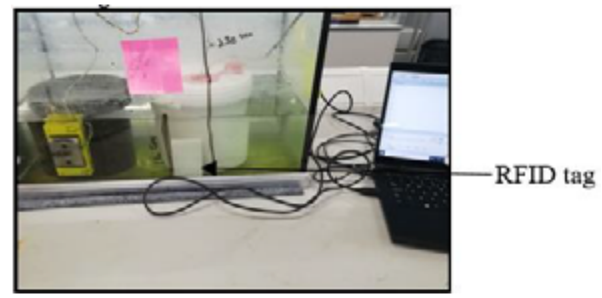

Figure 3. Magnetic circuit immersed in water along with RFID system

The magnetic circuit was immersed in the tank filled with water along with the RFID system, which comprises of Arduino microcontroller connected to the reader. The tag was placed close to it, all together inside a waterproof casing as in Figure 2. The Arduino microcontroller was connected to the laptop through a serial port connector. By running the code, the data from the GMR sensor was collected through the RFID system. Thus, the sensor data goes via the Arduino micro-controller to a writable RFID tag, and the reader reads this and sends to the PC as in Figure 3.

Table 1.Measurement ranges of 125 kHz and 13.56 MHz frequency transponders at different conditions

Tag-type	Frequency	Air	Fresh water	Salt water
PPS + Epoxy	125 kHz	10 cm	5 cm	3 cm
ABS	125 kHz	55 cm	53 cm	51 cm
Nylon	125 kHz	46 cm	42 cm	41 cm
PVC disc	125kHz	49 cm	36 cm	33 cm
Plastic	13.56 MHZ	12 cm	5 cm	4 cm

The maximum range obtained using RFID readable transponder at air is 55cm with ABS at 125 kHz and for salt water it is 51 cm. For 13.56 MHz frequency,the range obtained is 12 cm at air and 4 cm under saltwater.

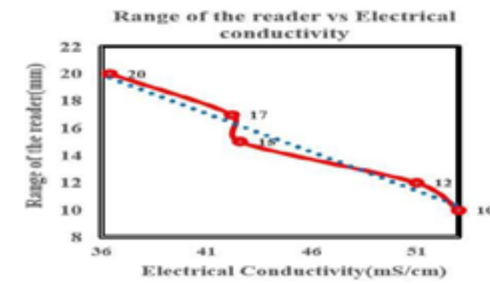

Figure 4. Range of the reader vs Electrical Conductivity for varying salinity level of water

Salinity level of water was slowly increased and the electrical conductivity was measured accordingly.

Range decreases with increase in electrical conductivity, as in Figure 4, due to the salinity level in water where it absorbs more electricity.

IV. DISCUSSION/CONCLUSIONS

A method to gather and store the data sent by the GMR sensor is required. RFID system provides data accuracy. The data sent by the GMR sensor must be stored in order to detect corrosion and reduction in wall thickness as it holds more sensitivity. The RFID system assures data integrity while also cutting down the time it takes to complete tasks. Each RFID tag has a different memory capacity.

The development of RFID sensor measurement has been presented and evaluated for underwater data collection. The findings show that RFID systems can be used to store data at near ranges regardless of frequency. The experimental investigations show satisfactory results in terms of data collection from the magnetic circuit for a 2mm thickness pipe sample.

V. FUTURE PLAN/DIRECTION

The system has been developed for data storage with a single RFID tag whereas testing can be carried out with multiple tags as well. Multiple RFID systems can be used for collection of data at various ranges within the reader, and this will be a subject of future research. However, the ability to use lower frequency bands has led to the advancement of certain RFID applications for particular purposes in both marine and freshwater environments.

REFERENCES

[1] Vasilescu, I.; Kotay, D.K.; Rus, L.D., Dunbabin, M., Corke, I.P.; Data Collection, Storage, and Retrieval with an Underwater Sensor Network, , page 154-165,2005 https://doi.org/10.1145/1098918.1098936.

[2] Michael Ho, Sami El-Borgi, Devendra Patil and Gangbing Song.; Inspection and monitoring systems subsea pipelines: A review paper, Sage Journals.2020 Vol. 19(2)606-645. https://doi.org/10.1177/1475921719837718.

[3] Ali, A.O.; Aiyeoribe.; M.A.; Lucky, O. O.; The Radio Frequency Identification Principles and Technical Impacts in Industrial Sectors, AR Journal of Engineering and Technology.2020 Vol.1: Issue:1, ISSN Print: 2708-5155 | ISSN Online: 2708-5163.

Matthew Weltevreden

In his third year of PhD with the University of Bristol, Matthew is currently based in the fracture integrity management section of TWI. He graduated from the University of Hull with a BEng in Mechanical Engineering and from the University of Bath with an MSc in Automotive Engineering. His PhD focusses on weld residual stress with specific application of probabilistic methods for pipeline girth welds.

Parametric Statistics using Austenitic Girth Weld Residual Stress Data

Isabel Hadley[1], Harry Coules[2]
[1]TWI, [2]University of Bristol
3rd Year of PhD

Keywords: type here

I. INTRODUCTION

Information regarding weld residual stresses in piping components is necessary for reliable and accurate results in fracture assessments. Standards such as BS 7910 [1], R6 [2] and API 579 [3] provide deterministic upper bound assumptions which can be readily applied to a range of welds using two key parameters: the material type (austenitic or ferritic steel) and the weld heat input (Figure 1).

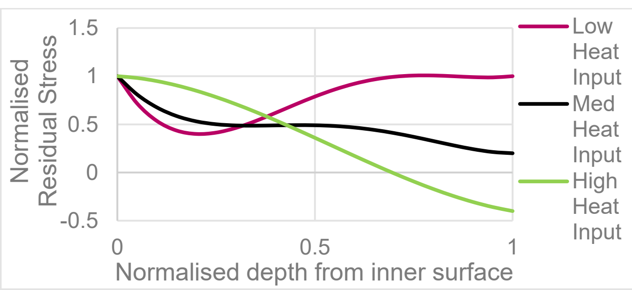

Figure 1. Pipe girth weld axial residual stress upper bound assumption recommended in BS 7910 Annex Q.

Although the generalised use of current upper bound assumptions are useful for encapsulating a large range of pipe girth welds, additional parameters which are currently not considered may provide more reliable and realistic values in fracture assessments. These additional parameters may include joint restraint, outer radius to thickness ratio (R/t), total weld thickness, weld sequencing among many more [4,5]. Introducing additional parameters into a residual stress profile estimation scheme may provide improved and more realistic assumptions for case-by-case analyses. So far, rigorous identification of key parameters has been largely limited to finite element (FE) analyses due to cost and surrounding difficulties involving the required manufacturing and measurement of many welded specimens.

In this work a residual stress database containing reliable weld centre line measurements are analysed in order to test R/t influence on weld residual stresses. Statistical t-tests are used to highlight correlations between various data populations gathered from experimental measurements found in literature.

Quantifying statistical evidence of parameter influence will allow for case specific assessments of girth weld residual stresses and provide guidance towards more accurate profile assumptions. Reducing the potential conservatism of the current upper bound assumption of residual stress could in turn reduce the need for unnecessary weld repairs, inform up-to-date manufacturing considerations and improve assessment criteria for existing and future girth welded components.

II. MEASUREMENT DATABASE & APPROACH

A database of austenitic girth weld residual stress measurements at low heat input (defined as electrical energy per unit weld run length, per unit weld thickness [1]) was assembled from existing literature. Austenitic measurements were considered in this study specifically due to the abundance of reliable studies from power generation applications.

One-sample Kolmogorov-Smirnov (K-S) tests [6] were used to test the relationship of the database measurements to a normal probability distribution. Two-sample t-tests [7] are used to investigate potential parameter influences. As discussed in a previous report [8], the variance of residual stress data was shown to follow a normal distribution throughout the component thickness. A similar assumption will be tested using the presented austenitic database and utilised further to determine parameter influence using two-sample t-tests.

III. RESULTS

The K-S analysis of the weld residual stress data (normalised by the measured parent material yield strength) clearly indicates a normal distribution correlation of the database measurements. The measurement frequency of R/t is represented primarily by lower values (< 6) while measurement data becomes less prominent towards higher R/t values (6 to 10). Two-sample t-tests are performed between each possible combination of the data categories to determine potential parameter influence. The results of the R/t t-tests (Figure 2 & Table 1) show a strong correlation between the datasets for low (< 4) and medium ($4 < R/t < 6$) R/t values, while comparisons between the datasets for high R/t (10) are significantly lower.

2 sample t-test (5% sig, unequal variance)			
Test combinations	Low vs Med	Med vs High	Low vs High
Average P-value	0.62	0.24	0.21

Table 1. Average P-value correlation between datasets.

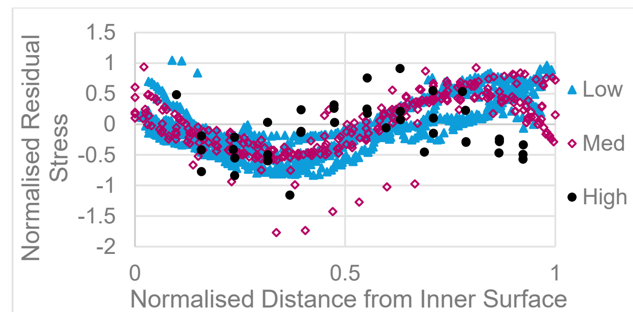

Figure 2. Database measurements separated into 'low', 'med' & 'high' R/t values.

IV. DISCUSSION & CONCLUSION

It is widely accepted that uncertainty and conservativeness exist regarding the current upper bound assumption of axial pipe girth weld residual stress [9]. Improving the accuracy of the residual stress assumption through the use of additional parameters will, in turn, influence treatment to represent more realistic values.

While parameter influence has been documented in previous studies using FE models [10], this work has aimed to establish statistical evidence using an experimental database of residual stress measurements. Based on the presented results it is sensible to assume that R/t is not a significant driving parameter regarding development of weld residual stress. Good agreement of the austenitic girth weld measurements has allowed for rather minimal variation between data groups. Therefore in context of treatment in fracture assessment it is likely that specific consideration of R/t will alter treatment data directly.

V. FUTURE WORK

1. Perform additional statistical tests on reported influential parameters using weld residual stress measurement database.
2. Investigate statistical evidence between weld centreline and heat affected zone measurements and implications for treatment residual stress in fracture assessments.
3. Analyse and compare results with existing FE weld process models regarding parameter influence.
4. Comment on practical implications and postulate approach for improving the residual stress assumption in fracture assessment.

REFERENCES

[1] BSI Standards Publication: Guide to Methods for Assessing the Acceptability of Flaws in Metallic Structures, British Standards Institution, 2019.
[2] EDF Energy (2001), R6 - Assessment of the Integrity of Structures Containing Defects, Revision 4, 2000, as amended, n.d.
[3] Fitness-For-Service API Recommended Practice 579-1 / ASME FFS-1, American Petroleum Institute, 2016.
[4] H. Teng, S.K. Bate, D.W. Beardsmore, Determination of Residual Stress Profiles of Pipe Girth Weld Using a Unified Parameteric Function Form, (2009) 1–8.
[5] M.R. Farahani, I. Sattari-Far, Effect of the Weld Groove Shape and Pass Number on Residual Stresses in Butt-Welded Pipes, Int. J. Press. Vessel. Pip. 86 (2009) 723–731.
[6] A. Kolmogorov, Sulla determinazione empirica di una legge di distribuzione, Inst. Ital. Attuari, Giorn. 4 (1933) 83–91.
[7] B.L. Welch, The Generalization of `Student's' Problem When Several Different Population Variances Are Involved, Biometrika. 34 (1947) 28–35.
[8] M. Weltevreden, I. Hadley, H. Coules, Probabilistic Treatment of Pipe Girth Weld Residual Stress in Fracture Assessment, Int. J. Press. Vessel. Pip. 192 (2021) 104397.
[9] J. Sharples, I. Hadley, Treatment of residual stress in fracture assessment: background to the advice given in BS 7910:2013, Int. J. Press. Vessel. Pip. 168 (2018) 323–334.
[10] P. Dong, On the Mechanics of Residual Stresses in Girth Welds, J. Press. Vessel Technol. 129 (2007) 345.

Oliver Logan

Oliver studied his Masters in Mechanical Engineering at the University of Bristol, graduating in June 2018. He started his PhD in September 2018 at the University of Bristol and TWI Ltd. He is a member of NSIRC and the Solid Mechanics Research Group. His PhD investigates the effects notch tip radius of non-sharp defects has on fracture toughness assessments. This work was co-funded by the Industrial Members of TWI as part of the Core Research Programme and the University of Bristol via a PhD programme. The work was enabled through, and undertaken at, the National Structural Integrity Research Centre (NSIRC), a postgraduate engineering facility for industry-led research into structural integrity established and managed by TWI through a network of both national and international Universities.

Using a Constraint Loss Approach to model Notch Fracture Toughness

Isabel Hadley[1], Yin Jin Janin[1], Nicolas Larrosa[2]
[1]TWI, [2]University of Bristol
3rd Year of PhD

Keywords: Notch Effect, Constraint, Two-parameter Fracture Mechanics, Modified Boundary Layer Models

I. INTRODUCTION

Structural integrity assessment procedures conventionally categorise flaws either as infinitely sharp cracks or local thinned areas (LTAs) [1], [2]. Defects failing an LTA geometry check are assumed to be sharp cracks and are assessed using a fracture mechanics-based approach.

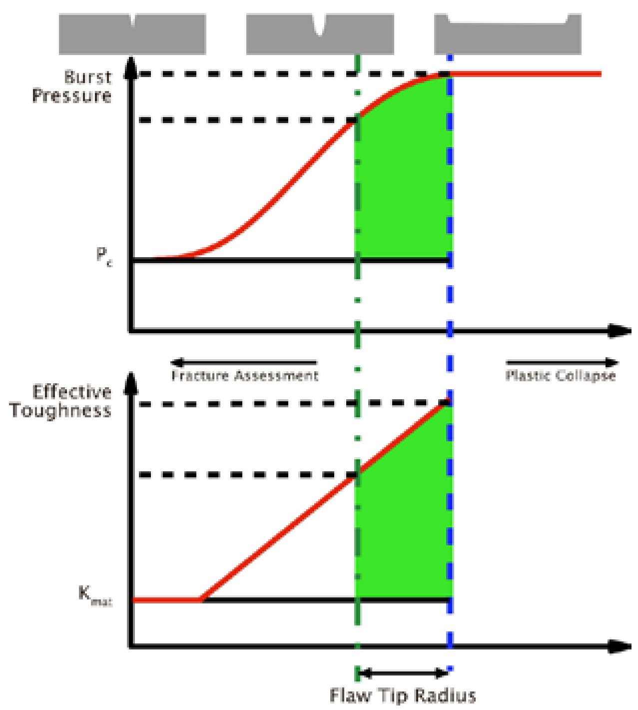

Figure 1: Effect of flaw tip acuity on plastic collapse load and apparent fracture toughness. The black line shows the current value used and the red line shows the expected behaviour.

Although real world defects are often sharp defects or LTAs, they can lie somewhere in between - a non-sharp defect. Figure 1 shows the expected behaviour as defects transition between sharp defects, on the left, into LTAs, on the right, highlighting the excessive conservatism that might be added to an assessment by simplifying a non-sharp defect into a sharp crack. As a result, there is the need to develop procedures that assess non-sharp defects less conservatively [3]–[5].

We propose a method of modelling notch effect on fracture toughness as a loss of crack tip constraint, in much the same way as a change of crack depth. The aim is to find an equivalent cracked specimen to represent a notched specimen by matching the notch load ratio, L_r^ρ and the limit load ratio L_R:

$$L_r^\rho = \frac{P}{P_L^\rho} = \frac{P}{P_L} = L_r \qquad (1)$$

where P is the applied load and P_L and P_L^ρ are the limit load and notch limit load respectively. L_r^ρ was found to remain weakly dependent on notch tip radius, ρ, when reviewed over a range of J values, as shown in Figure 2. Thus, a notch tip radius independent relationship between load levels could be assumed.

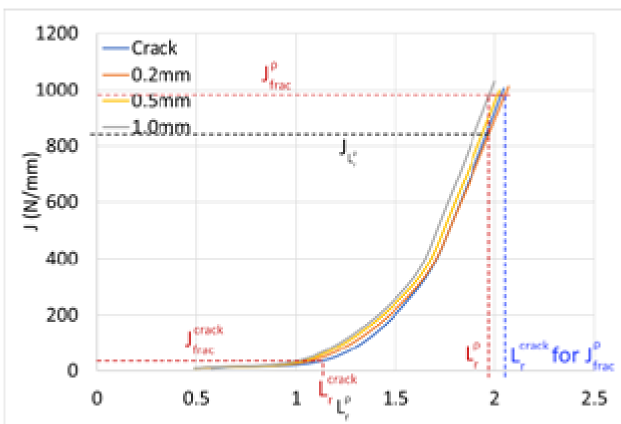

Figure 2: J vs Notch Load Ratio, L_r^ρ, for an elastic-plastic 3D SENB model.

II. MATERIALS AND METHODS

The material properties, defined by laboratory testing, used for computer-based modelling are shown in Table 1. Single Edge Notch Bend (SENB) elastic-plastic specimens were modelled with a range of notch tip radii in ABAQUS.

Table 1: S355 material properties

Property	Value
Yield Strength (MPa)	430
Poisson's Ratio	0.3
Young's Modulus (MPa)	207000
Hardening Exponent, n	13

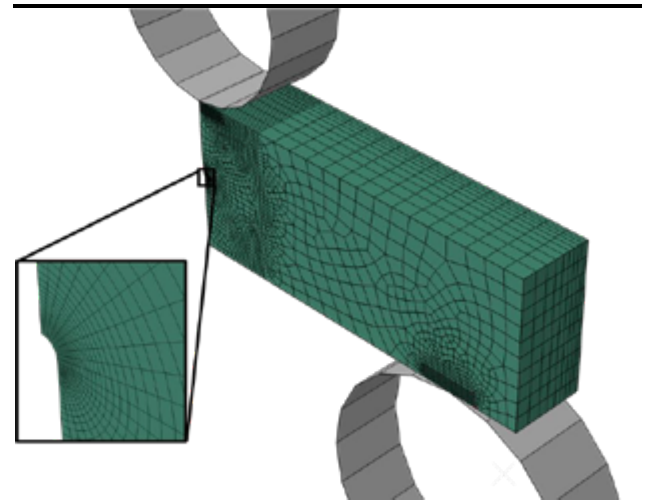

Figure 3: SENB quarter model with analytical loading parts and mesh zoom at the notch tip.

Two sets of SENB models were run; the first modelled each notch tip radius loaded to their value of J at fracture, J^ρ_{frac}, and the second loaded cracked models with values of $J_{L_r^\rho}$ for each notch tip radius. $J_{L_r^\rho}$ was found as shown in Figure 2, L_r^ρ was calculated for each notched model after applying J^ρ_{frac}. Then, by setting $L_r^{crack} = L_r^\rho$, a load could be found by rearranging equation (1); $P = L_r^\rho \times P_L^{crack}$. A value of $J_{L_r^\rho}$ could be found from the cracked model as well as the stress field.

Figure 4 shows the stress fields of the cracked SENB specimen with $J = J_{frac}^{crack}$, the 0.5mm notched SENB specimen with $J = J_{frac}^{0.5mm}$ and the cracked SENB specimen with $J = J_{L_r^\rho}$. A measure of constraint loss, $Q \equiv \frac{(\sigma_{yy})_{J_{L_r^\rho}} - (\sigma_{yy})_{J_{frac}^{crack}}}{\sigma_0}$, was calculated for the two cracked SENB specimen stress fields.

$(\sigma_{yy})_{J_{L_r^\rho}}$ is the stress field for cracked model with an applied load of $J = J_{L_r^\rho}$ and $(\sigma_{yy})_{J_{frac}^{crack}}$ is the stress field for the cracked model with an applied load of $J = J_{frac}^{crack}$, as shown in Figure 4. This Q could be used in a constraint analysis approach, described in standards such as BS7910 or R6 [1,2], to find a notch fracture toughness.

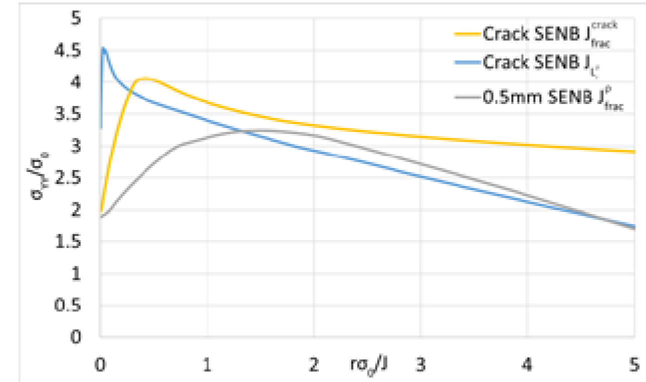

Figure 4: Normalised Stress fields vs normalised distance ahead of notch tip for elastic-plastic SENB models with a crack and 0.5mm notch tip radii

III. CONCLUSIONS

The proposed approach finds the crack stress field equivalent to the stress field of a notch for the same limit load ratio, L_r^ρ, at fracture. The stress field of the equivalent crack for a specific limit load ratio, L_r^ρ, is then used in the framework of two-parameter fracture mechanics to evaluate the constraint parameter, Q. We believe that this approach could be a simple and straightforward method for describing notch fracture mechanics with classical approaches for cracks. This would allow notches to be assessed in a less conservative manner.

IV. FUTURE PLAN

The next steps of the project will be to expand the modelling programme with Modified Boundary Layer (MBL) models. The SENB experimental data can inform the MBL models to create a more generic assessment method. The MBL models can be used to more easily replicate different crack tip loading conditions for assessment of different scenarios.

REFERENCES

[1] BSI, BS 7910:2019 Guide to methods for assessing the acceptability of flaws in metallic structures, (2019) 535.

[2] British Energy Generation Limited, R6: Assessment of the Integrity of Structures Containing Defects, Revision 4 (as amended), EDF Energy Nuclear Generation Ltd. Barnwood, Gloucester, 2013.

[3] J.-J. Han, N. O. Larrosa, Y.-J. Kima, and R. A. Ainsworth, "Blunt defect assessment in the framework of the failure assessment diagram," Int. J. Press. Vessel. Pip., vol. 146, pp. 39–54, 2016.

[4] J. S. Kim, N. O. Larrosa, A. J. Horn, Y. J. Kim, and R. A. Ainsworth, "Notch bluntness effects on fracture toughness of a modified S690 steel at 150 °C," Eng. Fract. Mech., vol. 188, pp. 250–267, 2018.

[5] A. J. Horn, S. Cicero, A. Bannister, and P. J. Budden, "Validation of the Proposed R6 Method for Assessing Non-Sharp Defects," Vol. 6B Mater. Fabr., p. V06BT06A010, 2017.

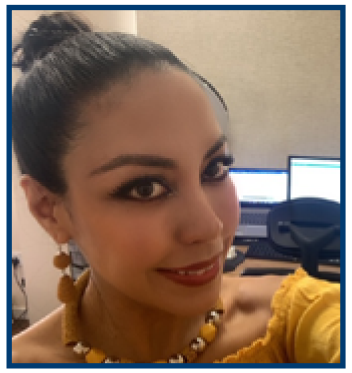

Ana Carolina Araujo-Lascano

Ana received her education in Chemical Engineering from the University San Francisco of Quito in Ecuador (BSc). To pursue her aspirations, she gained a partial scholarship to study Structural Integrity with Brunel University London (MSc), where she graduated with distinction. She carried out her second master program in Corrosion Control Engineering from The University of Manchester (MSc), where she also gained a distinction. Ana is currently an NSIRC PhD student of Coventry University funded by Lloyd's Register Foundation and Coventry University. Her research study is focused on the "Performance of Painted Thermally Sprayed Aluminium (TSA) in Simulated Marine Environment".

Performance of Painted TSA in Simulated Marine Environment

Shiladitya Paul[1], David Parfitt[2]
[1]TWI, [2]Coventry University
2nd Year of PhD

Keywords: Thermally sprayed aluminium, organic coatings, duplex coatings, coating degradation

I. INTRODUCTION

One common approach to mitigate corrosion in the offshore field requires the use of cathodic protection often in conjunction with dielectric coatings. Nevertheless, once the protective organic coating is damaged they offer little or no protection to the asset. As damage is almost unavoidable, these coatings may lead to an expensive inspection and maintenance regime.

An alternative mitigation method is the use of duplex coating systems that includes a sacrificial layer of thermal spray coatings (either aluminium or zinc-aluminium) top-coated with paint. The concept of duplex coatings intends to produce a synergy effect between metallic and organic coatings to extend the long-term protection of the asset and minimize the need of maintenance.

An overall service life of 50 years was expected to be achieved from these systems. Thermally sprayed aluminium has been widely used on large scale projects in marine environments with great success [1]. Difficulties arise, when a thick organic coating is applied on TSA. In fact, according to many in the field, degradation of TSA with the formation of blisters have been reported [2]. It has been assumed that the presence of blistering is primarily due to voluminious corrosion products under the organic coating [2].

The mechanism of this blistering, however, has not been fully explored. The aim of this project is to address this knowledge gap by exploring the corrosion mechanism of duplex TSA coatings. To study this degradation process, the duplex coating system consisting of TSA top coated with Epoxy and Polyurethane on S355 steel were immersed in synthetic seawater at room temperature. Electrochemical tests were carried out to monitor blistering on the duplex coating. Subsequently, microstructural characterisation of the immersed samples will be carried out to understand the blistering mechanism.

II. METHODOLOGY

A. Sample Preparation

Duplicate samples with dimensions of 75x50x6 mm were prepared with the coating systems listed in Table 1. S355 steel, supplied by Parker steel, was used as a substrate material. The impurities, adhered greases and residual surfaces debris were removed using ultrasonic cleaning in acetone. To produce a suitable roughness profile, the specimens were blasted with chilled iron grit media (G12) at 40 psi set pressure.

Table 1: Description of tests conditions

Test name	Sample type / Number of samples	Experiment description
Free corrosion test	Carbon steel + epoxy + PU / 2 samples	The open circuit potential (OCP) is being monitored
	Carbon steel + TSA + Epoxy + PU with defect / 2 samples	
	Carbon steel + TSA + Epoxy + PU / 2 samples	
Potentiostatic cathodic polarization test	Carbon steel + TSA + Epoxy + PU / 2 samples	The current is being measured with an applied potential of -1.1 V (Ag/AgCl)
Potentiostatic anodic polarization test	Carbon steel + TSA + Epoxy + PU / 2 samples	The current is being measured with an applied potential of -0.95 V (Ag/AgCl)

The substrate samples with the combination of the duplex system (TSA and organic coatings) were then sprayed with 1050 aluminium wire, supplied by Metallisation Ltd., to achieve a TSA thickness of ~200 µm using twin-wire arc spray.

After TSA application, these samples were coated (brush applied) with AkzoNobel's epoxy (intergard 410) and polyurethane (interthane 900). The wet layer was evened using a bar coater to attain a uniform dry film thickness of ~150 µm of each layer. The nominal dry film thickness was measured with PosiTest gauge at three locations on each panel to ensure the average value does not exceed the maximium thickness (less than 1.25 x the nominal dry film thickness) as stated by ISO 12944-6 [3].

A circular holiday (artificial defect) was introduced at the centre of two samples using a flat drill with a diameter of 10 mm and 0.9 mm depth corresponding to 5% of sample surface area to expose steel and imitate damage during service.

Additionally, to gain a better insight into the degradation mechanism of duplex coatings, two samples with only paint films were applied into S355 steel.

Finally, the electrical connection between the sample and the potentiostat was created by a threaded rod (insulated with heat-shrink tubing and lacquer). All faces of the samples, except the side with duplex coating, were also isolated with lacquer, as shown Figure 1.

B. Immersion Experiments

A conventional three electrode cell consisting of a working electrode (sample), Pt/Ti counter electrode and a referece electrode of Ag/AgCl (saturated with KCl) was used to conduct long-term tests in synthetic seawater ASTM D1141.

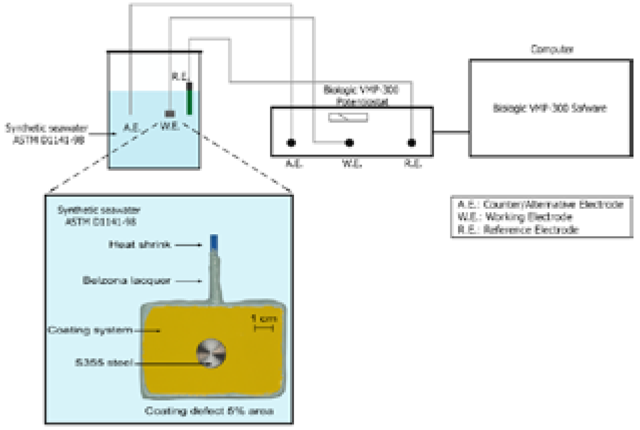

Figure 1:Three electrode cell for immersion tests

Three types of experiments are being performed with a Biologic VMP-300 potentiostat, as listed in Table 1. These are open circuit potential (OCP), cathodic polarization at -1.1 V vs. Ag/AgCl and anodic polarization at -0.95 V vs. Ag/AgCl. The samples have been under immersion for over 10 months.

C. Microstructural Characterization

Material characterization will be performed with Olympus BX41M-LED optical microscope and Scanning Electron Microscope (SEM) with Energy Dispersive X-Ray Analysis (EDX). The identification of corrosion products will be analyzed through Raman Spectroscopy.

III. FINDINGS/RESULTS

Figure 2 shows the sample with duplex coating (left-side) and the sample with the circular holiday to expose steel (right-side) after 10 months of immersion in synthetic seawater. One can notice that no blisters were developed in the protective paint for the sample with the undamaged duplex coating. This is indeed true for all tests except for the experiments with the artificial defect.

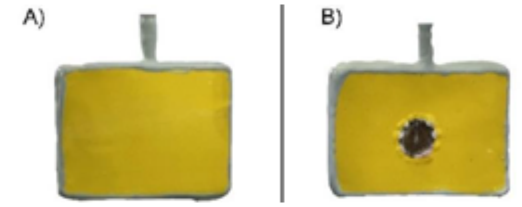

Figure 2: Sample surface after 10 months of exposure A) duplex coating B) duplex coating with artificial defect

When a circular holiday is introduced at the centre of the sample, corrosion deposits are developed below the organic coating located near to the defect region, promoting the appearance of blisters, as shown Figure 2B. Literature has reported aluminium sulphate hydrates as common TSA corrosion products [4]. Calcareous deposits (brucite, aragonite) are likely to develop on top of steel at the edge of the holiday.

IV. DISCUSSION/CONCLUSIONS

- The lack of blisters when no artificial holiday is introduced on the sample surface shows the effectiveness of aluminium metallic coatings with paint to protect steel at least in the short term.
- When the duplex coating is undamaged, very little degradation of aluminium was observed, thus preventing the formation of blisters in the short term.

V. FUTURE PLAN/DIRECTION

- The low anodic current density will be validated through analysing the results from the anodic and cathodic polarization tests.
- To study the degradation mechanism of TSA duplex coatings with artificial holiday, the corrosion products and calcareous deposits will be identified using microstructural characterization tests.

REFERENCES

[1] Fischer, K. P., Thomason, W. H., Rosbrook, T., & Murali, J. (1995). Performance history of thermal-sprayed aluminum coatings in offshore service. Materials Performance, 34(4), 27-35.
[2] Knudsen, O. O., Rogne, T., & Rossland, T. (2004). Rapid degradation of painted TSA. Corrosion 2004.
[3] European Committee for Standardization. (2018). BS-EN-ISO 12944-6. BSI standards publication. Paints and varnishes.
[4] Syrek-Gerstenkorn, B., Paul, S., & Davenport, A. J. (2019). Use of thermally sprayed aluminium (TSA) coatings to protect offshore structures in submerged and splash zones. Surface and Coatings Technology, 374, 124-133.

Adamantini Loukodimou

Adamantini graduated with a Chemistry degree in 2016, which was then followed by a Master of Science degree in Synthetic Chemistry and Advanced Polymeric and Nanostructured Materials in 2018, both undertaken at the University of Patras in Greece. In 2018 she started her PhD at NSIRC and the Innovative Metal Processing Centre for Doctoral Training (IMPaCT) at the University of Leicester. The aim of her PhD is the Development of Self-Healing Coating Systems for Mitigating Corrosion of Offshore Wind Turbines. Her research is supported by Lloyd's Register Foundation.

Development of Novel Coating Systems for Mitigating Corrosion of Offshore Wind Turbines

Shiladitya Paul[1,2], Alan Taylor [1], David Weston[2]
[1]TWI, [2]University of Leicester
3rd Year of PhD

Keywords: marine corrosion, thermal spray coatings, self-healing materials

I. INTRODUCTION

Offshore wind turbines are subjected to harsh and corrosive environments. Fluctuating temperatures, excessive sunlight exposure or bird droppings can cause irreversible damage to these metallic structures. An offshore wind turbine consists of three different zones, the submerged, the splash/tidal and the atmospheric zone, which is the zone under investigation in this research.

Usually cathodic protection is used for the corrosion protection of these structures. Because of the lack of continuous electrolyte (seawater) in the atmospheric zone, this method proves unsuccessful. Hence, the development of advanced coatings is essential. A coating which not only protects, but also enhances the system with self-healing properties is a desirable solution to the corrosive environment of offshore wind turbines. The self-healing materials are microspheres loaded with corrosion inhibitors (silanes). After their formation, these are going to be loaded into an epoxy paint, low in Volatile Organic Compounds (VOC).

When a scratch occurs, the microspheres will rupture and release their content. In contact with the atmosperic air this will solidify and protect the underlying material. In order to ensure the most sufficient protection of the carbon steel substrate, an additional protective layer will be applied on it. This is going to be Zn/Al thermal spray coating. Based on literature Zn/Al can provide corrosion protection acting as a sacrificial layer. In the galvanic series aluminium and zinc are less noble than steel. Subsequently, once the coating is damaged these metals will corrode readily protecting the substrate.

II. DESIGN/METHODOLOGY/APPROACH

Figure 1 visualises the design of the multilayer system, which will be developed.

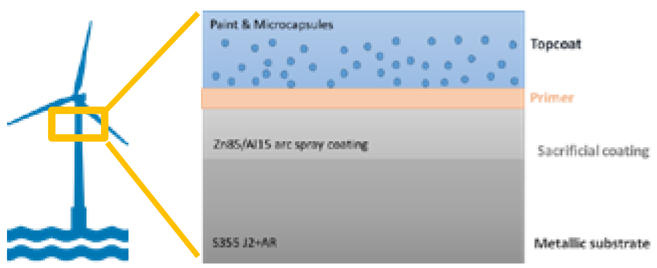

Figure 1: Design of multilayer coating system

The carbon steel samples with dimensions 100x150x5 mm were blasted with alumina (size F24) and then they were sprayed by using the arc spray process with Zn85/Al15. The microspheres consist of a polystyrene shell and are loaded with NXT silane, which has been hydrolysed in water and ethanol solution. The method that is followed for their formation is the solvent evaporation technique from an emulsion as decribed from Cavallaro and Vieira Aoki [1] in Figure 2. This technique is based on the water-in-oil-in-water (W1/O/W2) system, with W1 to be the microcapsule core (hydrolysed silane), which emulsifies in a polymeric solution, O, forming an emulsion of water in oil (W1/O). When the emulsion is stabilised, this phase is dispersed in a continuous medium (W2) according to Martins et. al [2] and microcapsules are formed.

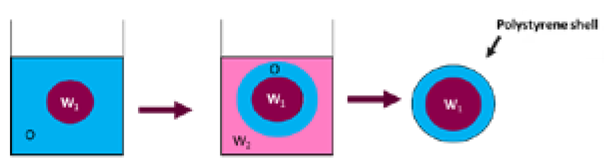

Figure 2: Solvent evaporation technique

Optical microscope and Scanning Electron Microscope (SEM) were used for the surface characterisation of Zn/Al coating in Figure 3a and of microspheres in Figure 5. Additionally for the Zn/Al coating EDX (Energy Dispersive X-Ray Spectroscopy) was used. In order to confirm the corrosion protection, which is offered from the sacrificial coating and the corrosion inhibitors, electrochemical measurements were performed for NXT silanol (Electrochemical Impedance Spectroscopy (EIS), Polarisation Curves and Linear Polarisation Resistance (LPR)).

III. FINDINGS/RESULTS

Figure 3 represents the used TSA gun.

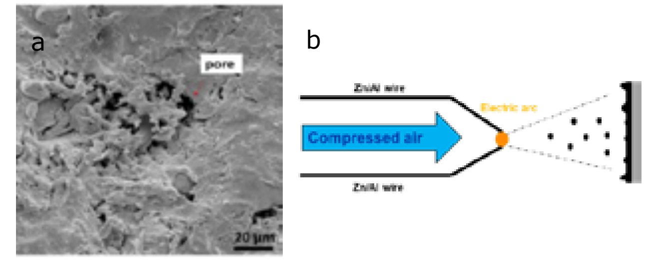

Figure 3: TSA representation and surface of sacrificial coating

It has been found that the size of the microcapsules is affected from the agitation rate of the magnetic stirring as well as from the emulsifier.

For the hydrolysed silane (80EtOH/20H2O) the agitation rates that were tested were 400, 500, 600 and 700 rpm. The following Table 1 gives the produced size of the microspheres.

Table 1

Agitation rate (rpm)	Average size (µm)
400	151
500	137
600	41.5
700	49.2

Another factor which affected the diameter of the microspheres was the used emulsifier for the preparation of the emulsion. When a anionic polysacharite (acacia gum) was used, the average size was much bigger compared to the use of a anionic (SDBS) emulsifier in Figure 4.

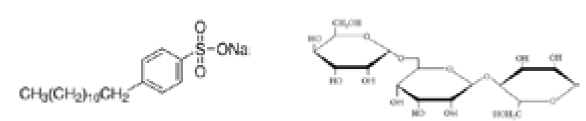

Sodium dodecylbenzene sulfonate (SDBS)

Acacia gum biopolymer (gum arabic)

Figure 4: Emulsifiers

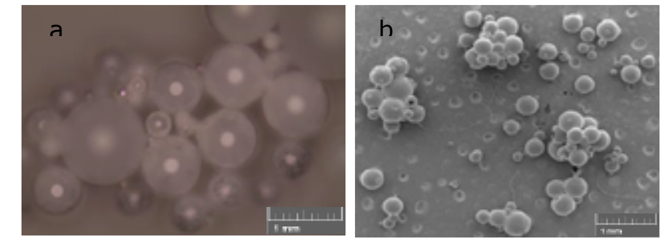

Figure 5: Optical microscope and SEM images of microcapsules

IV. DISCUSSION/CONCLUSIONS

The microspheres that were synthesised had white colour (white powder), a desirable size of around 80-100 µm and were round with smooth surface. Also they were seperated from the others, with each one of them to be loaded with self-healing liquid. The electrochemical measurements showed that NXT silanol provide good anti-corrosion properties to the system.

V. FUTURE PLAN/DIRECTION

Due to COVID, the reseach has been considerably impacted with many experiments having been cancelled. The next steps of this research focus on the chose of a compatible paint to the polystyrene microspheres. Different amounts of microspheres are going to be mixed into the paint and then applied on a primer coating, for better adhesion. Deliberated scratches will be inserted onto the metallic three-layer coupons. Droplet tests of 0.5% and 3.5% NaCl will be performed. Moreover, a simulation model will be developed, which will visualise the rupture of the microspheres and the release of the corrosion inhibitor. Kinetics of the reactions will also be determined.

VI. ACKNOWLEDGEMENTS

The author gratefully acknowledges financial support from the Centre for Doctoral Training in Innovative Metal Processing (IMPaCT) funded by the UK Engineering and Physical Sciences Research Council (EPSRC). This publication was made possible by the sponsorship and support of Lloyd's Register Foundation, a charitable foundation helping to protect life and property by supporting engineering-related education, public engagement and the application of research. http://www.lrfoundation.org.uk/. This work was enabled through and undertaken at the National Structural Integrity Research Centre (NSIRC).

REFERENCES

[1] S. H. Cavallaro, "Evaluation of the use of a sulfosilanol as corrosion inhibitor for galvannealed steel", 2018, University of São Paulo
[2] M. N Martins, E. T. Kubaski, T. Seguinel, S. Cava, M. L. Moreira, S. M. Tebcherani, "Processing conditions for the production of polystyrene microcapsules containing demineralized water", Advanced Powder Technology, Issue 28 (2017): pp. 1221-1227 here.

Aamna Asad

Aamna graduated with a first class BEng (Hons) from Lancaster University in 2017. She later pursued an MSc in Advanced Chemical Engineering from The University of Manchester where her research focused on the determination of self-diffusivities of gases in petroleum using Molecular Modelling techniques. In October 2018, Aamna started an industrial CASE PhD with the University of Cambridge and TWI Ltd. Her work focuses on establishing a methodology to characterise, design and optimise the functionalisation process of silica nano-particles.

Understanding the Structure Function Relationships of Super-Omniphobic Nano-Particles

Alan Taylor[1], Anna Wojdyla-Cieslak[1], Mick Mantle[2]
[1]TWI, [2]University of Cambridge
3rd Year of PhD

Keywords: Silica, nano-particles, functionalise, hydrophobic, nuclear-magnetic-resonance (NMR).

I. INTRODUCTION

Silica nano-particles (SNP) have various applications in many industries such as microelectronics, food, sorption, catalysis, coatings and healthcare [1], [2]. In most of these applications the advantages of silica arise from its structure and chemical nature of its surface, and hence most of its performance is controlled by these properties. The process of functionalising nanoparticles has been known for many years and is used to alter the properties of a surface. The surface of silica nano-particles can be made hydrophobic by functionalising or grafting with certain silanes (coupling agents), such as Hexamethyldisilazane (HMDZ), in order to form trimethylsilyl (TMS) groups (- Si(CH3)3). Grafting can also be achieved by using other modifying agents, these can be, namely alkoxy-, halo-, and aminosilanes and organosilazanes [3]. Surface functionalisation has different applications in a variety of applications including catalysis, biochemical sensing, biolabeling, coatings and photonics. Hydrophobized silica nanoparticles in general, are of interest from a practical point of view because these materials are more well-suited for other practical applications than unmodified hydrophilic silica particles.

This research revolves around developing an innovative method to select and produce new advanced inorganic additives for high performance coatings which will, in-turn, improve interfacial characteristics between the matrix and the additive. The main focus of this research is to quantify the surface of the additive so we may choose and select specific characteristics of the additive and gain an understanding of the relationship of the chemistry with the behaviour such as thickening effects, free flow aids, filler loadings, rheology control etc. The method adopted will aid to differentiate between currently available commercial additives and quantify and qualify the differences. The output shall set the background for future advanced materials, for example, being able to replace fluorinated polymers and coatings in the near future.

II. METHODOLOGY

As part of this research, a group of industrially functionalised and unfunctionalised fumed silicas (supplied by EVONIK Industries) were reacted via vapour deposition techniques with hexamethyldisilazane to facilitate and attain maximum functionalisation. Table 1 summarises physical properties of the respected silicas. Samples were dried at 200ºC for 24 hours in order to remove any residual HMDZ and physically absorbed water. Solid-state ^{1}H, ^{29}Si and ^{13}C nuclear magnetic resonance (NMR) techniques were used to qualify and quantify the extent of additional functionalisation/TMS coverage on the industrially functionalised silica particles.

Table 1 EVONIK fumed silica properties

Sample	R 8200	R 9200	A200	R 812S
Average Surface Area (BET) m²/g	160± 25	170± 20	200 ± 25	260 ± 30
Average Primary Particle size (nm)	-	-	12	7
Loss on drying 2hrs @105 C (%)	≤ 0.5	≤ 1.5	≤ 1.5	≤ 0.5
C content (wt. %)	2.0 – 4.0	0.7 – 1.3	-	2.0 – 3.0
Functionalising agent	HMDZ	HMDZ	-	HMDZ

III. RESULTS AND DISCUSSION

The chemistry of silica has been studied through history by various authors, using ^{1}H and ^{29}Si NMR methods. The various species that can be identified in the following spectra are summarised in Figure 1. Each species can be identified with a certain chemical shift on the NMR spectrum.

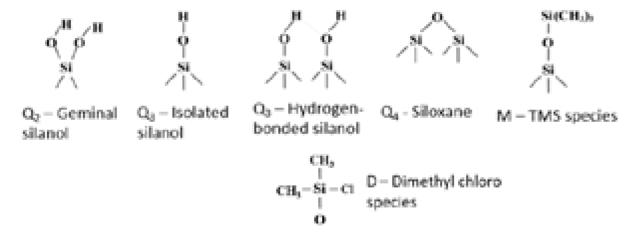

Figure 1 Species present on the silica surface

Figure 2 displays the ^{9}Si High powered (HPD)-MAS spectra of A200 and HMDZ functionalised A200. On functionalisation, an M peak at 13.6 ppm is evident on the spectrum which represents the formation of TMS groups.

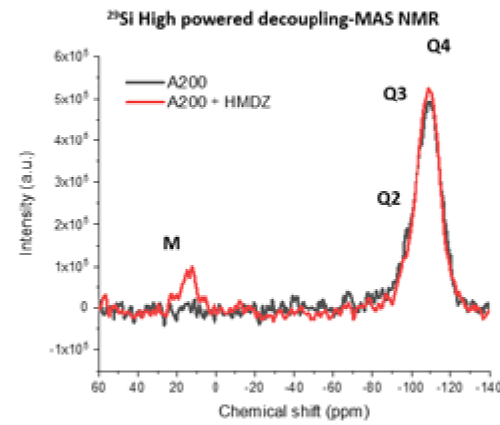

Figure 2 ^{29}Si HPD-MAS spectra of A200 and functionalised A200

The equivalent ^{29}Si Cross Polarisation (CP)-MAS spectra, Figure 3, displays a similar result to the HPD spectra. However, the M peak is 9 times more in intensity, this is due to high abundancy of hydrogen atoms on the TMS groups which provides greater cross polarisation energy transfer and results in a better signal. The Q3:Q4 decreases on functionalisation which indicates that the Q3 species are the active sites taking part in the functionalisation reaction.

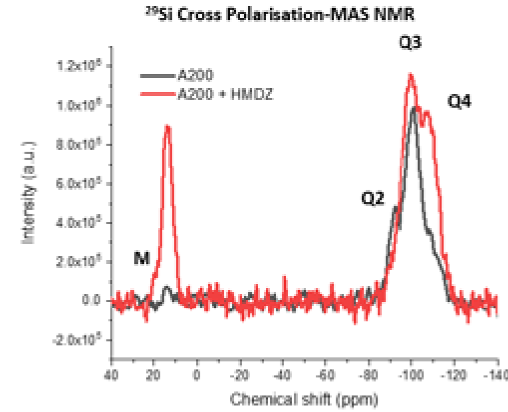

Figure 3 ^{29}Si CP-MAS spectra of A200 and functionalised A200

Figure 4 shows the ^{29}Si Cross Polarisation (CP)-collective MAS spectra of all the EVONIK supplied fumed silicas and the HMDZ functionalised A200. It is evident that all the fumed silicas, except A200, show a defined M region at 13.6 ppm indicating that they are all TMS functionalised with R812S showing the greatest M peak with respect to its Q3 intensity. The R9200 exhibits a D region which indicates that it is functionalised with a dichloro-dimethyl-silane. The presentation will discuss the characteristics of the further functionalised fumed silicas (R series) in greater detail.

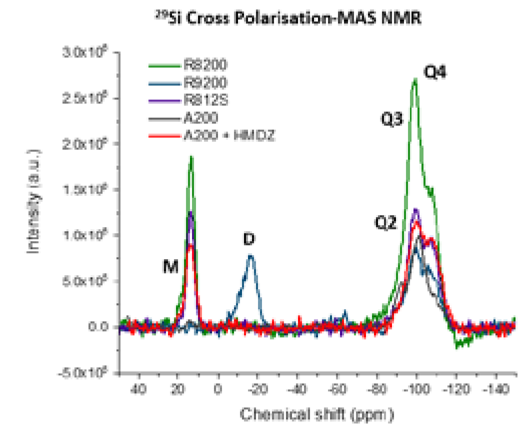

Figure 4 ^{29}Si CP-MAS spectra of A200, functionalised A200, R812S, R8200 and R9200

IV. CONCLUSIONS/FUTURE DIRECTION

In the current state, this research is focused in understanding the chemistry of the fumed silica surface and the changes made post additional functionalisation. It has been analysed that it is possible to further functionalise i.e. reach potential maximum functionalisation on the EVONIK R-series fumed silicas. Future work will consist of using other functionalising agents to investigate the possibilities of multi-functionalisation. Further investigation will also include the incorporation of these functionalised silica additives into model systems and explore its respected compatibility.

REFERENCES

[1] C. C. Liu et. al,, 'The Fumed Silica Surface: A Study by NMR', J. Am. Chem. Soc., vol. 118, no. 21, pp. 5103–5119, Jan. 1996.

[2] T. I. Suratwala et. al, "Surface chemistry and trimethylsilyl functionalization of Stöber silica sols." Journal of non-crystalline solids 316.2-3 (2003): 349-363.

[3] I. S. Protsak et. al, 'A 29Si, 1H, and 13C Solid-State NMR Study on the Surface Species of Various Depolymerized Organosiloxanes at Silica Surface', Nanoscale Res. Lett., vol. 14, no. 1, p. 160, Dec. 2019.

Dimitrios Gaitanelis

Dimitrios was awarded his Diploma in Mechanical Engineering by the Aristotle University of Thessaloniki, Greece in 2015. After working for two years as a Mechanical Engineer, he did his MSc at Cranfield University in 2017 where he studied Aerospace Vehicle Design. He received the Course Director's prize for achievement for his Individual Research Project, where he examined numerically the response of composite stiffened panels in compression after impact. Both of his individual research projects during his Diploma and MSc studies got published in well-acclaimed journals. From 2019, he is an NSIRC PhD student of Brunel University London, sponsored by TWI. His research focuses on high-temperature - short-duration processing of composites, with the overall aim of improving confidence in hybrid composite/metal joints.

Thermal degradation of thermoplastic composites in laser processing: An investigation for composite-metal joining

Dr Chris Worrall[1], Dr Mihalis Kazilas[2]
[1]TWI, [2]Brunel University London
3rd Year of PhD

Keywords: Joining, PEEK, thermoplastics, thermal degradation, Carbon fibre

I. INTRODUCTION

Driven by European Regulations (No. 2019/631) and the USA Corporate Average Fuel Economy (CAFE) standard, automotive and aerospace companies are increasingly looking to use carbon fibre composites to achieve up to 50% weight savings over metallic alternatives. Nonetheless, it is unlikely that these industries will adopt a 100% composite solution, and the optimum design will inevitably comprise both composites and metals.

Currently, mechanical fastening and adhesive bonding are the predominant methods for joining composites to metals [1]. However, these joining methods can suffer from several drawbacks. Mechanical fastening introduces bolts and rivets to the structure that can significantly increase the overall weight [2]. This issue can be overcome with adhesive bonding, which does not induce a flaw in the structure [2]. Nonetheless, to increase the quality of the resulting joint, surface preparation and treatments at optimal conditions have to take place before joining, which can make the process cost-ineffective [1]. Hence, there is a clear need for new, flexible, cost-effective and rapid methods for joining composites to metals, which often involves high-temperature processes.

A fundamental problem in hybrid joining though is that either during the joining process itself or in subsequent joining processes, the metal part is exposed to temperatures higher than the adjoining polymer composite can normally tolerate. The above can trigger the decomposition mechanisms of the polymer matrix and can consequently lead to the degradation of the joint's performance [3]. However, even though the temperature tolerance difference is unavoidable, by managing both temperature and exposure time the reduction in the joint's strength can be minimised.

II. METHODOLOGY

The PhD is focused on establishing the underpinning fundamental science of high-temperature - short-duration processing of polymer matrix composites. In addition, the research is focused on the fundamental science of the fibre/matrix interface, especially after undergoing a severe thermal cycle where the fibre coating may have been damaged. In detail, carbon fibre (CF) reinforced poly-ether-ether-ketone (PEEK) is examined and the applied methodology for identifying the optimum high-temperature - short-duration processing of CF-PEEK in hybrid joining applications is the following:

- Develop a coupled thermal-chemical model to identify the laser processing of CF-PEEK that does not thermally degrade the material;
    - Thermogravimetric analysis (TGA) to derive the kinetic parameters of PEEK (activation energy, reaction order, pre-exponential factor);
    - Use of user-defined subroutines to implement these parameters in Abaqus software;
- Develop a thermal degradation assessment methodology for laser processing of CF-PEEK;
    - Fourier-transform infrared spectroscopy (FTIR), differential scanning calorimetry (DSC) and nanoindentation to assess the thermally induced damage;
- Develop a fibre/matrix interface assessment methodology to assess the interfacial shear strength (IFSS), before and after the heating treatment;
- Experimentally evaluate the effect of excessive thermal degradation on the structural performance of a composite-metal joint.

III. FINDINGS

A coupled thermal-chemical model is developed to identify the processing conditions that can achieve high temperatures without inducing a severe thermal damage on the composite material. A maximum decomposition of 1% has been found tolerable [2] and the process window that leads to a decomposition less than 1% is therefore defined (Fig. 1).

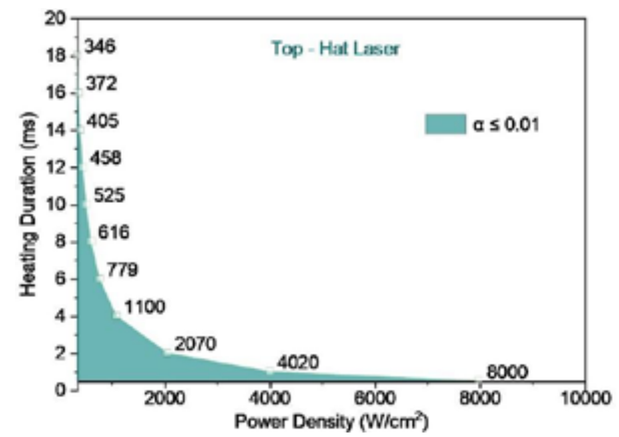

Figure 1: Laser processing of CF-PEEK for achieving a decomposition ≤ 1% (0.5 - 18ms).

In addition, an experimental assessment methodology is developed that can provide an answer on what is the approximate extent of the resulting degradation after high-temperature - short-duration processing is applied at PEEK and CF-PEEK.

In detail, an FTIR analysis of samples that were heated up to 600°C with heating rates of 5, 20, 50 and 100°C/min took place. Through this investigation, several spectral changes were noticed and a new peak was formed at 1711 cm^{-1}, which was found to be directly linked with the process of degradation (Fig. 2).

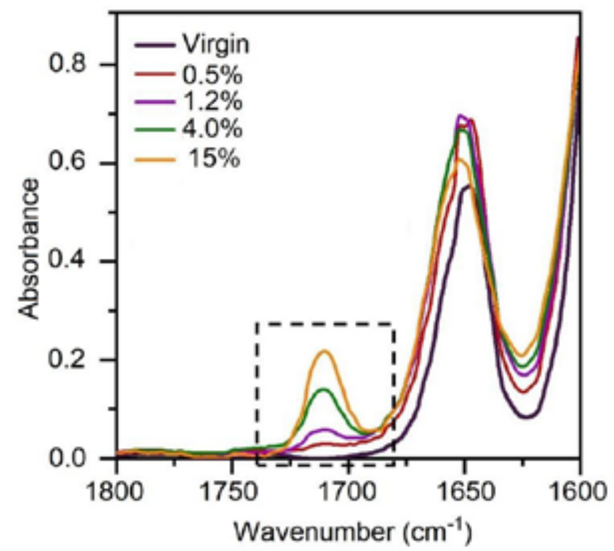

Figure 2: The development of the 1711 cm^{-1} peak in a PEEK sample heated with 100°C/min up to a mass loss of 0.5%, 1.2%, 4% and 15%.

IV. CONCLUSIONS

- A numerical model has been developed, capable of defining the processing conditions that can minimise the extent of the heat-affected zone of CF-PEEK in high-temperature applications.
- The process window for achieving high-temperature processing of CF-PEEK without triggering the degradation mechanisms of the PEEK matrix has been defined for a heating duration between 0.5ms and 18ms.
- For a top-hat laser, the required power density, where the material decomposes less than 1% has been found to vary from 8000 to 346 W/cm^2.
- An FTIR investigation of PEEK and CF-PEEK samples, heated at the controllable conditions of a TGA furnace, showed that a new peak is developed as degradation progresses.
- This new peak can be used as a detection tool to identify whether the material has been thermally affected after high-temperature - short-duration processing is applied.

V. FUTURE PLAN

To further establish the optimum high-temperature - short-duration processing of CF-PEEK in hybrid joining applications, a multi-scale and multi-technique analysis is taking place. In detail, the steps that are to be undertaken are described below:

- Identify the processing conditions that slightly degrade PEEK and CF-PEEK upon laser heating with FTIR;
- Evaluate the effect of laser heating on the composite's crystallinity with DSC;
- Assess the induced thermo-mechanical damage with nanoindentation;
- Perform single fibre pull-out tests (SFPTs) to assess the IFSS, before and after the heating treatment;
- Numerically and experimentally assess the effect of excessive thermal degradation on the performance of a CF-PEEK/Titanium joint;

REFERENCES

[1] C. Worrall, M. Mortello, Hybrid composite-to-metal joining, TWI Report 32221/1/2019 (2019).
[2] A. Pramanik et al., Joining of carbon fibre reinforced polymer (CFRP) composites and aluminium alloys - A review, Composites Part A: Applied Science and Manufacturing 101 (2017).
[3] X. Tan et al., Characteristics and formation mechanism of porosities in CFRP during laser joining of CFRP and steel, Composites Part B: Engineering 70 (1) (2015).

Bowei Li

Bowei Li received his MSc in Mechanical Engineering from Brunel University London in 2018, after completing a BEng in Mechanical Design, Manufacturing and Automation from Xi'an University of Science and Technology. Bowei started his PhD with Brunel University London in February 2019, and his research topic is 'Laser riveting: an innovative technique for dissimilar composite to metal joining' in collaboration with The Welding Insitute (TWI) and NSIRC. This research aims to create a novel rivet joint for dissimilar materials by laser-based metal wire deposition application.

Laser Riveting: An Innovative Technique for Dissimilar Materials Joining

Ali Khan[1], Bin Wang[2]
[1]TWI, [2]Brunel University London
3rd Year of PhD

Keywords: Laser metal wire cylinder deposition

I. INTRODUCTION

In the transport sector, there has been a recent emphasis on the practice of 'light-weighting' in which engineers attempt to reduce the overall weight of structures in order to:

- Meet emission targets and standards as required by both national and international legislation and policy
- Improve the fuel economy of the vehicle and reduce costs for the owner
- Meet the public's environmental expectations of the sector.

The main way in which aerospace manufacturers minimize the weight of transport structures is by selecting higher-strength construction materials to use. Such materials are not only metallic (Titanium and Aluminium); there are also non-metallic materials: Carbon Fiber Reinforced Polymer Composites (CFRPs) in further trials.

TWI has developed a technique it has termed 'laser riveting (LR)' which offers a quicker, cheaper, more flexible, and more effective way to circumvent the limits of existing mechanical fastening techniques.

II. METHODOLOGY

The final aim of this research is to create a dissimilar joint between composite and metal. In this case, the project consists of two main research processes: laser metal wire deposition (LMwD) to build a solid rivet on the metal substrate, and dissimilar joining to interlock composite sheet to the metal substrate. The different metals (titanium, aluminium, and steel) and CFRP are used to create dissimilar metal-to-metal/composite joints after designing and developing the experiments. Several analyses were conducted including, but not limited, to metallurgy (cross-section microstructure observation and alpha and beta phase change), chemical (fraction changes in Fe and V), strength, and fatigue tests. For the numerical analysis, the corresponding ABAQUS simulations of laser riveting also have been developed in this project.

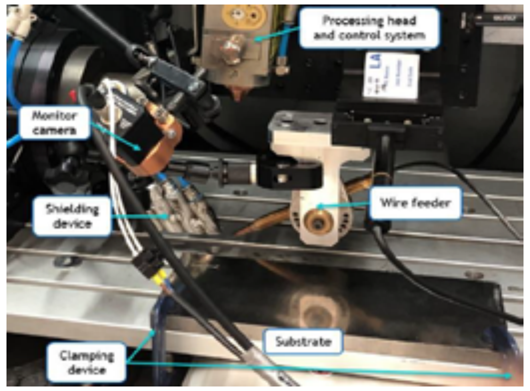

Figure 1 LMwcD processing system setup

In the preliminary experiment, the main investigation on the basic research objective, laser metal wire cylinder deposition (LMwcD) has been completed, the processing system is shown in Fig 1. The feasibility study confirmed the solid cylinder feature can be built on the substrate by additive layer method (ALM) with a proper circle path strategy. In the parametric studies of LMwcD, the industry-productivity-time of the process was shortened. Through control of the processing parameters, different deposition strategies have been designed: High Speed (HS) deposition by increasing the speed and reduce the cooling time. In addition, a new continuous spiral deposition method (CS) and improved high-speed spiral (HSS) method are developed which removed the cooling step between layers. The comparison results of different deposition methods were analyzed from productive and metallurgy aspects in the rivet building process.

The LMwcD was applied to the LR concept, the dissimilar Ti6Al4V/AA6062 joint has been built by HSS and the following post-wash procedure is high-frequency laser scanning, which improved the crown feature and welding condition of the rivet. The original build and various post-washed rivets were compared, and their qualities are evaluated by microstructural analysis, micro-hardness, and tensile shear tests.

Further LR application for dissimilar Ti6Al4V/CFRP joining trials were explored, the HSS and HS employed to create the initial joints, and the ceramic insert bush and Al thin cover plate were manufactured and used to protect the CFRP from the thermal damage in the process. Moreover, post-deposition and post-scanning methods were designed to reduce the heat input thus minimising the degradation of the joined sheets during the joining process. The cross-sections of rivets were analyzed by microstructural observation and their strength evaluated through the tensile shear tests.

RESULTS

1. Feasibility and parametric studies for LMwcD, productivity comparison from initial normal to final HSS method.

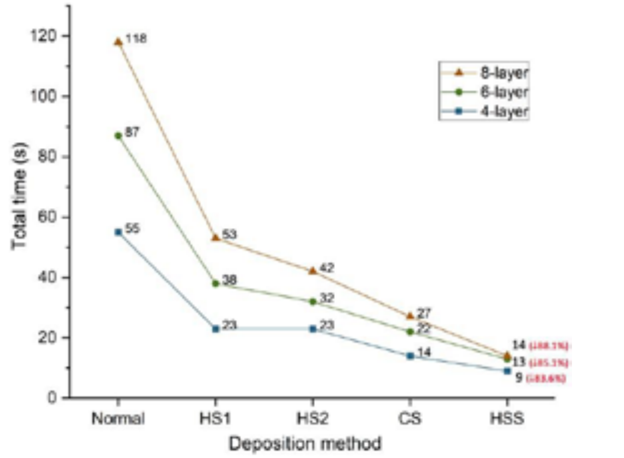

Figure 2 Comparison of results of different LMcwD methods processing times against LMcwD methods for increasing numbers of layers.

2. LR for dissimilar Ti6Al4V to AA6061 joining, original and 12s post-washed rivets.

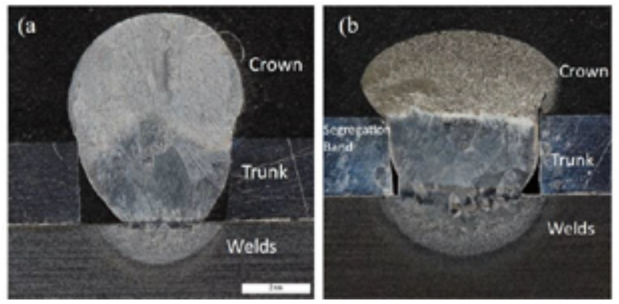

Figure 3 cross-section overviews of dissimilar Ti6Al4V/AA6061 joints of (a) original and (b) post-washed rivets.

3. LR for dissimilar Ti6Al4V to CFRP joining, cross-section of post-sccaning and post-deposition rivets.

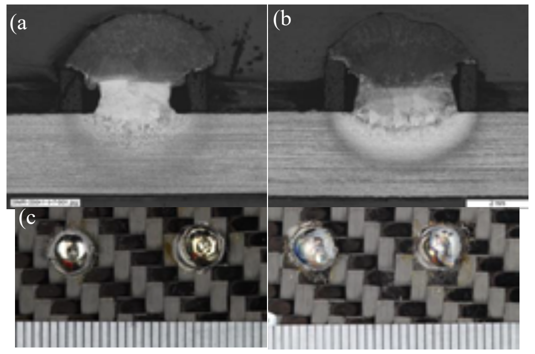

Figure 4 Cross-section overviews of dissimilar Ti6Al4V/CFRP joint for (a) post-scanning, (b) post-deposition rivets and (c) their topview outlooks.

III. DISCUSSION AND CONCLUSIONS

In the preliminary LMcwD feasibility study, the cylinder feature has been built by circle ALM deposition, showing a proper cross-section without major defects (porosity and crack) detected. Systematically designed parameter optimization studies have allowed the process mechanism to achieve increase productivity up to 7 times.

The original HSS deposited rivet has provided the basic strength, it was further post-processed by implementing a high-frequency laser washing technique to re-melt and deform the crown of the build to form a sound rivet joint. The quality (both aesthetics, metallurgy, and mechanical strength) of the rivet is highly dependent on the post-wash parameters, especially relates to the energy input, and the welding area was expanded from 3.42mm^2 to 8.6mm^2. In addition, further study investigated the potential influence of the deposition strategy for the rivet building.

Due to the serious degradation of CFRP in the direct LR joining process, the realized carbon decomposition contaminated the deposition in the initial layer, which significantly harmed the rivet strength. Alternatively, the contamination was much reduced and intact deposition was observed in post-scanning and post-deposition rivets. A positive correlation was found between the post-scanning time and the extension of the contamination.

IV. FUTURE WORK

Laser riveting as a novel concept has unique benefits compared to the current conventional joining method, the basic deposition process, and its feasibility study is introduced and investigated in this study, but it still needs further comprehensive research such as parametric studies and iterative optimization to achieve a mature industrial standard.

Amarachi Frances Obilor

Amarachi is an NSIRC PhD student of Loughborough University based at TWI. She received her education in Materials and Metallurgical Engineering from the Federal University of Technology Owerri (BEng) and University of Lagos (MSc) both in Nigeria, where she gained a distinction. Her research interest centers on processing of polymers for various functionalities. Sponsored by TWI and Loughborough University, her PhD study focuses on laser Processing for Surface energy control of polymers.

Laser Processing for Surface energy control of polymers

Dr. Andy Wilson[1], Dr Manuela Pacella[2], Prof Vadim V. Silberschmidt[2]
[1]TWI, [2]Loughborough University
2nd Year of PhD

Keywords: PEEK, Laser, surface modification, contact angle, adhesion, wettability, roughness

I. INTRODUCTION

PEEK is a high performance organic thermoplastic material with excellent mechanical and chemical properties. It has been used in several biomedical applications because of its interesting properties. In the aspect of reconstructive surgery, PEEK is used in the manufacture of joint implants and other bone replacements in human bodies. Similar to bone, PEEK is biocompatible with good load bearing capacity and high shear strength. However, it exhibits poor interfacial bonding due to its high chemical stability. The need to enhance the surface properties of PEEK has led to several areas of research. Laser surface engineering is an effective method towards improving the adhesive properties of this polymer. This method involves the modification of surface chemistry and topography with a view to increase surface wettability by reducing liquid contact angles. Modified surfaces with roughness values just below 1µm or above have shown improved adhesive bonding of implant to bone (Martin et al., 1995).

The influence of laser parameters in the surface modification or texturing of PEEK is reported in previous studies. However, no study has investigated picosecond laser processing of PEEK using varied beam delivery methods.

II. METHODOLOGY

The material used in this study is unfilled injection moulded PEEK from Victrex PLC. It was cut into rectangular coupons measuring 50 mm X 25 mm X 4 mm. Prior to laser processing, the samples were degreased with isopropyl alcohol. A mode-locked Yb-doped fibre laser pulsed laser with a wavelength of 1064 nm and output power of 25 W was used for the processing. Laser parameters were selected based on preliminary experiments. The pulse duration was 8.8 ps at 200 kHz and the laser beam was focused at 182 mm. The scan speed was set at 5000 mm/s and the sample stage remained stationary during the raster scan. The fluence was calculated using;

$$F = \frac{4P_m}{\pi {w_0}^2 f} \quad ,$$

where P_m is the pulse energy (J), w_0 is the beam's spot radius (cm) and f is the frequency (Hz) (Pacella et al., 2014).

III. FINDINGS/RESULTS

The laser treated surfaces were characterized using a Zeiss EVO LS15 scanning electron microscope, Alicona 3D profilometer and KRUSS DSA100 drop shape analyser. PEEK H1 (**Error! Reference source not found.**) had the lowest mean contact angle measurements of 75° and 50° with deionised water and diiodomethane, respectively. Generally, surfaces with contact angle values lower than 90° are considered hydrophilic or more wettable. Further surface analysis of PEEK H1 with the 3D profilometer showed a roughness value of 3.8 µm, while that of the control sample is 2.1 µm. Around a fluence of $1.79\ \mathrm{J/cm^2}$, the total surface energy increased from $37\ \mathrm{mNm^{-2}}$ to $42\ \mathrm{mNm^{-2}}$. SEM images were obtained after taking contact angle and roughness measurements to ensure that their results are not influenced by the sample preparation method which involves a thin layer of gold coating.

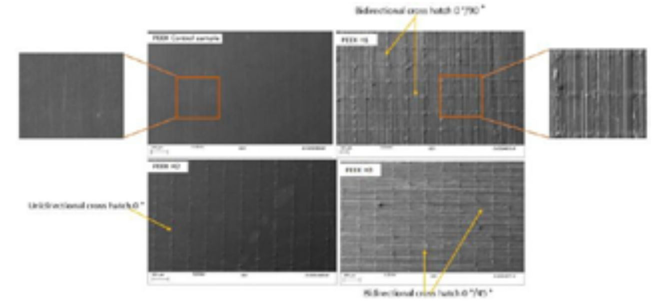

Figure 1: SEM micrographs of laser treated surfaces.

From SEM micrographs, slight surface protrusions/swellings along the laser paths are visible. These can be attributed to bond breakage in the sub-surface. Previous works have reported an inverse relationship between laser intensity and carbon/oxygen ratio as well as the formation of functional groups such as carbonyls and carboxylic acids (Wilson et al., 2015). It is not clear if the topography has influenced the contact angles. This is because of the negligible change in the dispersive coefficient of the surface free energy obtained.

IV. FUTURE PLAN/DIRECTION

In addition to direct laser writing on PEEK, this work focuses on developing a laser system that creates an interference pattern on the irradiated PEEK surface to produce features that are much smaller than the laser spot size used. This system works by the convergence of split beams on the sample surface. Further surface analysis using XPS and lap shear tests will give more insight on surface chemistry changes and the shear strength of the laser treated surfaces. Additional experiments will be done with varied parameters and beam delivery methods to investigate their influence on surface free energy alongside adhesive properties.

REFERENCES

[1] Martin, J. Y., Schwartz, Z., Hummert, T. W., Schraub, D. M., Simpson, J., Lankford, J., Dean, D. D., Cochran, D. L., & Boyan, B. D. (1995). Effect of titanium surface roughness on proliferation, differentiation, and protein synthesis of human osteoblast-like cells (MG63). Journal of Biomedical Materials Research, 29(3), 389–401. https://doi.org/10.1002/jbm.820290314

[2] Pacella, M., Axinte, D. A., Butler-Smith, P. W., & Daine, M. (2014). On the topographical/chemical analysis of polycrystalline diamond pulsed laser ablated surfaces. Procedia CIRP, 13, 387–392. https://doi.org/10.1016/j.procir.2014.04.066

[3] Wilson, A., Jones, I., Salamat-Zadeh, F., & Watts, J. F. (2015). Laser surface modification of poly(etheretherketone) to enhance surface free energy, wettability and adhesion. International Journal of Adhesion and Adhesives, 62, 69–77. https://doi.org/10.1016/j.ijadhadh.2015.06.005

George Brooks

George is a third year PhD student with NSIRC and Sheffield Hallam Univeristy (SHU). Following a year in industry with Knorr-Bremse Rail services as part of his aerospace engineering BEng, he returned to SHU where he undertook his final year project investigating Simultaneous Double Sided Friction Stir Welding - a project that was supported by TWIs technology centre in Sheffield. From this collaboration he applied for the PhD position funded by TWI's Core Research Programme to continue and expand upon this work.

Investigation into the Influence of Friction Stir Welding in Thick Section Aluminium Alloys

Stephen Cater[1], Stephen Magowan[2]
[1]TWI, [2]Sheffield Hallam University
3rd Year of PhD

Keywords: Friction Stir Welding, Aluminium, FSW, Joining

I. INTRODUCTION

Friction Stir Welding (FSW) is a solid-state joining process that in its simplest form, uses a non-consumable tool with a specially designed shoulder and probe to stir material softened by friction to form a joint, such as demonstrated in Figure 1.

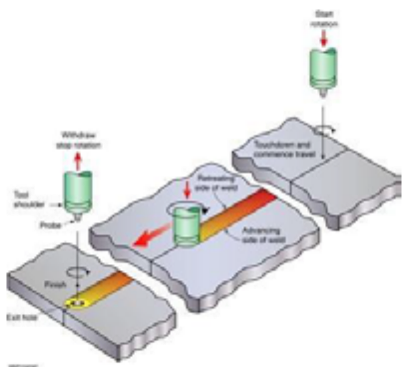

Figure 1 - Schematic of the FSW process [1].

The primary aim of the research project is to investigate the influence of welding variables on the microstructure and mechanical of welds created in thick section aluminium and thereby develop the technical and commercial benefits of the FSW process.

II. METHODOLOGY

Plates of 900x130x50mm AA5083-H111, AA6082-T651 and AA7050-T7451 were welded to the same grade of alloy by Weld-Flip-Weld (WFW-FSW) and Simultaneous Double Sided (SDS-FSW) and subsequently tested. The composition of the alloys is presented in Table 1.Further plates of 500x130x50mm were welded using Supported Stationary Shoulder (SSS-FSW) as this technique was untested in the thickness of material, investigation into tool life was first necessary. All welds were produced using the PowerStirTM available at TWI Ltd in South Yorkshire.

Wt. %	AA5083	AA6082	AA7050
Al	94.200	97.5	90.600
Cr	0.110	0.011	0.008
Cu	0.070	0.016	1.850
Fe	0.350	0.19	0.120
Mg	4.430	0.74	1.830
Mn	0.480	0.53	0.010
Other	0.028	0.076	0.04
Si	0.240	0.92	0.054
Ti	0.017	0.010	0.058
Zn	0.075	0.007	5.290
Zr	-	-	0.140

Table 1 - Composition of alloys.

Microstructural analysis of the material included Optical Emission Spectroscopy, Energy dispersive X-ray spectroscopy (EDX) Optical Light Spectroscopy (OL). Mechanical testing focused on Micro-hardness and tensile testing. In addition, energy input into the weld and swept volume per revolution were calculated.

III. RESULTS

Results for the WFW-FSW in AA7050-T7451 are presented below. The weld was produced using traverse and spindle speeds of 130mm/min and 130rpm respectively. Figure 2 and Figure 3 show the macrograph and microstructure. Within the stir zone (Figure 3d, e & f) the grains are equiaxed and particles appear intergranular. Where the probes overlapped and produced a double processed region, e, the grains are much smaller. Whereas in the Heat Affected Zone (HAZ), where the heat input was sufficient to allow the precipitates and grains to grow, there are several larger grains surrounded by smaller grains.

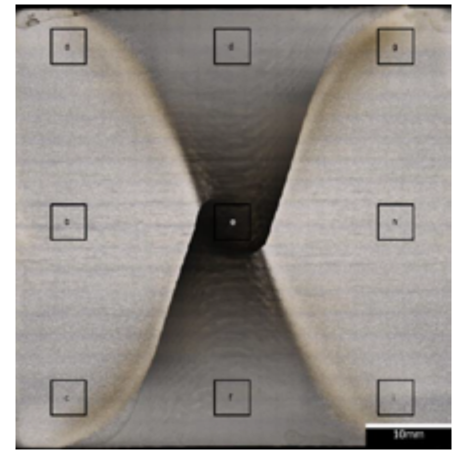

Figure 2 - Macrograph of the WFW identifying regions of microstructural analysis.

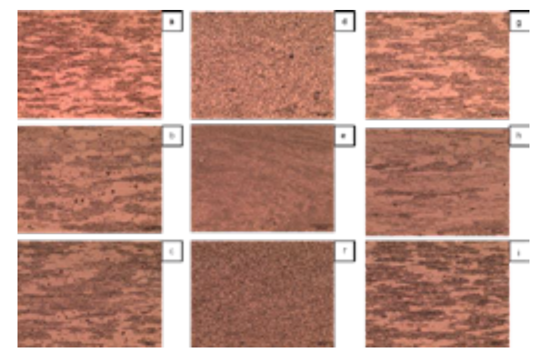

Figure 3 - Microstructure of the WFW once etched in Krolls reagent.

The tensile data shown in Table 2 indicates that the WFW has retained 77.90% the strength of the parnt material. All three of the samples tested, failed on the retreating side of the weld and passed through the double processed region as pictured in Figure 4. The failure has followed the region that hardness testing identified as the softest region as demonstrated in Figure 5.

ID	Avg UTS (MPa)	Avg Elongation (%)
PM	537.52	12.50
WFW	418.76	4.02

Table 2 - Tensile data for WFW vs PM.

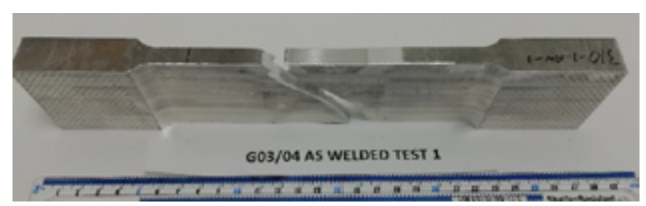

Figure 4 - Failed WFW tensile sample.

The hardness of the weld, shown in Figure 5, suggests that where the Thermo-Mechanical Affected Zone (TMAZ) meets the HAZ, the material retains 55% of the hardness of the Parent Material (PM).

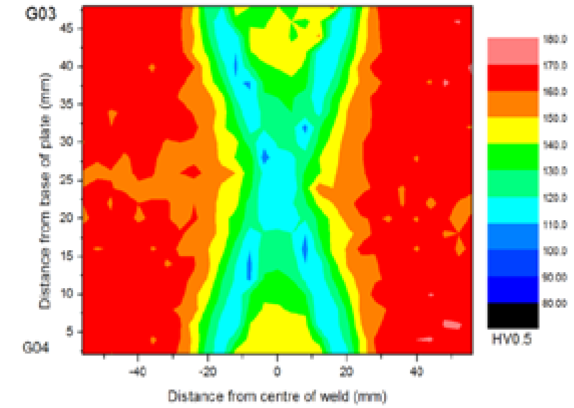

Figure 5 - Micro-hardness contour map of G03/04.

This relates to the larger grains shown in Figure 3, which were influenced by the heat from the weld. However in the stir zone there is a 70% retention in hardness compared to the PM. Although this region is hotter than the HAZ, the mechanical deformation of the grain structure by the rotating probes produces grains typically a factor of 10x small than the PM and equiaxed. This reduces the effect of the heat input by forming more grain boundaries for the dislocations to pass through.

IV. CONCLUSIONS

Overall, eleven welds have been produced in 50mm thick aluminium alloys. These have been produced using Friction Stir Welding (FSW) variants; Weld-Flip-Weld (WFW-FSW), Simultaneous Double Sided (SDS-FSW) and Supported Stationary Shoulder (SSS-FSW).

The following observations have been made with regards to the microstructural and mechanical properties of the welded materials;

- The macrograph of WFW-FSW shows a clear hourglass shape to the stir zone.
- Grains within the stir zone appear equiaxed and refined compared to the grains in the HAZ.
- Tensile data suggests a retention of 77.90% strength vs the parent material.
- Retention of ~70% hardness is observed in the stir zone but only 55% at the TMAZ/HAZ transition.

V. FUTURE PLAN

Future work on this project will continue the investigation into the microstructure of the welded material by conducting EBSD and TEM analysis.

REFERENCES

[1] Cater, Stephen, Dick Andrews, and TWI Ltd. 2014. Fundamentals of Friction Stir Welding.

Nigar Gul Malik

Nigar has an MSc degree in Mechanical Engineering from Queen Mary University of London and her BSc degree is in Metallurgy and Materials Engineering from University of Engineering and Technology, Pakistan. Currently, she is undertaking a PhD at the University of Leicester. Her project focuses on the production of REACH-complaint coatings for corrosion protection of high strength steels in aerospace environment. She is carrying out her research at, the National Structural Integrity Research Centre (NSIRC), a postgraduate engineering facility for industry-led research into structural integrity established and managed by TWI through a network of both national and international Universities.

Development of Novel REACH-Complaint Coatings for the Protection of High Strength Steels

Shiladitya Paul[1], Karl S Ryder[2]
[1]TWI, [2]University of Leicester
2nd Year of PhD

Keywords: zinc-nickel coatings; ED-Aluminium coatings; ionic liquids; salt spray test; embrittlement test; scanning electron microscopy; energy dispersive X-ray spectrometer.

I. INTRODUCTION

The toxic and carcinogenic nature of cadmium and its compounds is of high concern to the EU. It falls under the category of candidate list of substances of extremely high concern for authorisation, https://echa.europa.eu/candidate-list-table. Therefore, its usage is discontinued across various industrial sectors. Some industrial sectors namely aerospace, defence, mining, offshore and nuclear sectors have a sunset date and continue to utilise cadmium, though special authorisation is required for certain applications. These sectors impose high safety requirements. Nonetheless, there is research going on for REACH* compliant cadmium substitutions.

Some of the candidates include zinc, zinc-nickel (Zn-Ni) alloy and electrodeposited Aluminium (ED-Al). Among these, Zn-Ni and ED-Al have the most potential. Zn-Ni alloy coatings contain qualities of both; zinc and nickel, thereby demonstrating an acceptable corrosion rate. Zn-Ni coatings containing 10 – 15% Ni [1-] are considered to possess the best corrosion protection. However, these coatings have not been tested in the environment suitable for aerospace and testing methods are typically based on visual examination. Furthermore, current method of development of these coatings is limited to certain types of steel.

II. METHODOLOGY

Electrolyte was prepared by dissolving 25g of boric acid in 500ml of DI water. After boric acid had completely dissolved, 40g of zinc chloride was added to the solution and mixed to dissolve. This was followed by addition of 100g of nickel chloride hexahydrate which was also mixed to dissolve and then finally 200g of potassium chloride was added. The solution was continuously stirred at 300rpm and once it was completely clear, pH was adjusted by using either KOH or HCl solution. Ni sheet was used as the anode whereas copper (hull cell panels and strips) was used as the cathode.

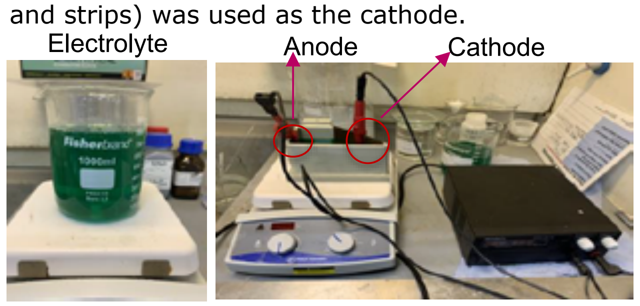

Copper panels and strips were polished using 600 and 1200 grade emery paper. Pre-treatment of copper panels and strips was carried out by using sulphuric acid solution (50ml of H_2SO_4 and 450ml of H_2O) as an activator. Copper was immersed in the activator for 15 seconds. After this, these panels and/or strips were rinsed with DI water and placed in the electrolyte. Anode was also immersed in the electrolyte. Electrodeposition was carried out for 10 minutes at different pH, current densities and temperatures. After deposition, samples are dried using a compressor gun.

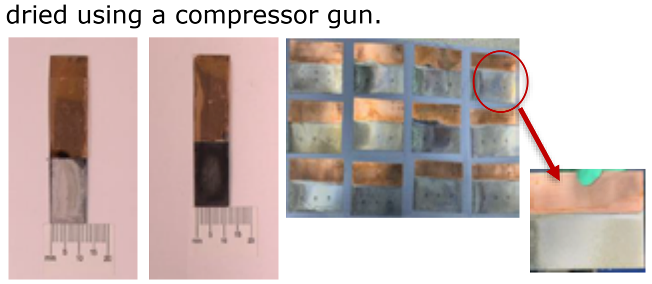

III. RESULTS AND DISCUSSION

Zn-Ni coatings produced were observed to be uneven and coarse. SEM analysis demonstrated the coatings to have a globular morphology and there was no sign of gamma phase whose existence provides optimum corrosion protection to the substrate.

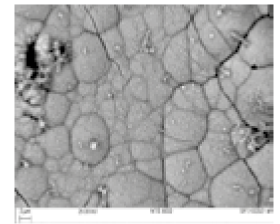

Figure 1

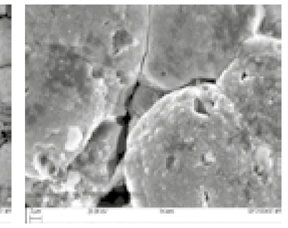

Figure 2

Figure 1 and 2 demonstrate SEM images (at 2 µm) of Zn-Ni samples at pH 4.35 and 5, respectively, when the temperature was 25C and the current density was 3 A/dm2.

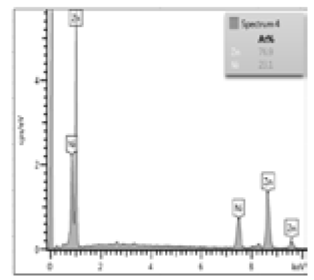

Figure 3

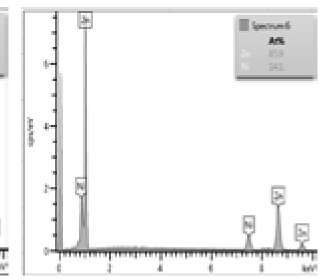

Figure 4

Figure 3 displays the EDX analysis of Zn-Ni sample at pH 5, temperature 30C and current density 0.2 A/dm2. It reveals that this sample constitutes of 76.9% zinc and 23.1% nickel. Figure 4 exhibits that this Zn-Ni sample had 85.9% of zinc and 14.1% of nickel. Operating conditions for this sample were pH 5, temperature 25C and current density 1 A/dm2. According to literature, Zn-Ni coatings have 10-15% Ni exhibit the best corrosion protection [1-3].

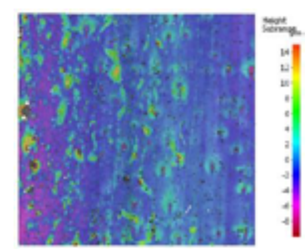

Figure 5

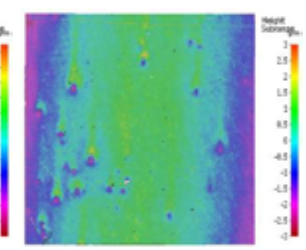

Figure 6

The above figures show profilometry images of a Zn-Ni sample (pH 5) produced at a temperature of 25C and a current density of 2A/dm2. Figure 5 is an image taken at a distance of 2.5cm of the Hull cell panel and figure 6 reveals profilometry image at a distance of 7.5cm, respectively. It can be observed from the images that figure 6 reveals a smoother surface as compared to figure 5. This could be due to the diagonal alignment of the panel during electrodeposition, thereby leading to a higher current density at 2.5cm as compared to the current density at 7.5cm.

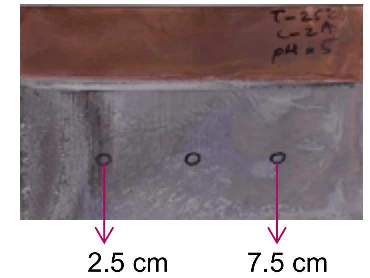

Figure 7: A copper hull cell panel with Zn-Ni deposition at pH 5, temperature 25C and current density 2A/dm2.

IV. FUTURE PLAN

1. To perform the Zn-Ni deposition using different electrolytes

- Chloride (acidic)
- Sulphate (acidic to slightly neutral)
- NaOH (alkaline)
- Citrate/Acetate (low toxic new electrolyte)

2. Electrodeposition on high strength steel (AISI 4340)

3. Parameters to be studied

- Deposition conditions: applied current density, deposition temperature, time
- Electrolyte conditions: pH, concentration of metal precursors, influence of anions (chloride, sulphate, acetate, citrate)
- Mode of deposition: Pulse plating, reverse pulse plating

V. ACKNOWLEDGEMENTS

I would like to express my gratitude to my supervisors Professor Karl Ryder, Dr Shiladitya Paul and Professor Andy Abbott who kindly accepted me as their PhD student and also for their guidance and support. I would also like to thank Ben Robinson for his assistance and encouragement in the project. Additionally, I am extremely appreciative for the help and support provided by my family and friends. Lastly, I pay highest regards to all the staff members who helped me with the training for working in laboratories.

REFERENCES

[1] Byk T V., Gaevskaya T V., Tsybulskaya LS. Effect of electrodeposition conditions on the composition, microstructure, and corrosion resistance of Zn-Ni alloy coatings. Surf Coatings Technol. 2008 Aug 15;202(24):5817–23.

[2] Benballa M, Nils L, Sarret M, Mü C. Zinc-nickel codeposition in ammonium baths [Internet]. Vol. 123, Surface and Coatings Technology. 2000. Available from: www.elsevier.nl/locate/surfcoat.

[3] Gavrila M, Millet JP, Mazille H, Marchandise D, Cuntz JM. Corrosion behaviour of zinc-nickel coatings, electrodeposited on steel [Internet]. Vol. 123, Surface and Coatings Technology. 2000.

*REACH is European Union regulation concerning the Regulation, Evaluation, Authorisation and restriction of Chemicals. It came into force on 1st June 2007.

TWI

CORE RESEARCH PROGRAMME

DAY 2 ABSTRACTS

Channa Nageswaran

Dr Channa Nageswaran has been working with ultrasonic phased array technology for 12 years and has published several papers on the subject. His primary field of interest is the research, development and application of the technology towards industrial inspection of critical components and structures. Channa has developed his knowledge and skills through large collaborative research and development projects. His present role in TWI includes providing tailored site inspection services to major clients in all industrial sectors throughout the world. Channa joined TWI in 2007 and holds a EngD in the field of phased array technology development and a MEng in Aeronautical Engineering.

Influencing Parameters for the Ultrasonic Inspection of Austenitic Welds

Author: J Lambert and C Carpentier

Download **Available to TWI Industrial Members**

Industrial Need

Improving the ultrasonic inspection of austenitic stainless steel (and nickel alloy) welds requires a good understanding of the influence of welding parameters on the metallic structure of the weld. By understanding the impact of these parameters on inspection capability, both welding and inspection procedures can be designed with due consideration for the required level of quality in the joint.

Key Findings

- In order to improve the likelihood of detection across the full volume of the weld, it is recommended that several techniques should be utilised to cover the same region of weld. Low frequencies are more suitable for detection of discontinuities, whereas higher frequencies are better suited for any sizing requirements.
- Generally for weld thickness in the range considered in this project, and likely for lower and higher thicknesses, the recommended sound frequencies is between 1 and 5MHz. Frequencies outside this range can be utilised but with likely loss in resolution and increased sensitivity to attenuation.
- The metallurgical structure of the weld appears to ‘guide’ the sound towards the root, which was observed on all welding positions regardless of the level of asymmetry in the solidification structure. Along with other factors related to focusing and convergence point of transmit-receive probe types, this appears to increase the likelihood of detecting root flaws.
- Even though only stainless steel was included in this project, similar results could be expected for other austenitic material that develop textured grain growth guided by cooling gradients. This statement is supported by experience in TWI, but it should be noted that the use of nickel alloy in welds and cladding are generally lower in thickness than the 60mm joints in this project, so it is possible that effects could be more pronounced in comparison to 300-series stainless steel in similar thicknesses.
- It is possible to measure through-wall height of planar flaws and using tip diffraction signals. However, it should be noted that in cases where the weld can only be inspected from a single-side, there is a risk that flaws on the opposite side may not be detected and, if detected, may not be sizeable. Care should also be taken with root flaws, which may be under sized, in particular with lower frequency probes. This again reinforces the earlier recommendation that several techniques and frequencies should be used to inspect austenitic welds.
- Imaging techniques such as FMC/TFM and PWI did not demonstrate a clear benefit in comparison to the different phased array techniques, but further work should be done to seek any such benefit, because there are many operational modes that remain to be investigated and under development.
- The evidence in this report supports the need for stringent qualification of selected techniques when the welds to be inspected are of a sufficient critical nature, to establish the necessary performance for detection, and sizing if necessary. Several formal methods for qualification are available to industry.

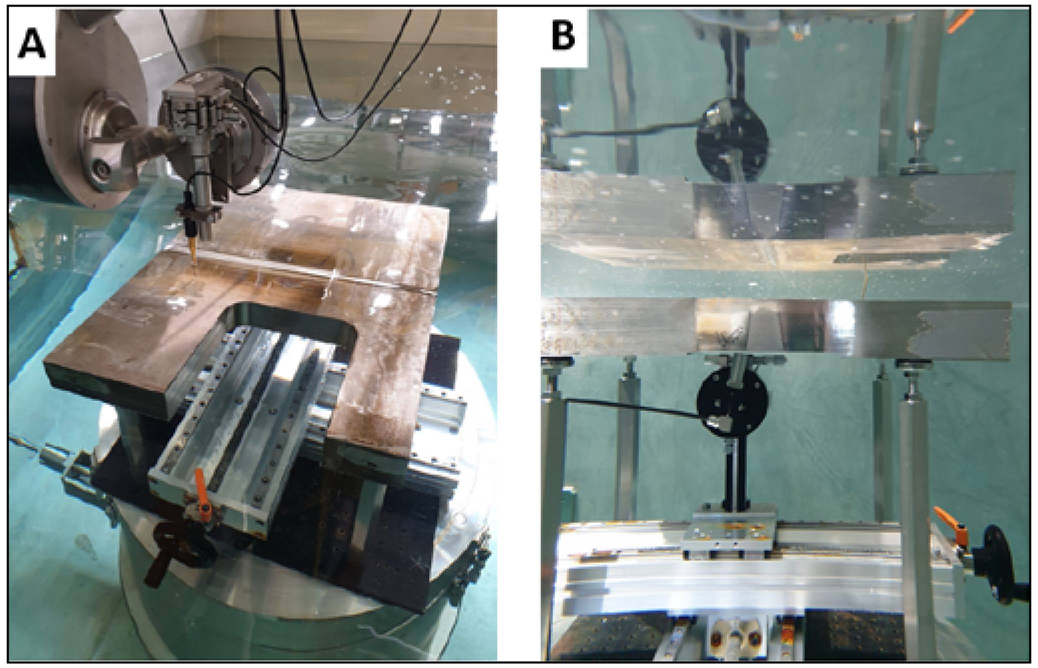

Figure 1: Multiple piercing head, with 100 pin blocks attached

Muhammad Ali

Muhammad joined TWI in 2007 and has been working in the field of Fracture Mechanics and Testing within the Materials and Structural Integrity Group of TWI. Muhammad has been working on projects involving Fitness-For-Service assessment of structures used in various industrial sectors, i.e., oil and gas, process industry, power and transport. Many of these projects involved materials testing and fracture mechanics based Engineering Critical Assessment to various standards. Muhammad is also experienced in fracture mechanics testing in sour environments and had been involved in developing new techniques for testing in this area. He has also been working on projects involving technical disputes and has experience of working as an expert witness in arbitrations.

Refill Friction Stir Spot Welding Parameter Development for Transport Industry Aluminium Alloys

Author: P Santos and A McAndrew

Download **Available to TWI Industrial Members**

Industrial Need

Refill friction stir spot welding (RFSSW) has several advantages compared with other mainstream single-point joining or mechanical fastening processes. Although many organisations recognise these advantages and benefits, further research is required in order to implement this technology into large-scale production and increase the current technology readiness level. This report describes the collection of baseline mechanical properties and microstructure characterisation of RFSSW welds on various transport aluminium alloys used in the transport sector, intending to promote industrial uptake.

Schematic of the RFSSW process:

a) Shoulder-plunge variant

b) Probe-plunge variant

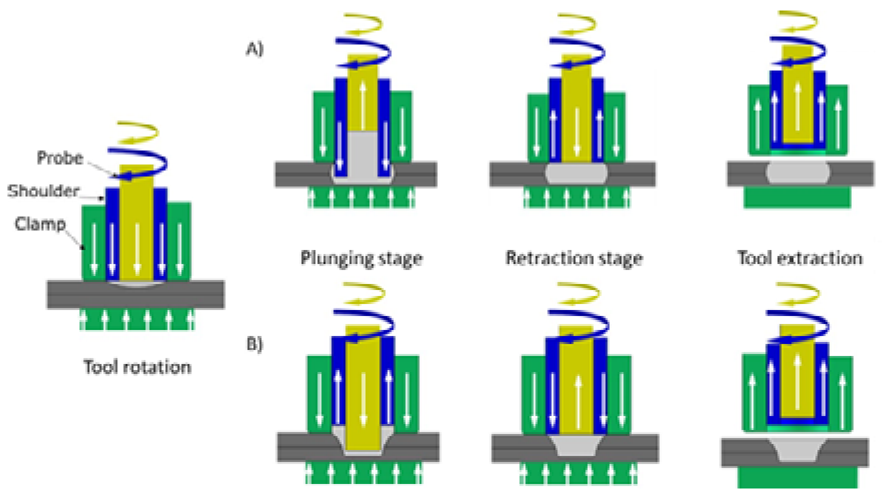

Key Findings

- Welding of most AM materials by conventional means is both possible and relatively insensitive to the configuration of the AM material relative to the weld interface.
- At the macro scale, the structures in the HAZ and weld metal of the joints were entirely conventional in their nature and no unusual or unexpected microstructure was seen to form as a result of the incorporation of AM material into the joint.
- It was noted that significant porosity occurred adjacent to the fusion boundaries of the joints between aluminium PBF specimens. It is felt that the most likely cause of this is dissolved gas being released from the PBF microstructure and boiling out through the weld metal.

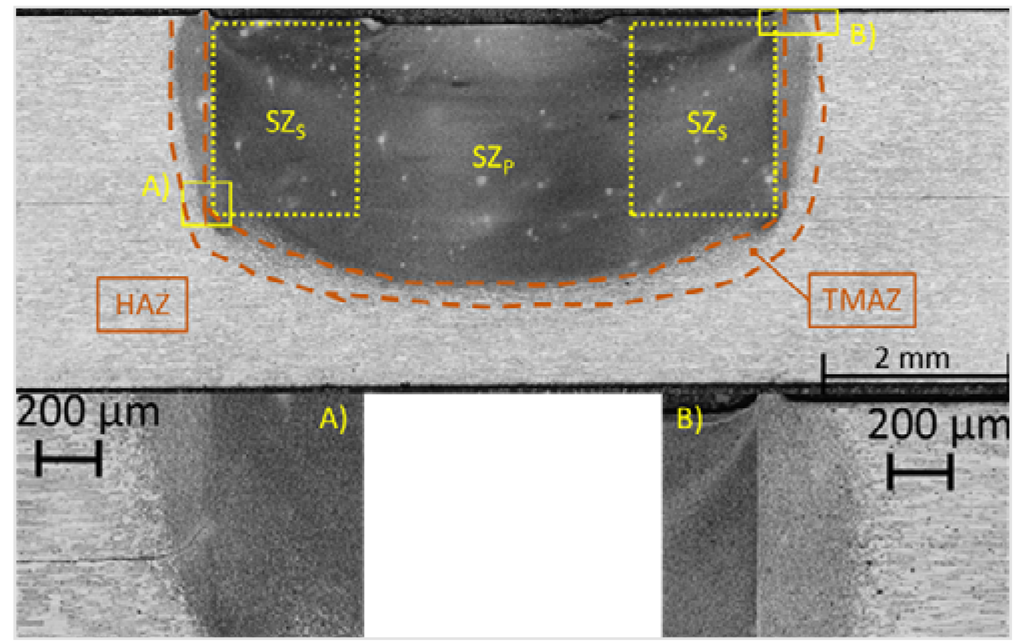

Cross-section of RFSSW AA7075 (in T6 condition). SZp and SZs are the stir zones of the probe and shoulder respectively. HAZ is the wider heat affected zone surrounding the weld:

a) Hook region (transition from unjoined region to welded area);

b) Stir zone/thermo-mechanically affected zone (SZ/TMAZ) interface

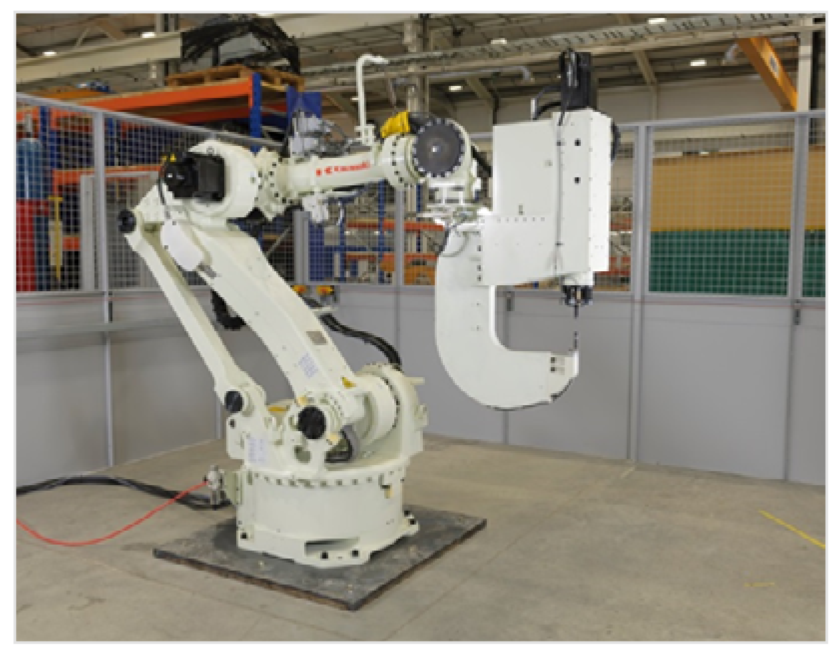

TWI's FW-35 KHI RFSSW system

Ewen Kellar

Ewen has over 25 years' experience in the field of adhesive bonding and related processes at TWI. Since joining the company, he has led or been involved in many projects within almost every industry sector including assessing the use of adhesive systems within the marine industry, adhesive fractography, adhesive debonding and medical adhesive systems. In parallel with this work he has also been active in the area of pre-treatments for bonding, with a particular focus on plasma and related processes. He has presented at many conferences and published extensively, in addition to being an author or contributor to several books.

Gas Plasma as a Universal Dry Pre-treatment for Structural Bonding Applications

Author: : D Williams and E Kellar

Download

Available to TWI Industrial Members

Industrial Need

One area of the structural adhesive bonding of metals is the pre-treatment stage. This is a critical phase of the joining process as it prepares the surfaces prior to the application of the adhesive with the aim of ensuring that the resulting joint is strong and durable. Currently, many metal pre-treatments use wet chemical based processes to etch the metal surface and modify its chemistry. The largest issue with this practice is that different metals require different types of chemical etchant. When bonding two or more metals, each etchant will have its own set of immersion processes to clean and treat each material; which, in turn, will affect the energy consumption, consumables and time required.

This work explored the use of cold atmospheric plasma (CAP) to treat metals prior to adhesive bonding as a means to move away from wet processing. It focused on two different metals, commonly used in industrial settings i.e. stainless steel (316), and titanium alloy (Ti 6Al 4V). In industry, plasma is predominantly used on metal substrates as a low-pressure batch process, which limits its viability for use on a production line. The plasma treatment investigated in this work operates at ambient pressure and therefore has the potential for use on a production line. The CAP torch also allows for the precise treatment of discrete areas of a structure prior to adhesive bonding, which could be an additional benefit.

Key Findings

- A significant increase in dry bond strength, above the untreated state, is realised through the application of CAP as a pre-treatment on both stainless steel and titanium. The CAP treated stainless steel joints performed more than 10% better than oxalic/sulfuric acid etched samples. The performance of CAP treated titanium joints was about 5% lower than chemically etched samples.
- The durability of the bonded joints produced within this project using CAP was similar when considering stainless steel, when used in conjunction with grit blasting, but does not perform as well for titanium.
- The CAP process is less complicated with fewer stages and input/output streams. This may mean there are fewer control systems required and the material wastage for the process is easier to manage.
- CAP has the potential to be a multi-material pre-treatment system that can be scaled up by linear addition of components such as nozzles etc and automated using off-the-shelf equipment.
- It has been shown to offer a less energy intensive route over current 'wet' pre-treatment systems in addition to being greener with a low health and safety impact.
- Current studies on the effect of CAP have shown that the treatment window is relatively wide and has relatively low substrate sensitivity, i.e. the technology can treat a range of substrates effectively with only minor modifications to the process parameters.

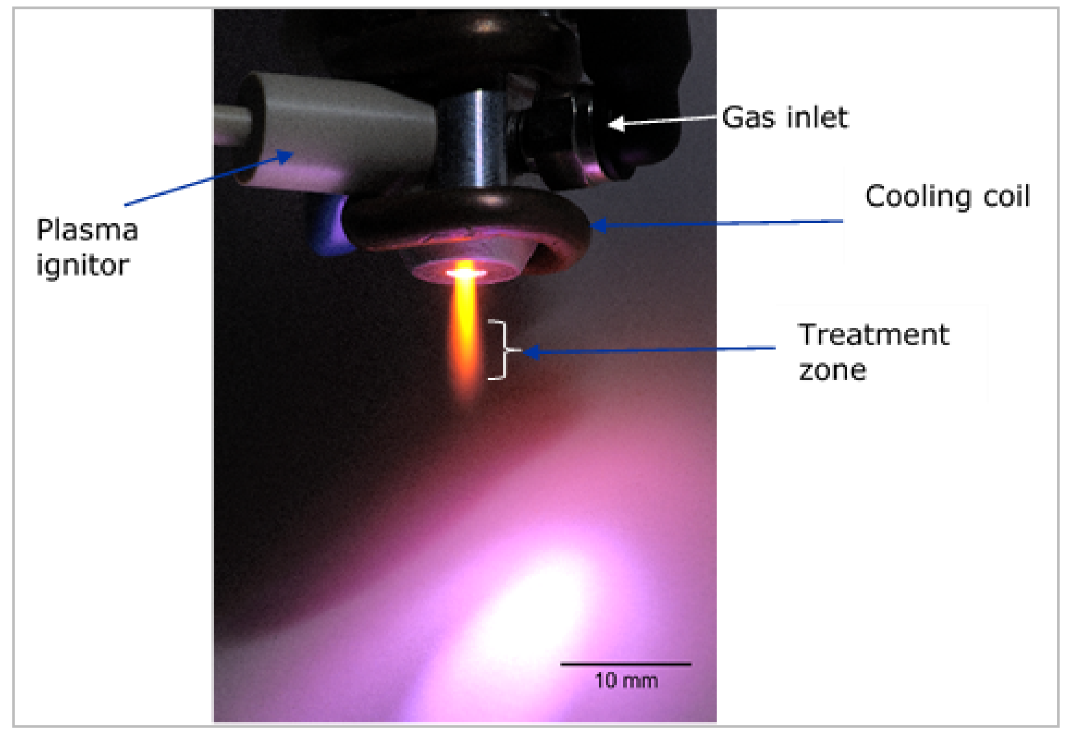

Cold atmospheric plasma plume.


At Teesside University, we develop solutions that shape the future, today.
We foster research and innovation to generate new knowledge that addresses global challenges and changes lives for the better.
DISCOVER MORE
tees.ac.uk/ambition
AMBITION
DELIVERED
TODAY
Teesside University


floteks
Engineered
Plastic Products
Rotomoulding Solutions
Your Experienced Partner for
Product Innovation,
Research and Development
EU PROJECTS:
SafeHPower
DeICE-UT
DEICING OF WIND TURBINE BLADES
MONITANK
ISOPREP
LeakFree
OHSAS 18001
ISO 14001
AS 9100
IATF 16949
Exhibitions:
ARMI
ARMI MEMBER
ARMO MEMBER
IAA
Driving tomorrow
AGRITECHNICA
2019
Floteks Plastik Sanayi ve Ticaret A.Ş
DOSAB Fulya Sk. No:7 16245 Osmangazi Bursa / TURKEY info@floteks.com.tr www.floteks.com.tr

TWI Innovation Network

FACILITATOR AND HUB FOR TECHNOLOGY DEVELOPMENT AND INNOVATION

INNOVATION ACCELERATION STRATEGIC PLANS



FUNDING SUPPORT

- Technology innovation management
- Proposal management and delivery
- Consortium management
- Ideas development
- Investment and financing

UNLOCKING OPPORTUNITIES

- Key partner matching
- TWI Innovation Network (TWIIN):
    - Innovation Centres
    - Technology Acceleration Programmes (TAPs)
    - Private Technology Innovation Partnerships (PTIPs)
    - Access to TWI Industrial Members and SMEs
- Dissemination and marketing
- Events management
- Innovation consultancy

ROADMAPPING

- Technology mapping
- Ideas generation
- Concept development
- Idustrial targets
- Trends analysis
- Roadmap canvas
- SWOT analysis
- Future development focus
- Value chain analysis
- Key Performance Indicators (KPIs)

TECHNOLOGY FOCUS

- Foresight review
- Product innovation
- Trending subjects
- CPD courses
- Technology development
- Marketplace strategies




#COLLABORATEANDINNOVATE

info@twi-innovation-network.com twi-innovation-network.com +44 (0)1223 899 000